

Correlated activity in the mammalian retina

Von der Fakultät für Medizin und Gesundheitswissenschaften der Carl von Ossietzky Universität Oldenburg zur Erlangung des Grades und Titels eines

Doktors der Naturwissenschaften (Dr. rer. nat.)

vorgelegte Dissertation

Von Frau Elaheh Lotfi Karkan geboren am 24.03.1989 in Tehran, Iran

Gutachter: Prof. Dr. Martin Greschner

Weitere Gutachter: Dr. Udo Ernst

Tag der Disputation: 21.11.2024

Table of contents

Table of figuresV	
SummaryVII	
1 Introduction	
1.1 The structure of the Retina	1
1.1.1 Photoreceptors	
1.1.2 Horizontal cells	
1.1.3 Bipolar cells	
1.1.4 Amacrine cells	
1.1.5 Ganglion cells	
1.2 Correlated activity in the retina ganglion cells	
1.2.1 Underlying mechanisms of correlation in the RGCs	
1.2.2 Isolating signal and noise correlation	
1.2.3 Characteristics of correlated activity in RGCs	
1.3 Effect of correlated activity on retinal population coding	
1.3.1 Information theory	
1.3.2 Stimulus reconstruction	
1.4 Objectives	
1.4.1 Project 1: Electrical coupling of heterotypic ganglion cells in the	17
mammalian retina	14
1.4.2 Project 2: Asymmetric polyaxonal amacrine cell type delivers directional	
sensitive inhibition to retinal ganglion cells	15
1.4.3 Project 3: Multineuronal firing patterns in retinal ganglion cells of guinea	10
pig	15
P ¹ S	10
2 Electrical Coupling of Heterotypic Ganglion Cells in the Mammalian Retina 17	
2.1 Introduction.	18
2.2 Results	18
2.2.1 Reciprocal firing of ganglion cells indicates homotypic and heterotypic	
coupling	18
2.2.2 Heterotypically coupled ganglion cells form two independent mosaics	19
2.2.3 Identification of sON α-ganglion cells as one of the heterotypically	
coupled types	20
2.2.4 Tracer injections of sON α-ganglion cells reveal homotypic and	
heterotypic coupling	21
2.2.5 Electrical images show homotypic and heterotypic coupling patterns	
2.2.6 Stimulus-dependent modulation of heterotypic reciprocal firing	
2.2.7 sON α-ganglion cells influence spiking in medium sON cells more	
effectively than vice versa	25
2.3 Discussion	25
2.3.1 Electrical coupling via gap junctions	25
2.3.2 Coupling patterns of ganglion cells	
2.3.3 Functional roles of electrical coupling	27
2.3.4 Interactions across neuronal pathways	
2.4 Materials and Methods	28

2.4.1 Animals and tissue preparation	28
2.4.2 Multi-electrode array recordings	
2.4.3 Light stimulation	29
2.4.4 Receptive field and classification analysis	29
2.4.5 Correlated activity measurement	
2.4.6 Electrical Image	
2.4.7 Electrical Image Model	
2.4.8 Neurobiotin injections	
2.4.9 Immunohistochemistry and light microscopy	31
2.4.10 Alignment and matching	
2.4.11 Statistical analyses	
3 Asymmetric polyaxonal amacrine cell type delivers directional sensitive inhibition	
to retinal ganglion cells	
3.1 Introduction	
3.2 Results	
3.2.1 Functional identification of an ON PAC cell type	37
3.2.2 Functional organization and light response of ON asymmetric PACs and	
medium sON RGCs	
3.2.3 Physiological properties of ON asymmetric PACs	
3.2.4 Correlated activity of ON asymmetric PACs and medium sON RGCs	
3.2.5 The light response of medium sON RGCs to moving bar stimulus	45
3.2.6 ON asymmetric PACs contribute to the direction-sensitivity of medium	
sON RGCs	
3.3 Discussion.	48
3.3.1 Modulatory effect of ON asymmetric PACs: positive and negative	
correlation	
3.3.2 Direction sensitivity of medium sON RGCs by ON asymmetric PACs	
3.3.3 ON asymmetric PACs: sparse and asymmetric axonal arbors	
3.3.4 Prospects for future studies	
3.4 Materials and Methods	
3.4.1 Animals and tissue preparation	
3.4.2 Multi-electrode array recordings	
3.4.3 Light stimulation	
3.4.4 Receptive field and classification analysis	
3.4.5 Correlated activity measurement	51
3.4.6 Measurement of conduction velocity of PAC	
3.4.7 Polar and raster plots	
3.4.8 Model	52
43.6.1	
4 Multineuronal firing patterns in retinal ganglion cells of guinea pig	7.0
4.1 Introduction	
4.2 Results	
4.2.1 Spatial organization of correlated activity	5 /
4.2.2 Receptive field properties of pairwise synchronous and asynchronous	50
spikes	39
4.2.3 Quantification of the receptive field properties of pairwise synchronous	(1
and asynchronous spikes across cell types	
4.3 Discussion	

4.3.2 Synchronous spikes vs asynchronous spikes		65
4.3.3 Prospects for future studies		
4.4 Materials and Methods		67
4.4.1 Animals and tissue preparation		67
4.4.2 Multi-electrode array recordings		
4.4.3 Light stimulation		
4.4.4 Receptive field and classification analysis		
4.4.5 Correlated activity measurement		
4.4.6 Synchronous spike trains		
4.4.7 STA calculation and receptive field parameters		68
4.4.8 Quantification		69
4.4.9 Violin plot		69
5 General Discussion		
5.1 Electrical coupling between parallel pathways of different RGC types		
5.2 Direction-sensitive response of medium sON RGCs		
5.3 A Polyaxonal amacrine cell population in the guinea pig retina		
5.4 Systematic patterns of correlated activity across six RGC types		
5.5 Linear response of synchronous and asynchronous firing activities		
5.6 Final remarks		75
A11	7.0	
Abbreviations	/6	
Curriculum Vitae	78	
Currentum vitae	/ 0	
List of publications	79	
References	80	
Acknowledgments	91	
Frklärung	92	

Table of figures

Figure 1.1: The structure of the retina.	3
Figure 1.2: Electrical image of an RGC and a PAC.	5
Figure 1.3: Correlated activity within and across RGC types.	6
Figure 1.4: Common input and reciprocal interactions mediating noise correlation	8
Figure 1.5: signal and noise correlation	9
Figure 1.6: Isolating signal and noise correlation in cross-correlation function	10
Figure 1.7: Effect of correlation on information coding	12
Figure 2.1: Cross-correlation functions of spiking activity between homotypic and heterotypic RGC pairs in one preparation.	19
Figure 2.2:Receptive field mosaics of heterotypically coupled cell types.	20
Figure 2.3: sON α-RGCs are heterotypically coupled.	21
Figure 2.4: sON α-RGCs are tracer coupled to a heterotypic RGC type.	22
Figure 2.5: The electrical images of the medium sON RGCs revealed the homotypic and heterotypic coupling pattern.	23
Figure 2.6: Heterotypic reciprocal firing of RGCs is modulated by their stimulus-driven activation.	24
Figure 3.1: Electrical images of ON asymmetric PACs and medium sON RGCs	38
Figure 3.2: Receptive field mosaics of medium sON RGCs and ON asymmetric PACs	39
Figure 3.3: Electrical images of ON asymmetric PACs reveal asymmetry in their axonal arbor pattern.	40
Figure 3.4: Conduction velocity of ON asymmetric PAC's axonal spikes.	41
Figure 3.5: Correlated activity of ON asymmetric PACs and medium sON RGCs	41
Figure 3.6: Delay in the negative correlation of ON asymmetric PACs and medium sON RGCs is consistent with conduction velocity.	42
Figure 3.7: Stimulus-driven activity of medium sON RGCs in close proximity to ON	43

Figure 3.8: Spatial patterns of correlated activity of an ON asymmetric PAC and the medium sON RGCs population.	44
Figure 3.9: Medium sON RGCs response to moving bar stimulus reveals their direction-sensitivity.	46
Figure 3.10: Direction-sensitive inhibition of medium sON RGCs through ON asymmetric PACs.	47
Figure 4.1: Receptive field mosaic of six RGC types.	57
Figure 4.2: Spatial organization of correlated spiking activity within and across RGC types.	58
Figure 4.3: The spatial receptive field of the synchronous and asynchronous spike trains.	60
Figure 4.4: The temporal receptive field of synchronous and asynchronous spike trains	61
Figure 4.5: Quantification of the receptive field of pairwise synchronous and asynchronous spikes across cell types.	63

Summary

The retina is the first stage of visual processing in the mammalian brain. It transforms the light signals captured by the photoreceptors into spike trains that are sent to the higher visual centres via the optic nerve. Retinal ganglion cells (RGCs) are the output neurons of the retina, and they have diverse types and functions. RGCs of one type do not act independently but rather interact with each other and with amacrine cells (ACs). These interactions can generate correlated activity between RGCs, which means that nearby RGCs tend to fire spikes synchronously, depending on the stimulus and the network properties. Correlated activity can shape the visual signal transmitted to the brain in different ways. Therefore, studying correlated activity in the retina is important for understanding how retinal neural networks process visual information. This thesis investigates the existence and properties of correlated activity within and across different types of RGCs and between RGCs and spiking ACs using large-scale multi-electrode array recordings.

The retina is comprised of heterogeneous groups of RGCs that are selective to distinct features and tile the visual space with minimal overlap. RGCs form parallel pathways, projecting their responses to specific regions in the higher visual areas. This configuration is assumed to be the optimal method for information coding, as it allows a large scale of visual information to be transmitted through the bottleneck of the optic nerve efficiently. Consequently, strong cross-type synchrony such as heterotypic electrical coupling between RGCs, would appear to conflict with the retina's objective of independently sampling visual features. It was thought that electrical coupling occurred solely among identical RGC types or between RGCs and amacrine cells. Revisiting this dominant view, we employed large-scale multi-electrode array recordings to reveal heterotypic electrical coupling between two types of RGCs via gap junctions. Immunohistochemical labeling techniques allowed us to identify one of the participating RGC types as the sustained ON alpha RGC (sON α RGC). Tracer injections into sON α RGCs confirmed these findings and exhibited the electrical coupling of this cell type to the neighboring cells of the same type, amacrine cells, and smaller medium-sized RGCs within the dendritic field of the sON α RGC. The existence of cross-talk in the parallel pathways hints at potential benefits similar to those provided by homotypic electrical coupling in visual coding.

RGCs exhibit correlated activity with ACs via both electrical and chemical synapses. The extensive diversity of ACs presents a challenge in systematically characterizing their contributions to retinal circuitry. A subgroup of ACs, known as polyaxonal amacrine cells (PACs), are distinguished by their axons that extend several millimeters across the retinal surface. These PACs fire action potentials to relay signals due to the considerable length of their axons. Consequently, their activity can be simultaneously recorded along with RGCs using multi-electrode arrays. The distinctive spatial

configuration of PACs' axons permits their differentiation from RGCs via electrical imaging approaches. Utilizing these methodologies, a distinct functional PAC type was identified. Electrical images revealed that this PAC type exhibits a sparse and asymmetric axonal pattern. Characterization of the populations of these PACs exhibited uniform signaling properties and a mosaic organization. Analysis of cross-correlation functions showed a correlation between this ON asymmetric PAC type and the medium sustained ON RGC type. Medium sON RGCs, whose receptive fields were in close proximity to the axons of ON asymmetric PACs, displayed negatively correlated activity with these PACs. We showed that ON asymmetric PACs convey a directional sensitive inhibitory signal to medium sON RGCs. Additionally, our findings indicated that medium sON RGCs exhibit a direction-sensitive response. By developing a conceptual model we showed that directional sensitive inhibitory signals of ON asymmetric PACs could mediate the direction-sensetivity of the medium sON RGCs.

It has been suggested that the synchronous activity of the RGCs could convey fine spatial details about the visual world to the brain. Additionally, it has been suggested that the common input from ACs might be the mechanism behind this phenomenon, facilitating multiplex coding via the synchronous activity of RGCs. In our study, we revisited this concept by analyzing large-scale multi-electrode array recordings from RGCs of guinea pigs. We assessed the functional organization of six RGC types across four retinas using the reverse correlation method. Our investigation into the structure of correlated activity both within and across these six RGC types revealed a systematic dependence of the correlated activity on distance. Utilizing the receptive field, we characterized the stimulus-response properties of the pairwise synchronous activity of RGCs within the same cell type. For the six RGC types examined, the receptive fields of their synchronous activity exhibited distinct characteristics in terms of size, intensity, and latency compared to the asynchronous activity of the pairs.

1 Introduction

1.1 The structure of the Retina

The retina is a thin light-sensitive tissue, about 200 µm thick, that lines the back of the eye (sterling & Demb, 2004). It has a laminar structure, where five neuronal classes form a dense network of feed-forward and feedback, excitatory and inhibitory synapses. The cell bodies of these neurons are located in nuclear layers, while their neural processes interact with each other in the plexiform layers.

Image processing begins when light passes through the cornea and the lens, which focuses it onto the back of the eyeball, where the retina is located. In vertebrates, the retina has an inverted structure. Therefore, light has to travel through all five layers of the retina to reach the photosensitive neurons, called photoreceptors, whose cell bodies are located in the outer nuclear layer (ONL). The two retinal neuronal classes that provide feed-forward excitatory input to their target cells, in order of signal propagation, are photoreceptors and bipolar cells. There are also two other classes, called horizontal and amacrine cells, that receive feed-forward excitatory input and inhibit their target cells via feedback and feed-forward signals. In the last step of signal processing in the retina, ganglion cells send out their output through the optic nerve to the higher visual areas. The light that is transduced into a neural signal by photoreceptors is relayed to bipolar cells, while being modified by horizontal cells at the first synaptic level in the outer plexiform layer (OPL). In the next step, ganglion cells receive excitatory and inhibitory inputs, respectively, from bipolar and amacrine cells in the inner plexiform layer (IPL). The cell bodies of bipolar, horizontal and amacrine cells are located in the inner nuclear layer (INL), and those of ganglion cells are in the ganglion cell layer (GCL).

1.1.1 Photoreceptors

Photoreceptors are divided into two subclasses: rods and cones. They can be distinguished by their shape, distribution, and function. Cones have a cone-shaped outer segment, while rods have a longer and thinner one. Cones are the photoreceptors that are responsible for daylight and color vision, while rods take over under scotopic conditions. Rods and cones, like every other cell type in the retina, form a mosaic pattern, and cones have a higher density in the fovea. Therefore, the size of cones' cell bodies increases gradually from the fovea to the periphery, and their density decreases.

Rods and cones release the excitatory neurotransmitter called glutamate in response to light. The process of converting light into a neuronal response is a complex biochemical cascade, which is called phototransduction. Light level modulates glutamate release: both rods and cones hyperpolarize at high light levels, hence releasing less glutamate, while they depolarize at low light levels, and the glutamate release increases (Mustafi et al., 2009; Masland, 2012a; Grimes et al., 2018).

1.1.2 Horizontal cells

Horizontal cells are GABAergic inhibitory interneurons that have a distinct morphology. They come in two shapes: axon-bearing and axon-less cells, which extend their processes laterally in the OPL. Most mammals, including primates and guinea pigs, have two types of horizontal cells, while some rodents, such as rats and mice, have only one type.

Horizontal cells receive input from cones via dendritic invaginations into cone pedicles, and from rods via their axons. The feed-forward input from photoreceptors, as mentioned before, is in the form of glutamate release, and horizontal cells express ionotropic AMPA- and kainate-type glutamate receptors to form synapses with them. Horizontal cells modulate cones' output via feedback signaling, and also modify bipolar cells' output in a feed-forward fashion. There have been extensive studies on the feedback synapses of horizontal cells to cones, suggesting three different mechanisms: ephaptic, pH-mediated and GABA-mediated. Although, the mechanism of horizontal cell to bipolar cell signaling is poorly understood, there are studies that show evidence of GABA receptors on bipolar cell dendrites in some species. Therefore, horizontal cells can have a feed-forward inhibitory effect on bipolar cells.

Some functions attributed to Horizontal cells' feedback and feed-forward interactions in the OPL are contrast enhancement, color opponency and center-surround formation for cones and bipolar cells. In addition to chemical synapses, horizontal cells are strongly electrically coupled to each other via gap junctions. The expression of connexin 57 in mice has formed a dendro-dendritic and axo-axonal coupling, resulting in a dense network. Therefore, the receptive field of horizontal cells is larger than the extension of their dendritic arbors. As a result, a horizontal cell can laterally integrate the information relayed from multiple cones through its wide network and send it back as an inhibitory feedback signal to a single cone. This procedure is the well-known global signal processing of horizontal cells, which can play a role in the formation of center-surround antagonism. In addition to global signaling, there are recent studies (Jackman et al., 2011; Vroman et al., 2014) suggesting a contribution of horizontal cells to local signal processing. The coexistence of both modes at the earliest stage of signal processing can prevent the loss of information as a result of lateral integration in horizontal cells (Wässle, 2004; Chapot et al., 2017).

For licensing reasons, this figure is not visible in the online version. Please see https://shop.elsevier.com/books/guyton-and-hall-textbook-of-medical-physiology/hall/978-0-443-11101-3, Figure 51.1

Figure 1.1: The structure of the retina. In the first step, photoreceptors transduce the image and relay it to more than a dozen distinct bipolar cell types, which provide input to more than 40 types of retinal ganglion cells (RGCs). Interneurons such as horizontal and at least 42 amacrine cell types modify the signal which initiates from photoreceptors and will be transmitted to the brain via RGCs. Different types of RGCs tile the retina and form independent mosaics for efficient encoding. Figure from (Hall & Hall, 2020).

1.1.3 Bipolar cells

Bipolar cells are the second-order cells in the visual pathway that project the light-evoked response of photoreceptors to ganglion cells. They have two types of processes extending vertically: one going up to the OPL and the other going down to the IPL (Euler et al., 2014). There are at least 15 types of bipolar cells in the mouse retina, with more ON than OFF types (Shekhar et al., 2016). Additionally, there is one type of rod bipolar cell (Wässle et al., 2009; Hartveit & Veruki, 2012).

ON and OFF bipolar cells can be differentiated by the stratification level of their axons in the IPL and their dendritic morphology. The IPL has five strata, where OFF bipolar cells project their axons to layers 1-2 in the outer part and ON bipolar cells project their axons to layers 3-5 in the inner part of the retina. There are also bistratified bipolar cells that have terminals in both ON and OFF sublaminae (Cajal; Euler et al., 2014). OFF bipolar cell dendrites contact the base of cone pedicles, expressing ionotropic AMPA- and kainate-type glutamate receptors. On the other hand, ON bipolar cell dendrites invaginate into the cone pedicle and form a metabotropic synapse via mGluR6 receptors (DeVries, 2000; Vardi et al., 2000; Puller et al., 2013). The expression of different types of receptors results in different kinetics in the responses of bipolar cells. Synapses that are mediated by kainate are sustained, while those mediated by AMPA are more transient. Bipolar cell axons with transient signals stratify in the central strata of the IPL, while axons with sustained responses terminate in the peripheral strata in the borders of GCL and INL (Awatramani & Slaughter, 2000; Wu et al., 2000).

1.1.4 Amacrine cells

Amacrine cells are the most diverse and least understood retinal neuronal classes. Cajal named them "amacrine" because he initially thought that they lacked axons and used only dendrites for both receiving and sending signals (Cajal, 1892). More than 42 types of amacrine cells have been identified in the mammalian retina, which can be roughly classified based on the lateral extension of their dendritic tree and their stratification level in the IPL (MacNeil & Masland, 1998; Helmstaedter et al., 2013). Amacrine cells are broadly categorized into two main groups, depending on the size of their dendritic tree: small-field and wide-field cells (Mariani, 1990; MacNeil & Masland, 1998). They express ionotropic glutamate receptors, such as AMPA, kainate and NMDA, and receive feedforward input from bipolar cells (sterling & Demb, 2004; Dumitrescu et al., 2006). Amacrine cells mainly form inhibitory synapses and modulate the responses of bipolar cells with feedback signaling, while sending feedforward signals to ganglion cells and lateral signals to other amacrine cells (Masland, 2012b). In mammalians, small-field amacrine cells are glycinergic (Menger et al., 1998) and wide-field amacrine cells are GABAergic (Pourcho & Goebel, 1983). Besides these two main inhibitory neurotransmitters, some amacrine cells also co-release modulatory neurotransmitters (sterling & Demb, 2004; Masland, 2012b; Diamond, 2017) such as dopamine (Contini & Raviola, 2003), acetylcholine (Pourcho & Goebel, 1983) and glutamate (Lee et al., 2014).

A distinctive subgroup of wide-field ACs are the polyaxonal amacrine cells (PACs). Unlike some AC types whose dendrites mainly have presynaptic and postsynaptic specializations, PACs have separate dendrites and axons. PACs can be distinguished based on their specific axonal pattern that extends radially several millimeters in the IPL but does not exit the retina. The receptive fields of the PACs are mainly similar in size to the size of their dendritic trees and are much smaller than their axonal field, suggesting the separate role of dendrites in receiving signals and axons in transmitting signals. Due to the long-range axons, PACs fire spikes to transmit their signals over long distances without much signal attenuation compared to other ACs that generate graded potentials (Freed et al., 1996; Taylor, 1996; Stafford & Dacey, 1997; Völgyi et al., 2001). PACs are also found to extensively form homotypic coupling within their type and heterotypic electrical coupling with RGCs and PACs (Völgyi et al., 2001). Despite the fact that PACs extend their axons in the IPL, multiple studies were able to record the spiking activity of PACs along with RGCs using large-scale multi-electrode array recordings (Greschner et al., 2014; Greschner et al., 2016). The specific axonal pattern of PACs makes them distinguishable from RGCs using an electrical imaging approach. RGCs exhibit single axons with strong axonal spikes propagating toward the same direction, which is the optic nerve (Figure 1.2). However, PACs show multiple axons with relatively weaker axonal spikes propagating simultaneously in different directions over the retina.

For licensing reasons, this figure is not visible in the online version. Please see https://doi.org/10.1523/JNEUROSCI.3359-13.2014, Figure 1

Figure 1.2: Electrical image of an RGC and a PAC. The electrical image is the average spatiotemporal spike waveform recorded across the electrode array during the spikes detected from a specific cell. A, B, Electrical image of an OFF parasol cell. Large somatic spikes were detected at the main electrode (1), opposite-sign dendritic spikes were detected at the nearby electrode (2), and triphasic axonal spikes were detected along the axon directed toward the optic nerve (3–7). Larger circles indicate more negative voltage deflections. C, D, Electrical image of a simultaneously recorded ON-OFF PAC. The large somatic spike (1) was accompanied by dendritic spikes nearby (2) and by axonal spikes propagating simultaneously in multiple directions away from the soma (3–10). Figure from (Greschner et al., 2014)

1.1.5 Ganglion cells

Ganglion cells are the output neurons of the retina and their long axons assemble in the optic nerve. They integrate the information from the upstream neurons and transmit it to the brain areas downstream. Ganglion cells receive glutamatergic input mainly from bipolar cells and express mostly ionotropic NMDA, AMPA and kainate receptors (Massey & Miller, 1988; Brandstätter et al., 1998), but they may also express metabotropic glutamate receptors (Yang, 2004). Ganglion cells also receive inhibitory inputs from amacrine cells and express various GABAergic and glycinergic receptors. They vary in morphology, level of dendritic stratification in the inner plexiform layer, axonal projection sites, light response properties and molecular identities. In the mouse retina, more than 40 different RGC types have been classified (Kong et al., 2005; Coombs et al., 2006; Völgyi et al., 2009; Sümbül et al., 2014; Baden et al., 2016). RGCs can be classified into two main types of ON and OFF cells that exhibit firing activity to light increment (ON cells) and light decrement (OFF cells). In addition, some RGCs respond to both light increments and decrements and are called ON-OFF RGCs. ON ganglion cells stratify their dendritic tree in layers 3-5 of the IPL (ON-sublamina) and OFF ganglion cells stratify their dendritic tree in layers 1-2 of the IPL (OFF-sublamina) while ON-OFF ganglion cells stratify their dendrites in both ON- and OFF-sublaminas enabling them to receive input from both ON and OFF bipolar cells. ON and OFF RGCs can be divided into more specific types based on their light response kinetics, which can be transient and sustained. Transient RGCs stratify their dendrites in the middle of the IPL whose boundaries are specified by the dendritic stratification level of ON and OFF starburst amacrine cells and Sustained RGCs stratify their dendrites outside this boundary near the INL and GCL. Different RGC types sample various features of the visual field such as color, size, orientation, direction, and speed of motion and form parallel pathways to the brain. Based on the type of information that each cell type contains about the visual world they project their axons to a specific region in the higher visual

pathway. The two main sites that receive visual information from the retina are the dorsal lateral geniculate nucleus (dLGN) and the superior colliculus (SC).

1.2 Correlated activity in the retina ganglion cells

Correlated activity is a fundamental feature of neural networks. Neurons do not act as independent encoders but rather tend to fire simultaneously more often than would be expected by chance (Usrey & Reid, 1999; Averbeck et al., 2006; Shlens et al., 2008). The correlated activity in the RGCs was first reported by Rodieck, 1967 and was followed by Arnett, 1978 (Rodieck, 1967; Arnett, 1978). However, a series of seminal studies by David Mastronarde gave valuable insights into the different forms of correlation and mechanisms underlying them in cat retina (Mastronarde, 1983a, 1983b, 1983c).

The correlated activity between a pair of RGCs can be quantified by the cross-correlation function of the firing activity of the two cells. The cross-correlation function assesses how much the activity of one retinal ganglion cell affects the activity of another across various time intervals. The cross-correlation function of an RGC pair can show a peak or a trough at the zero time offset (Figure 1.3). The peak indicates that the two cells are positively correlated, while the trough is an indication of negative correlations. RGCs with the same light response polarity mainly exhibit a positive correlation, and RGC pairs with opposite light response polarities show negative correlation.

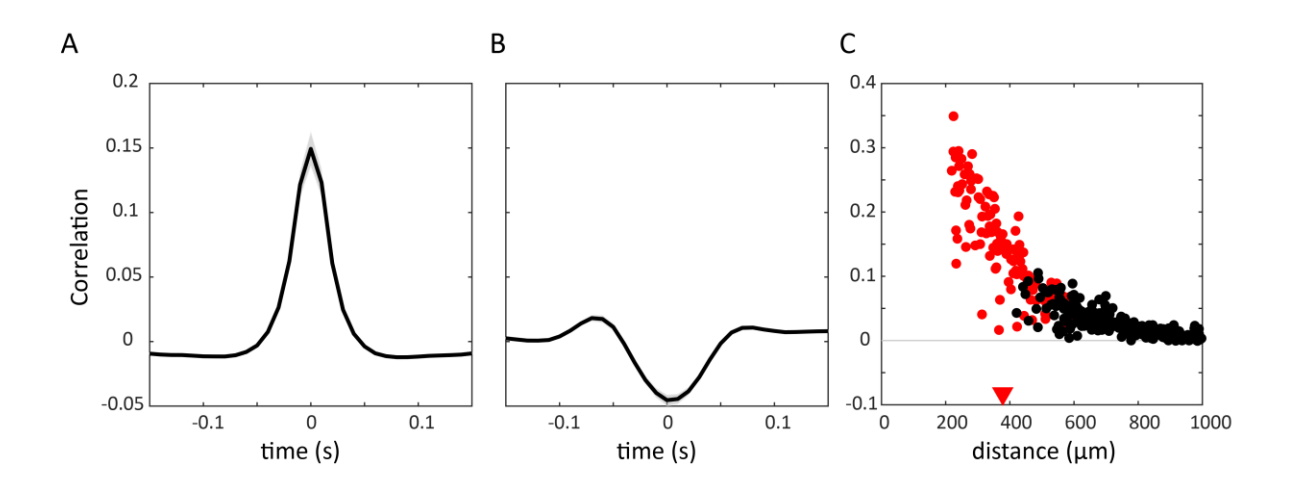


Figure 1.3: Correlated activity within and across RGC types. A, Average cross-correlation function of first direct neighbouring RGCs of the same type. B, Same as in A for pairs of two RGC types of opposite polarity. The pairs included have a distance of less than 200 μ m. Bin size, 10 ms. C, Correlation coefficient at time zero as a function of distance for pairs of the same type. The first direct neighboring pairs in the mosaic of the cell type are illustrated in red, and pairs that are more distant are shown in black. The average distance between the first direct neighboring pairs is marked with a red arrowhead

1.2.1 Underlying mechanisms of correlation in the RGCs

Correlated activity in the RGCs is mediated by two main mechanisms: common input and reciprocal interactions. These are qualitative categories of the mechanisms of correlation, which can be further analyzed in terms of biophysical properties.

Common input. Studies on ON and OFF parasol cells of the primate retina have revealed that the excitatory synaptic inputs of the neighboring ON parasol cells and neighboring OFF parasol cells in the absence of visual stimulations are correlated (Trong & Rieke, 2008; Ala-Laurila et al., 2011). These correlations mainly originate from common noise while the rest can be due to independent noise. Based on the circuitry of the retina there are several potential candidates for the source of the common noise such as cone photoreceptors, bipolar cells and amacrine cells (Brivanlou et al., 1998; Mastronarde, 1983a). Noise can originate from any of these cells and diverge into multiple RGCs and produce correlated activity in their response. However, there has been a long-standing debate on the contribution of the cone photoreceptors due to the discrepancy between the slow kinetics of cone light responses and the fast noise correlations in RGCs (Brivanlou et al., 1998; Mastronarde, 1983a). Indeed, the light response of cone photoreceptors is too slow to account for these correlations. However, cone noise has a faster kinetic than cone light response, which makes it a possible source of noise correlations in RGCs. Examining the excitatory synaptic inputs of pairs of ON and OFF parasol cells and pairs of ON parasol and ON midget cells that have little common circuitry except the cones, and pharmacological blockage of cone input to ON bipolar cells which resulted in a reduction of correlation in the excitatory synaptic inputs of ON parasol pairs, suggested cone photoreceptors can be the major source of noise in the retina (Ala-Laurila et al., 2011).

Reciprocal interaction. The cross-correlation function of the firing activity of some RGC types such ON parasol cells (Dacey & Brace, 1992; Trong & Rieke, 2008; Greschner et al., 2014), sON alpha (Puller et al., 2020), ON and OFF Y cells (Mastronarde, 1983a, 1983b, 1983c), OFF α and OFF brisk transient (DeVries, 1999; Hu & Bloomfield, 2003) exhibits sharp peaks at \sim 2 ms offset from 0. This type of rapid correlated activity is likely to be mediated by electrical synapses via gap junctions. When the connected pair belongs to the same RGC type, it is referred to as homotypic gap junction coupling. If the pair consists of different RGC types, or if one is an RGC and the other an amacrine cell, it is known as heterotypic coupling. The existence of gap junction coupling is mainly investigated by using intracellular tracer injections. Tracers are small substances such as Lucifer Yellow, a fluorescent dye, and Neurobiotin, a small bioactive molecule, that are not membrane permeable but are small enough to diffuse through gap junction pores to the neighboring cells after injection into the target cell (Vaney, 1991).

In addition to the direct gap junction coupling between RGC pairs that contributes to their correlated activity, it has been shown that the indirect gap junction coupling via an amacrine cell is likely to introduce correlated activity in the firing activity of an RGC pair. This form of correlated

activity falls in the category of common input where an amacrine cell is heterotypic gap junction coupled to two RGCs and provides simultaneous correlated synaptic input to them (Brivanlou et al., 1998)

For licensing reasons, this figure is not visible in the online version. Please see https://doi.org/10.1152/jn.1999.81.2.908, Figure 4

Figure 1.4: Common input and reciprocal interactions mediating noise correlation. A, Cross-correlation function of a pair of ON brisk RGCs. The cross-correlation function is unimodal with a sharp peak centered at zero. The cross-correlation function's width is ~10 ms, indicative of noise correlation mediated by a common input, primarily originating from cones. B, Cross-correlation function of a pair of OFF brisk transient RGCs. The bimodal cross-correlation function with sharp peaks offset from zero is indicative of a rapid correlation between pairs mediated by gap junctions. Figure from (DeVries, 1999)

Signal correlation. The correlated activities that have been discussed so far are noise correlation which is intrinsic to the retina and its specific circuitries. There is another type of correlation that is induced by the highly correlated visual scene and is called signal correlation. The spatial correlation of the stimulus can introduce correlated synaptic input to the RGCs and result in their correlated firing activity. Moreover, ganglion cells that have overlapped receptive fields are very likely to receive similar signals from shared presynaptic circuits. In elucidating the principles of signal and noise correlation, one may observe the tuning curve responses of two cells to a set of stimuli (Figure 1.5). These curves represent the mean responses of each neuron to multiple presentations of the same stimulus. Cells that belong to the same cell type typically exhibit tuning curves that closely resemble one another, suggesting a tendency for positive signal correlation. In contrast, neurons with tuning curves that diverge significantly are indicative of a negative signal correlation (Figure 1.5 A). When examining the responses of two neurons to a specific stimulus, s*, their mean response in the scatter plot is a single point. Nonetheless, the presence of noise introduces variability in their responses to each iteration of the stimulus, resulting in a distribution for each s*. Consequently, in the scatter plot that depicts the response of two cells, a distribution emerges in response to each stimulus. If the variations in the responses of the two neurons to s* are similar, the noise correlation is positive; if the variations are dissimilar, the noise correlation is negative (Figure 1.5 B).

For licensing reasons, this figure is not visible in the online version. Please see https://doi.org/10.1016/j.tins.2004.02.006, Figure 1

Figure 1.5: signal and noise correlation A, The tuning curves, which show the mean responses of two neurons (in red and blue) to a set of stimuli, are depicted in the left and right panels. The tuning curves of neuron 1 and neuron 2 have a small phase shift in the left panel, where they respond similarly to the stimuli. However, they have a 180-degree phase shift in the right panel, where they respond oppositely to the stimuli. Therefore, the left and right panels exhibit positive and negative signal correlation, respectively. **B**, The distributions of response variation around the mean responses of neuron 1 and neuron 2 to stimulus s* are shown on top of their tuning curves (left). The response space of the two neurons to stimulus s* is depicted in the right panel. The trial-to-trial responses of the two neurons to s* can vary in the same or opposite direction, indicating positive or negative noise correlation, respectively. Figure from (Averbeck & Lee, 2004).

1.2.2 Isolating signal and noise correlation

The signal correlation is assumed to be additive with the noise correlation hence the cross-correlation function of RGC pairs often exhibits them superimposed on each other (Figure 1.6). The signal correlation is slower than the noise correlation generated by the common input and the noise correlation that is mediated by the gap junctions is the most rapid one. To separate the signal and noise correlation in the cross-correlation function, specific stimuli or the shuffling method can be used (Perkel et al., 1967). Signal correlation depends on the stimulus, so it can be isolated when the stimulus is constant. In an experiment using repeated stimuli for n trials, the noise in the spike train of neurons is the variable parameter, while the stimulus is the constant parameter. Therefore, by calculating the cross-correlation function for neuron A in the i^{th} trial versus neuron B in the j^{th} trial, where $i \neq j$, several times, and averaging these cross-correlation functions, the signal correlation can be obtained. This method is called shuffling. The noise correlation, which is the corrected correlation in many cases, can be obtained by subtracting the signal correlation from the total cross-correlation function. Another way to measure

the noise correlation is to calculate the cross-correlation function when the stimulus is time-invariant (see Figure 1.6,(Greschner et al., 2011).

For licensing reasons, this figure is not visible in the online version. Please see https://doi.org/10.1113/jphysiol.2010.193888, Figure 5

Figure 1.6: Isolating signal and noise correlation in cross-correlation function A, Cross-correlation function (CCF) between two ON parasol RGCs under constant illumination. **B**, As in A, but under stimulation with a spatially correlated visual stimulus (raw CCF: red dashed lines). The shuffled CCF (signal correlation) is shown with black dashed lines. The spatial correlation of the stimulus increases from left to right, and as a result, the raw CCF and the shuffled CCF also increase in magnitude. The corrected CCF (noise correlation) is displayed with black solid lines, which are obtained by subtracting the shuffled CCF from the raw CCF. **C**, As in A, but for a pair of ON parasol and OFF parasol RGCs. **D**, As in B, but for the same RGC pair as in C. Figure from (Greschner et al., 2011)

1.2.3 Characteristics of correlated activity in RGCs

The noise correlation among RGCs depends on their type and distance. Pairs from the same RGC type are more likely to exhibit stronger correlations compared to pairs of the same polarity that do not belong to the same type. The cross-correlation function of pairs that do not belong to the same type is often asymmetric while the cross-correlation function of pairs that belong to the same cell type is symmetric. The pairwise correlation decreases as a function of distance and RGCs are more likely to be correlated with their direct neighbors in the mosaic and the strength of correlation with RGCs beyond the direct neighbors is reported to be very weak.

These observations are reminiscent of the mosaic organization of RGC's receptive fields and can be explained by the mechanism that mediates the noise correlation (Gauthier et al., 2009). The spatial limitation of correlation to the direct neighbors can reflect that these cells are more likely to receive the divergent noise of the cone photoreceptors since they have overlapped receptive fields and as the cells grow further the shared noise becomes less. Although some cell types such as ON parasol cells in primates have shown positive correlation with RGCs that are slightly beyond their direct neighbors and this could be due to the existence of a polyaxonal amacrine cell or chain coupling. The difference in the strength of correlation across cell types, the asymmetric correlated activity of cross-type pairs may indicate that although reciprocal interactions and common input mainly from cone

photoreceptors are the major mechanisms underlying correlated activity the presynaptic circuitries and the intrinsic properties of the cell and its nonlinearities modify the noise correlation observed in the response of the RGCs.

1.3 Effect of correlated activity on retinal population coding

Noise is a natural component of all sensory systems, including the retina. If the noise present in the responses of retinal ganglion cells were independent or uncorrelated, averaging their responses over multiple trials could effectively reduce this noise. However, RGCs often exhibit either positive or negative noise correlations in their firing activities. This makes it crucial to comprehend how noise correlation affects the information coding.

To further explain how noise correlation can affect information coding, some possible pairwise interactions of two cells in response to different stimuli in the presence of noise correlation are studied. Consider a pair of cells with similar tuning curves, meaning they typically tend to respond to visual stimuli similarly, exhibiting positive signal correlation. If these cells also display positive noise correlation, their response distribution to two stimuli would overlap. This overlap could reduce the amount of information encoded in the pair's response, leading to potential errors when trying to identify the observed stimulus based on the pair's response. However, if the positive noise correlation of the pair is eliminated using a shuffling method, the shape of the pairwise response distribution changes. This change decreases the overlap area, reducing the detrimental impact of noise correlation on coding (Figure 1.7A). In a different scenario, consider a pair with negative signal correlation and positive noise correlation. In this case, there would be no overlap between their response distributions to two stimuli, and the noise correlation would not negatively affect coding. However, if the noise of this pair is assumed to be uncorrelated, an overlap in the response distribution of the pair would appear, negatively impacting coding (figure: B). These observations lead to the concept of the sign rule (Averbeck et al., 2006). According to this rule, if the signal and noise correlation share the same sign, the noise correlation is likely to harm coding. Conversely, if their signs differ, noise correlation is unlikely to negatively impact coding.

In these two examples for simplification, the dependency of noise correlation to stimulus was not considered. Indeed, the noise correlation can be modulated by the stimulus. For example, OFF parasol cells receive stronger correlated excitatory presynaptic noise during modulated light relative to constant light (Trong & Rieke, 2008). Moreover, multiple studies in Direction-selective RGCs suggested that the stimulus dependency of noise correlation can decrease the harmful effect of noise (Franke et al., 2016; Zylberberg et al., 2016). Considering direction-selective RGC pairs that have a 90-degree tuning offset, cell A is tunned to upward motion (90°) and cell B to leftward motion (180°), the sign of signal and noise correlation change as the stimulus changes. The stimulus is suggested to serve as a modulatory gain factor for the input noise correlations, exhibiting stronger positive noise correlation

when the cells are both more active. This happens for stimuli that are between the peaks of the two cells' tuning curves from 90° to 180°. However, for these stimuli, the signal correlation is negative and the opposite sign of signal and noise correlation leads to the non-detrimental effect of noise correlation. The influence of noise correlation on information processing in the RGCs has been quantified using various approaches such as information theory(Puchalla et al., 2005), stimulus reconstruction using linear regression (Warland et al., 1997; Brackbill et al., 2020), and model-based stimulus reconstruction (Pillow et al., 2008).

For licensing reasons, this figure is not visible in the online version. Please see https://doi.org/10.1038/nrn18888, Figure 1

Figure 1.7: Effect of correlation on information coding A, The response space shows the response distributions of two neurons to two different stimuli s₁ and s₂. The x-axis and y-axis represent the response of neuron 1 and neuron 2, respectively. The green and yellow dots show the mean response (signal) of two neurons to s₁ and s₂ respectively, and the green and yellow ellipses show the 95% confidence interval of the response distributions to each stimulus (noise). The two ellipses are elongated along the diagonal, indicating a positive signal and noise correlation between neuron 1 and neuron 2. Using the shuffling method, the responses of the two neurons are decorrelated, and the ellipses become circles (right panels). The diagonal lines show the optimal decision boundary. The ellipses in the unshuffled (correlated) condition overlap more than the shuffled (decorrelated) condition, which makes the decision-making task of distinguishing the two stimuli based on the two neurons' response more error-prone. Therefore, the correlated condition carries less information about the stimulus. B, As in A, for two neurons with negative signal and positive noise correlation. The correlated condition has no overlap, unlike the decorrelated condition. Therefore, the optimal decision boundary for the correlated condition discriminates the two stimuli from neuronal responses without error, compared to the decorrelated condition. This indicates that the correlated condition carries more information about the stimulus than the decorrelated condition. Figure from (Averbeck et al., 2006).

1.3.1 Information theory

Information theory is the most used approach to study information encoding in the brain, as this method has the privilege of minimizing the number of assumptions about the structure of interactions between studied variables. The amount of information in the response of cells about the set of stimuli can be quantified by an information theoric measure called mutual information. Cells could jointly

convey less (redundant code), equal (independent code), or more (synergic code) information than the sum of the information they deliver individually. RGCs in the salamander retina exhibit major redundancy in their response to various stimulations such as natural scenes and flickering checkerboard and they show almost no synergy (Puchalla et al., 2005). However, another study showed that the RGCs in the mouse retina are mainly independent encoders (Nirenberg et al., 2001). These conflicting results could arise from the difference in the species and more importantly, the fact that the cell type information was neglected. In general, the redundancy could be due to similar response properties, for example, the signal correlation of the neighboring RGCs of the same type leads to redundant code. In such a case the redundancy could improve the signal-to-noise ratio and increase the fidelity of the signal. Alternatively, the noise correlation originating from common input could introduce redundancy in which the error-correcting role that was assumed for redundancy cannot be accomplished (Barlow, 2001). Finally, the highly spatiotemporal correlated nature of the visual scene could increase the redundancy in the joint response of RGCs. However, the optic nerve has a limited capacity for information transmission and the redundant code in the retina in earlier studies was thought to be against the efficient information coding and the redundancy reduction hypothesis was proposed (Attneave, 1954; Atick & Redlich, 1990; Barlow, 2001). This hypothesis suggests that there are mechanisms in the retina that mediate redundancy reduction such as the decorrelation of visual stimulus using the centersurround structure of the receptive field as a bandpass filter. In the visual scene, low spatial frequencies have more power than high spatial frequencies therefore a bandpass filter can remove low frequencies and reduce redundancy.

1.3.2 Stimulus reconstruction

Linear regression is one of the methods that is used widely to estimate the visual stimulus from the response of ganglion cells (Warland et al., 1997). Reconstruction of full-field stimulus using the response of salamander ganglion cells has shown that the optimal filter of each cell is likely to be acquired if the response of other cells is also included. However, this improvement in reconstruction is very small when the additional cell is from the same type compared to when the additional cell has an opposite polarity. This is consistent with the concept of correlated activity and redundancy. Since RGCs of the same type exhibit a positive correlation and contain duplicate information about the stimulus, addition of each cell from the same type slightly improves the joint information of the cells and the amount of information finally saturates and cannot be equal to the sum of the information of the individual cells. However, RGCs of opposite polarities are mainly negatively correlated and encode different visual features. Therefore, the joint information of the two cells could be equal to the sum of the information of individual cells and combining their response can enhance the reconstruction more. Additionally, it was shown where the signal fidelity was relatively low, the consideration of the existence of noise correlation improves the reconstruction (Brackbill et al., 2020). This is consistent with the observation that in scotopic conditions where the correlated noise is greater, considering it as

independent noise is detrimental to stimulus reconstruction (Ruda et al., 2020).

To further evaluate the importance of correlated activity in the information processing of RGCs, stimulus reconstruction methods that incorporate the nonlinear model of RGCs and correlations have been used (Pillow et al., 2008). This approach exploits the generalized linear model (GLM) that includes coupling filters which capture the influence of firing activity of cells on each other. The cross-correlation function of a neighboring pair of modeled ON parasols that do not have coupling filters has shown only a slow positive correlation that is likely the signal correlation while the cross-correlation function of neighboring pair of modeled ON parasols that include coupling filters has shown a faster positive correlation superimposed on the slow correlation that indicates the coupling filters are likely to model the noise correlation. Using the modeled ON parasol cells to reconstruct the stimulus has shown that taking noise correlation through coupling filters into account improves the reconstruction by 20%. Considering these two approaches, it can be understood although noise correlation does not carry information, noting its structure is important in the accuracy of information processing.

1.4 Objectives

Each Retina ganglion cell type tiles the retina and samples distinct features of the visual world and forms parallel pathways to higher visual areas. However, studies on RGCs in various species have shown that RGCs are not strictly independent encoders as their responses are correlated through various mechanisms. The correlated activity between RGCs of the same type, RGCs of different types and RGCs and amacrine cells could alter the way RGCs process visual information. The following studies investigate the existence and properties of correlated activity within and across different types of these cells.

1.4.1 Project 1: Electrical coupling of heterotypic ganglion cells in the mammalian retina

Electrical coupling via gap junctions serves as one of the mechanisms mediating correlation. The correlated activity produced by this mechanism is rapid in a timescale of approximately 2 ms. Such correlation has been exclusively observed in RGCs of the same type, known as homotypic coupling, which aligns with the principle of parallel encoding in the retina. Conversely, heterotypic coupling was presumed to occur solely between RGCs and ACs. Here we revisit the possibility of the existence of heterotypic coupling between RGC types. In this study, large-scale multi-electrode array recordings, intracellular tracer injections, and immunohistochemistry were combined to:

- Analyze the correlated activity of RGC pairs using their cross-correlation function.
- Identify two functional RGC types that exhibit homotypic and heterotypic coupling.
- Match the two recorded RGC types with the immunohistochemistry labeled RGCs.
- Verify the heterotypic and homotypic coupling of the two RGC types using tracer coupling and electrical imaging approaches.

1.4.2 Project 2: Asymmetric polyaxonal amacrine cell type delivers directional sensitive inhibition to retinal ganglion cells

In the retina, certain functions require signal processing over large distances. Polyaxonal amacrine cells (PACs) are significant in this context. These cells have long axons that cover several millimeters of the retinal surface, supporting long-range spatiotemporal interactions. PACs form inhibitory GABAergic synapses with retinal ganglion cells along their axons. This network of connections leads to a correlated activity, which shapes the RGCs' responses. Here we investigate if the correlated activity of a specific type of PAC and a type of RGC contributes to the direction-sensitive response of that RGC type. In this study large-scale multi-electrode array recording is employed to:

- Identify a distinct functional PAC type based on its specific electrical signature using an electrical imaging approach.
- Characterization of the functional organization of the PAC type using the reverse correlation method.
- Investigate the interaction of a specific PAC type with RGCs and determine its modulatory impact on a particular RGC type through cross-correlation function analysis.
- Illustrate the direction-sensitive response of the specific RGC type using the response of the cell type to moving bar stimulus.
- Develop a conceptual model to exhibit that the directional sensitive inhibitory signal of the specific PAC type is consistent with the direction-sensitivity of the RGC type.

1.4.3 Project 3: Multineuronal firing patterns in retinal ganglion cells of guinea pig

Correlated activity shapes the response of RGCs that are projected to higher visual areas. Correlated activity is mediated by different mechanisms and each mechanism can characterize the role of correlation in information processing. One of the main questions in this field of study is how the brain deals with the correlation and what else the synchronous spikes offer when the correlation is believed to be against the universal rule of efficient coding. In this study, we use large-scale multi-electrode array recordings of four retinas to:

- Characterize the functional organization of six RGC types using the reverse correlation method.
- Quantitative description of correlated activity within and across the six RGC types using pairwise cross-correlation function analysis.
- Investigate how the correlated activity alters the receptive field of cell pairs of the same type using spike-triggered average as a linear estimator of the receptive field.
- Quantification of the impact of correlated activity on the receptive field across cell types.

2 Electrical Coupling of Heterotypic Ganglion Cells in the Mammalian Retina

The Journal of Neuroscience, February 5, 2020 • 40(6):1302–1310

The manuscript is identical in content and adjusted to thesis format.

Declaration

I hereby confirm that Elaheh Lotfi contributed to the aforementioned study as stated below:

Article:

Electrical Coupling of heterotypic ganglion cells in the mammalian retina

Christian Puller*, Sabrina Duda*, Elaheh Lotfi*, Yousef Arzhangnia, Christoph T. Block, Malte T. Ahlers, and Martin Greschner

Department of Neuroscience and Research Center Neurosensory Science, Carl von Ossietzky University, 26111 Oldenburg, Germany

* Authors contributed equally to this work

Authors contribution:

C.P. and M.G. designed research; C.P. and S.D. performed research; M.T.A. contributed unpublished reagents/analytic tools; C.P., S.D., E.L., Y.A., C.T.B., and M.G. analyzed data; C.P. and M.G. wrote the paper. C.P. S.D., and E.L. prepared the figures and all authors edited and commented on the manuscript.

Prof. Dr. Martin Greschner
Supervisor

Date

2.1 Introduction

The separation of visual information into parallel streams starts at the first retinal synapse formed between photoreceptors and more than a dozen distinct bipolar cell types (Euler et al., 2014). By the time the information leaves the retina via >30 types of retinal ganglion cells (RGCs; (Baden et al., 2016), the visual information is separated into parallel pathways, in which each RGC type carries a distinct signal to the higher visual centers of the brain (Nassi & Callaway, 2009). Reciprocal electrical coupling between neurons via gap junctions is a recurrent scheme throughout the CNS including the retina (O'Brien & Bloomfield, 2018). At the level of RGCs, examples of electrical coupling between cells of the same type (homotypic) are well known (Vaney, 1991; DeVries, 1999; Hu & Bloomfield, 2003; Hidaka et al., 2004; Trong & Rieke, 2008; Greschner et al., 2011; Trenholm et al., 2013; Völgyi et al., 2013; Trenholm et al., 2014), whereas functional heterotypic coupling of cells has so far only been reported to occur between RGCs and inhibitory interneurons (Ackert et al., 2006; Völgyi et al., 2013; Greschner et al., 2016). The same conclusions were drawn from tracer coupling patterns of neurobiotin-injected RGCs indicative of gap junction coupling in various species (Vaney, 1991; Dacey & Brace, 1992; Xin & Bloomfield, 1997; Schubert, Degen, et al., 2005; Völgyi et al., 2005; Zhang et al., 2005) as well as from electron microscopic reconstructions of synaptic circuits (Marc et al., 2018).

Here, we performed a large-scale analysis of spike correlation patterns between various cell types by multielectrode array (MEA) recordings of adult guinea pig retinas. We provide functional and anatomical evidence for heterotypic electrical coupling between two types of sustained ON center (sON) RGCs, which is not in line with the common notion of a functional separation of the neuronal pathways at the level of the retinal output.

2.2 Results

2.2.1 Reciprocal firing of ganglion cells indicates homotypic and heterotypic coupling

We recorded the spiking activity of RGCs in adult guinea pig retinas with a large-scale multielectrode array to investigate their pattern of correlated electrical signaling. Reciprocal electrical coupling of RGCs via gap junctions causes highly correlated spiking activity that is reflected in a bimodal cross-correlation function with sharp peaks offset from 0 (Mastronarde, 1983c; Brivanlou et al., 1998; DeVries, 1999; Völgyi et al., 2013). Homotypic electrical coupling was readily observed between neighboring cells of a large-size (Figure 2.1A–D) and a medium-size (Figure 2.1E–H) type of sON RGCs among other types. Bimodal peaks occurred with an offset of approximately ± 2 ms from 0 [medium sON, 2.4 ± 0.4 ms, n = 136; large sON (sON α , see below), 2.6 ± 0.4 ms, n = 108; mean \pm SD]. These pronounced peaks were superimposed on slower correlations elicited by shared network noise and correlations of the light stimulus during recordings (Trong & Rieke, 2008; Greschner et al., 2011). Intriguingly, the same pattern of correlation was observed for heterotypic pairs of the medium and large sON RGCs (Figure 2.1I–L). Slow light-driven correlations were off centered, which pointed

to a difference in the light response kinetics of the two cell types (Figure 2.2). The bimodal peaks, however, were centered around 0 with a short delay of 2.1 ± 0.6 ms (n = 38), which indicated direct, functional coupling between two distinct RGC types. This heterotypic coupling pattern was cell type specific across preparations.

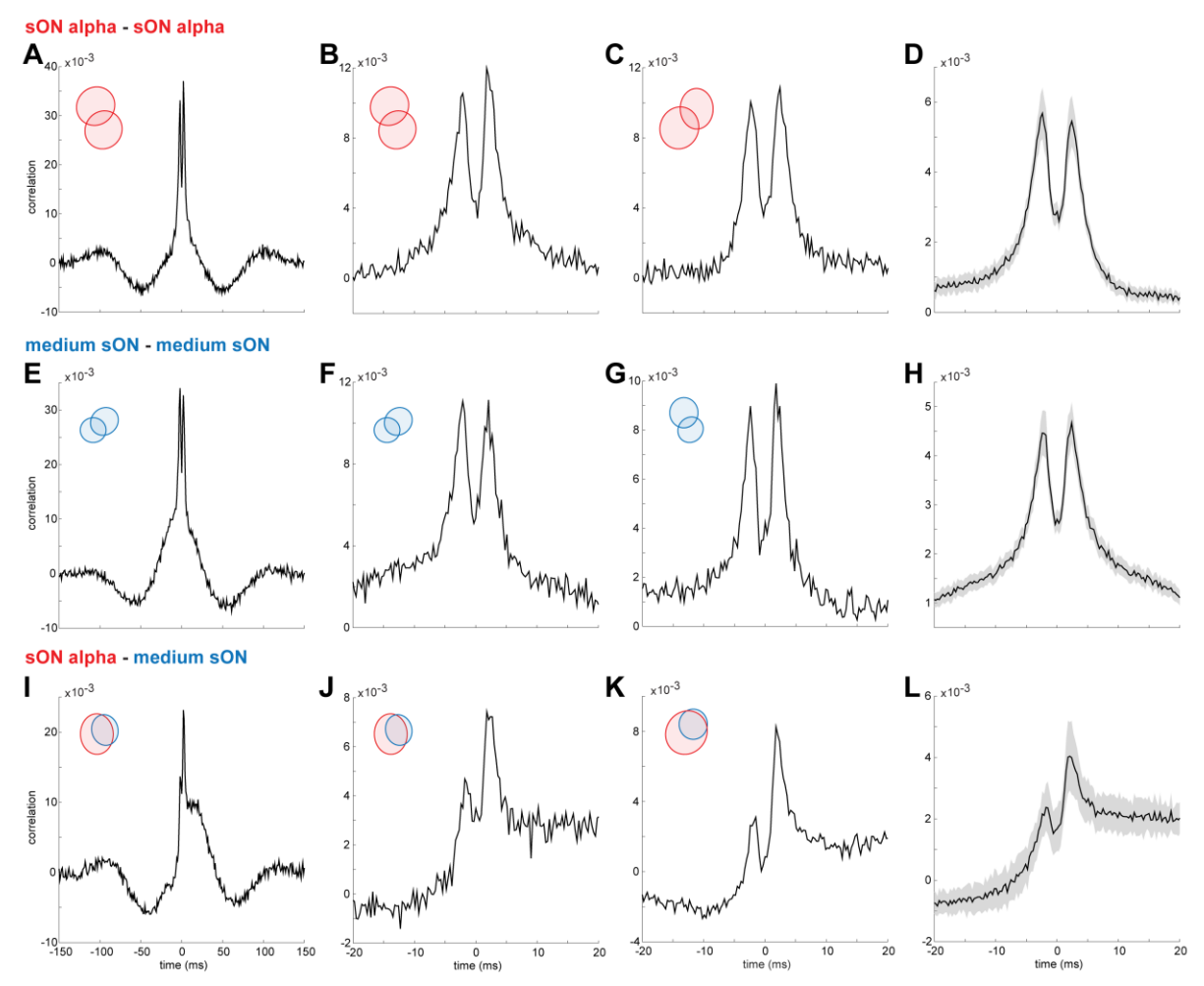


Figure 2.1: Cross-correlation functions of spiking activity between homotypic and heterotypic RGC pairs in one preparation. The retina was stimulated with a spatiotemporal random noise stimulus. A, Cross-correlation function between two sON α-RGCs. Insets show receptive field fits of the cell pair, as in Figure 2.2A. Bin size, 1 ms. B, Same cell pair as in A at a smaller time scale. Bin size, 0.3 ms. C, Same as in B for a different cell pair. D, Average cross-correlation function of neighboring sON α-RGC pairs (n = 54). Gray shaded region represents the 95% confidence interval. E–H, As in A–D for homotypic medium sON pairs (n = 68). I–L, As in A–D for heterotypic cell pairs of sON α- and medium sON cells (n = 14). Time 0 indicates a spike of the sON α-RGC.

2.2.2 Heterotypically coupled ganglion cells form two independent mosaics

RGCs of individual types tile the retina with their dendritic trees and thus form mosaics with their receptive fields (Wässle et al., 1981). Accordingly, the receptive fields of the two types of heterotopically coupled RGCs formed two independent mosaics and showed distinct ON center light response properties (Figure 2.2). The first cell type exhibited large receptive fields ($\emptyset = 499 \pm 38$ µm, n = 45) and a triphasic temporal filter, while the second cell type had medium-sized receptive fields

($\emptyset = 313 \pm 35 \mu m$, n = 89) and a more biphasic temporal filter. Both types showed sustained light responses to full-field light intensity steps.

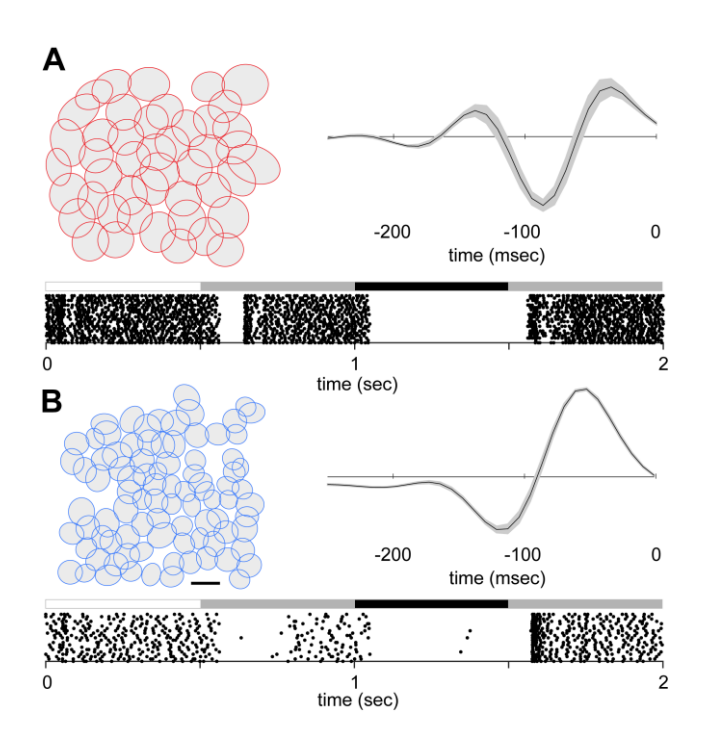


Figure 2.2:Receptive field mosaics of heterotypically coupled cell types. A, Receptive field outlines of an sON α -RGC mosaic (see Materials and Methods). Right, Mean spike-triggered average stimulus time course. Shaded region represents the 95% confidence interval. Bottom, Spike responses of an example sON α -cell to 20 repeats of full-field light intensity steps (indicated above the spike trains). B, As in A for medium sON RGCs. Scale bars: B (for A, B), 400 μm.

2.2.3 Identification of sON α-ganglion cells as one of the heterotypically coupled types

Next, we immunolabeled retinas after having recorded their physiological responses with the multielectrode array to reveal the morphological identity of one of the functional types (Li et al., 2015). Some of the functional features of the larger cell type resembled those of the sON α -RGCs of the guinea pig retina (Demb et al., 1999). sON α -RGCs are intensely labeled with antibodies against the neurofilament marker SMI-32 in mice (Bleckert et al., 2014; Krieger et al., 2017). Therefore, we used SMI-32 in combination with RBPMS, which labeled all RGCs (Rodriguez et al., 2014), and ChAT to label starburst amacrine cells as reference points for dendritic stratification depth in the inner plexiform layer (Manookin et al., 2008). In addition to horizontal cells, several types of RGCs were labeled with SMI-32 similar to the mouse retina (Figure 2.3A–G). Among the most intensely labeled cells, an ON RGC type had polygonal-shaped cell bodies, which were remarkably large (\emptyset = 29 ± 2 µm, n = 52) when compared with all other cell bodies (\emptyset = 17 ± 3 µm, n = 714). In addition, the primary dendrites of these cells stratified just beneath the dendritic plexus of ON starburst amacrine cells. These features were highly suggestive of the sON α -RGCs in the guinea pig retina (Demb et al., 1999; Manookin et al., 2008; Beaudoin et al., 2019). The putative sON α -RGC cell body locations matched the recording

locations of the large sON type derived from the electrical signals of the cells on the multielectrode array (Figure 2.3H, I, permutation analyses: p < 0.001). Thus, the results suggested that one of the cell types of interest corresponds to the sON α -RGCs.

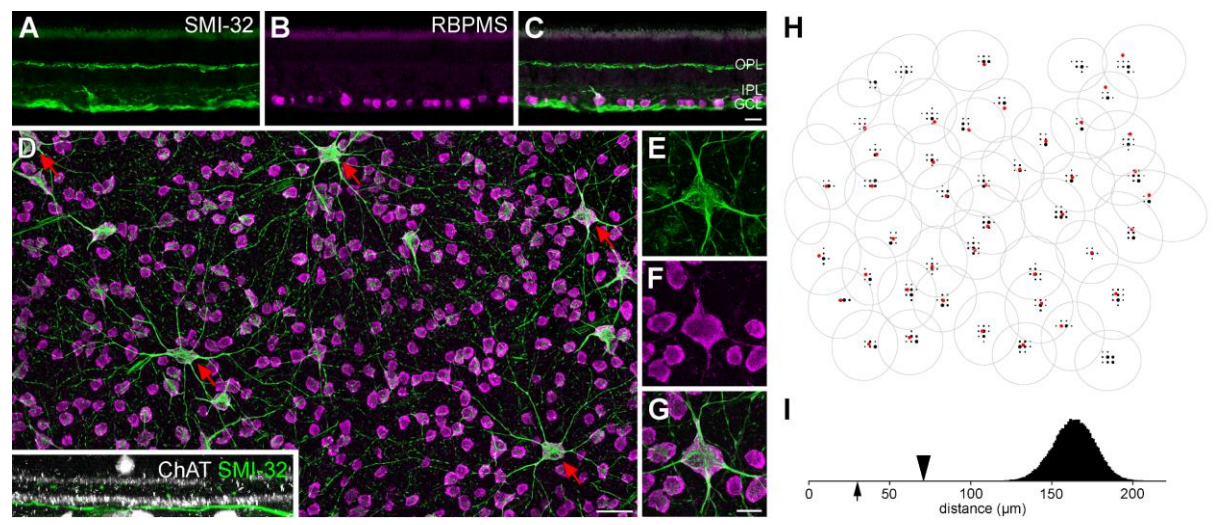


Figure 2.3: sON α**-RGCs are heterotypically coupled.** A**-**C, Vertical cryosection labeled with RBPMS and SMI-32. OPL, Outer plexiform layer; IPL, inner plexiform layer; GCL, ganglion cell layer. **D**, Staining as in A-C together with ChAT (inset) in a whole-mounted retina. Red arrows indicate sON α-RGCs. Inset shows the stratification of dendrites of an sON α-RGC relative to the dendritic tier of starburst amacrine cells in an x/y-projection of D. **E-G**, Magnification of the sON α-cell body in the top right corner of D. **H**, Overlay of soma locations from immunolabeled sON α-cells (red dots), with strongest electrodes from recorded large sON type RGCs (black dots) and respective receptive field outlines (gray ellipses). **I**, Permutation analysis indicates a probable match of recorded cells with immunolabeling. Black arrowhead indicates the observed mean distance between cell somas and recording locations. Histogram represents the mean distances for >165,000 random permutations of the mosaic. Black arrow indicates the mean distance after optimization (see Materials and Methods). The distance between electrodes (black dots) is 42 μm. Scale bars: C, G,20 μm; D, 50 μm.

2.2.4 Tracer injections of sON α -ganglion cells reveal homotypic and heterotypic coupling

We performed intracellular injections of the gap junction-permeable tracer neurobiotin (Vaney, 1991) to further confirm the heterotypic coupling of the sON α -RGC to another RGC type. sON α -RGCs were targeted with sharp microelectrodes based on their cell body shape and size. The characteristic morphology and dendritic stratification levels (Figure 2.4A) confirmed that the targeted cells (n = 14) were sON α -RGCs (Demb et al., 1999; Manookin et al., 2008; Beaudoin et al., 2019). The tracer-coupling pattern revealed additional neurobiotin-positive cell bodies, which were all located in the RGC layer. Large, strongly SMI-32-labeled cell bodies ($\emptyset = 26 \pm 2 \, \mu m$, n = 46; observed maximum coupled to one cell = 6) were observed at the outer perimeter of the dendritic tree of the injected sON α -cells (Figure 2.4 A, red arrows, B–E) in agreement with the homotypic coupling patterns between α -like RGCs in other species (Vaney, 1991; Hidaka et al., 2004; Völgyi et al., 2005). Medium-sized cell bodies ($\emptyset = 17 \pm 2 \, \mu m$, n = 12, observed maximum coupled to one cell = 5) that were positive for RBPMS but only weakly labeled with SMI-32 were consistently located closer toward the cell bodies of the injected sON α -RGCs (49 \pm 17% along the radial axes; Figure 2.4 A, blue arrow, F–I). These

significantly smaller cell bodies (p < 0.001, Wilcoxon rank sum test) belonged to heterotypically coupled RGCs, most likely the medium sON RGCs. Additionally, small-diameter cell bodies, which did not colocalize with RBPMS, were observed and therefore corresponded to electrically coupled, displaced amacrine cells (Figure 2.4A, black arrowheads, J–M).

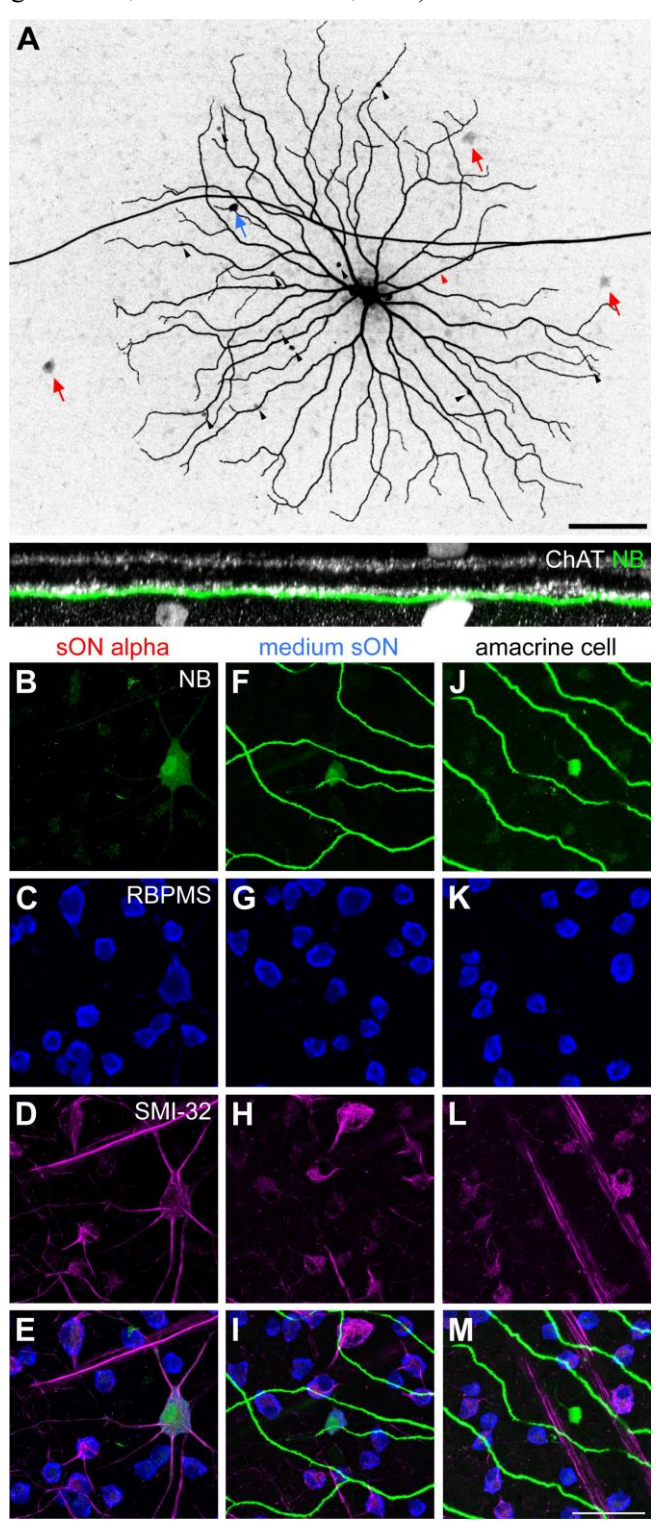


Figure 2.4: sON α -RGCs are tracer coupled to a heterotypic RGC type. A, Top, An injected sON α -RGC shows neurobiotin (NB) spread into large (red arrows), medium (blue arrow), and small (black arrowheads) cell bodies. The axon of the injected cell (red arrowhead) converges to an axon of another NB-injected, neighboring sON α -RGC, which passes horizontally through the image. Bottom, The x/y-projection of a dendrite

of the same cell relative to ChAT labeling. **B–E**, Magnified view of the leftmost NB-positive RGC body in A (red arrow), counterstained with RBPMS and SMI-32. **F–I**, As in B–E for the cell body marked with a blue arrow in A. **J–M**, As in B for an exemplary amacrine cell body. Scale bars: A, 150 μm; M, 50 μm.

2.2.5 Electrical images show homotypic and heterotypic coupling patterns

Heterotypic electrical coupling between sON α -RGCs and medium sON RGCs was also evident from the electrical images (i.e., the spike-triggered electrical activity across all electrodes; Figure 2.5). The electrical image of individual RGCs showed the expected spatial organization (Li et al., 2015), which is a high-amplitude somatic area, a lower-amplitude dendritic area, and an axon extending toward the optic disk (Figure 2.5A,D). However, if electrical signals were averaged only across a short time window before the somatic spike occurred, pronounced additional areas of electrical signals with larger amplitudes (hot spots) became visible (Figure 2.5B,C,E,F). These hot spots coincided with the location of neighboring homotypic (medium sON) and heterotypic (sON α) RGCs and thereby revealed the spatial organization of the coupling pattern. Medium sON RGCs were coupled to multiple neighboring sON α -RGCs and medium sON RGCs (Figure 2.5C,F). A simple model was used to test the idea that the hot spots are mainly based on the gap junction-driven correlations, while the signals of the less precisely correlated spikes average out. The hot spots could be reproduced using the electrical signatures of the neighboring cells from their electrical images and their spike correlations (Figure 2.5G). As expected, the hot spot amplitude was strongly reduced when the precise gap junction-driven correlations were removed (Figure 2.5H, inset).

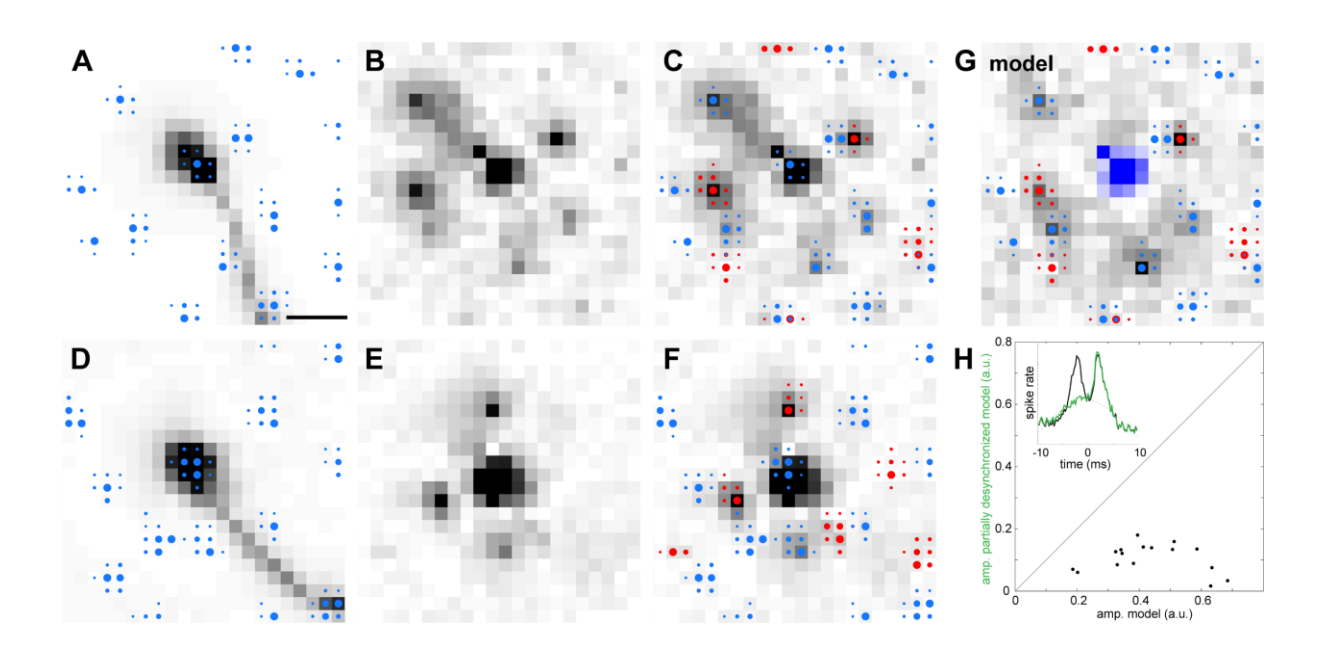


Figure 2.5: The electrical images of the medium sON RGCs revealed the homotypic and heterotypic coupling pattern. A, The minimum projection of the spike-triggered electrical activity of a medium sON RGC from 4.48 ms before to 6.72 ms after the somatic spike. Darker intensities indicate more negative voltage deflections. Largest amplitudes are saturated to increase visibility. Clusters of blue dots mark the electrode locations with the strongest signals for individual medium sON RGCs. **B**, The mean spike-triggered electrical activity from 2.1 to 0.39 ms before a spike of the cell in A reveals hot spots of activity surrounding the soma of the cell. **C**, As in B with the locations of strong signals of medium sON RGCs (blue dots, as in A) and

sON α -RGCs (red dots). **D**–**F**, As in A–C for a different medium sON RGC. **G**, Model of the medium sON RGC hot spots in C, based on the highly synchronized spikes and the somatic mean waveforms of neighboring cells, reproduces the correlation pattern. The center RGC position was marked with blue squares according to its appearance in B and C for visual guidance. **H**, Scatterplot of the hot spot amplitudes in the original model (G) versus a partially desynchronized model. Inset, Original cross-correlation function (black) of a sON α pair and their cross-correlation function after the partial removal of precise correlations (green). The dashed line is a Gaussian fit to the slower correlation component. Amplitude is given in arbitrary units. Scale bars: A (for A–G), 200 μ m.

2.2.6 Stimulus-dependent modulation of heterotypic reciprocal firing

To get some insights into the interaction of heterotypic coupling and stimulus processing, we searched for stimulus conditions that increased or decreased the coupling. As above, we used a random noise stimulus with a natural spatiotemporal frequency falloff as a generic visual stimulus. First, we used the spatiotemporal receptive field of the medium sON RGCs to predict their linear response to the stimulus. Then, the linear prediction was used to subdivide cross-correlation functions according to the amount of stimulus-driven activation the cells received (Figure 2.6). We removed the slower correlations elicited by shared network noise and correlations of the light stimulus by subtracting the average cross-correlation function of uncoupled pairs with similar receptive field overlap. Reciprocal firing increased when medium sON RGCs were increasingly activated by the visual stimulus. This was expected from previous observations of homotypic coupling properties (Mastronarde, 1983c; Trong & Rieke, 2008; Trenholm et al., 2014). Dividing the cross-correlation functions based on the stimulus-driven activation of the sON α -RGCs led to qualitatively identical results (data not shown). Instances in which one cell of the coupled pair was strongly activated by the stimulus while the other cell was inhibited hardly occurred due to the high receptive field overlap of the coupled pairs and their similar response properties.

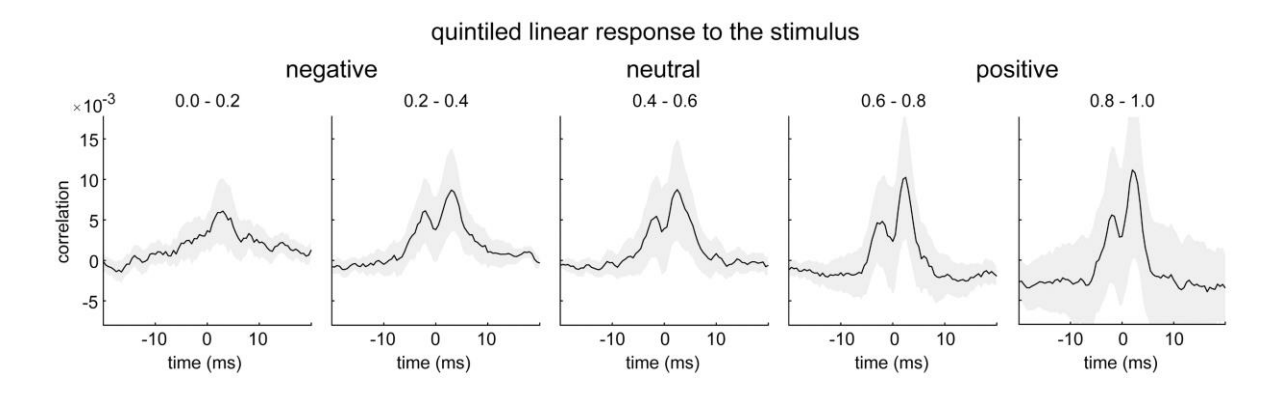


Figure 2.6: Heterotypic reciprocal firing of RGCs is modulated by their stimulus-driven activation. Cross-correlation function between cell pairs of sON α -RGCs and medium sON RGCs conditional on the stimulus-driven activation of the medium sON RGCs. The stimulus-driven activation was estimated as the linear response to the stimulus. Quintiles of the linear response were used to subdivide the spikes. Stronger activation from left to right. Stimulus and noise correlations were removed by subtracting the average cross-correlation function of uncoupled pairs with similar receptive field overlap. Data are as in Figure 2.5L (n = 14). Time 0 indicates a spike of the sON α -RGC. Gray shaded region represents the 95% confidence interval. Cross-correlation function bin width, 2 ms; bin center shift, 0.5 ms.

$2.2.7\ sON\ \alpha$ -ganglion cells influence spiking in medium sON cells more effectively than vice versa

Across all stimulus conditions, the left peak of the cross-correlation function is smaller than the right one (Figure 2.6; i.e., a spike in sON α -RGCs led to a spike in the medium sON RGCs more effectively than vice versa). Therefore, the question arose whether the medium sON RGC thereby inherited some of the stimulus filter properties of the coupled sON α -RGC. Indeed, the receptive fields of heterotopically coupled medium sON RGCs were larger than those of neighboring medium sON RGCs that showed no detectable heterotypic coupling (134 \pm 17% area; n = 12, p < 0.001, Wilcoxon rank sum test). To test whether this increase in receptive field size was consistent with being elicited by coupling, spatiotemporal receptive fields of medium sON RGCs were calculated only from spikes that occurred shortly after spikes in the sON α -RGCs. The receptive fields were larger than those calculated from the remaining spikes (127 \pm 31% area; n = 14, p < 0.002, Wilcoxon signed-rank test). Furthermore, these medium sON receptive fields were extended toward the coupled sON α -RGC, as indicated by a reduced distance between their receptive field centers (76 \pm 18%; n = 14, p < 0.001, Wilcoxon signed-rank test).

2.3 Discussion

In summary, the correlated spiking activity, tracer coupling, and spatial patterns of shared electrical activity in the electrical images all pointed to heterotypic coupling between two distinct types of RGCs.

2.3.1 Electrical coupling via gap junctions

The narrow, bimodal peaks in cross-correlation functions of spiking activity between heterotypic RGC pairs presented here closely resemble those of homotypic pairs in our study and previously published examples in terms of amplitude and timing (Mastronarde, 1983c; Brivanlou et al., 1998; DeVries, 1999; Trong & Rieke, 2008; Völgyi et al., 2013). The fast reciprocal firing has been attributed to gap junction coupling of the corresponding cells based on temporal firing properties and pharmacological manipulations. The bimodal shape indeed reflects direct reciprocal RGC coupling via gap junctions formed by connexins (Völgyi et al., 2013). In addition, tracer coupling of RGCs is commonly interpreted as evidence of gap junction coupling via connexins (Vaney, 1991; Dacey & Brace, 1992; Xin & Bloomfield, 1997; Zhang et al., 2005). This was confirmed in studies of genetically modified mice lacking the connexin subunit proteins Cx36 or Cx45 (Schubert, Degen, et al., 2005; Schubert, Maxeiner, et al., 2005; Pan et al., 2010; Völgyi et al., 2013; Roy et al., 2017). Cx36 is the major connexin subunit involved in RGC coupling (Pan et al., 2010) in addition to Cx45 and possibly Cx30.2 (Schubert, Maxeiner, et al., 2005; Mueller et al., 2010), and the guinea pig retina shows a

distribution of Cx36 common to mammals (Kovács-Öller et al., 2017). Therefore, it is likely that heterotypic coupling between sON α -RGCs and medium sON RGCs occurs via direct, connexincontaining gap junctions between the two cell types, while the connexin subunit that mediates the electrical coupling of these cell types remains unknown. We observed a bias toward medium sON cells in the spiking probability during reciprocal firing (Figure 2.1, Figure 2.6), which could possibly reflect rectification caused by differences in input resistance or membrane capacitance between the two cell types (Veruki & Hartveit, 2002), with the latter caused by different cell sizes (i.e., sON α -cells being larger than medium sON cells as estimated from cell body and receptive field sizes; Figure 2.2 ,Figure 2.3).

2.3.2 Coupling patterns of ganglion cells

Even though homotypic coupling has been known for decades, heterotypic electrical coupling between RGCs has not been observed in previous studies. Similarly, electrical coupling of neurons in other parts of the CNS is thought to occur in a homotypic manner (Traub et al., 2018). Based on our investigations, homotypic electrical coupling is a common phenomenon in the guinea pig retina, which occurs among several types of ganglion cells, similar to what has been shown in other species (O'Brien & Bloomfield, 2018). The coupling pattern of sON α-RGCs, however, is not consistent when compared across species. Homotypic coupling was not observed between ON α-RGCs of mouse and rabbit retinas (Xin & Bloomfield, 1997; Völgyi et al., 2005; Zhang et al., 2005). In contrast, ON α-RGCs were shown to be homotypically coupled in rat and ferret (Penn et al., 1994; Hidaka et al., 2004). While the analogies between rodent ON α- and primate ganglion cell types are still under debate, ON parasol cells are a well known example for homotypically coupled RGCs in primates (Dacey & Brace, 1992; Trong & Rieke, 2008; Greschner et al., 2014). Therefore, our findings regarding the heterotypic coupling of sON α-RGCs in guinea pig retinas cannot be treated as a general rule for electrical coupling of this cell type, as coupling patterns greatly differ between species. Nevertheless, it is likely that heterotypic electrical coupling of RGC types exists across species. Functional analyses across many cells in conjunction with a reliable cell type classification, which have rarely been conducted in the past, are required to reveal these interactions between pathways. Evidence for heterotypic RGC coupling in previous tracer injections may have been missed because of the complex coupling patterns, with labeled cell bodies of different shapes and sizes. Tracer-coupled cell bodies that did not match the injected cell body size were by default identified as large amacrine cells, where additional molecular markers would have been required to reveal the identity of cells. Finally, the interpretation of results may have been further confounded by the prevailing premise of RGC types never being heterotypically coupled to preserve their function as parallel and independent processing units.

2.3.3 Functional roles of electrical coupling

Insight into the functional roles of reciprocal coupling at the level of RGCs was gained from studies of homotypic coupling among certain RGC types. The coding benefits have been shown to include enhanced signal-to-noise ratio and stimulus saliency (Bloomfield & Völgyi, 2009; Trenholm et al., 2013; Yao et al., 2018). The heterotypic coupling of RGCs described here introduces a new network motif that extends these mechanisms across parallel output channels. Moreover, heterotypic coupling may give rise to an efficient circuitry, where certain stimulus features are passed on from one pathway to another only after the filter properties of the spiking nonlinearity. Heterotypically coupled cells may take advantage of this feature-selective filter residing in their coupled partners, as it does not exist in the presynaptic circuitries of the cells. First, the stimulus features must match the preferred filter properties of the cells to overcome the strong nonlinearity of the spike generation. Then, if the spike threshold has been reached in one of the cells, a spike in the second, electrically coupled cell is produced only if its membrane potential is already close to threshold (Mastronarde, 1983c; Trong & Rieke, 2008; Trenholm et al., 2014), which is further supported by the results of our study (Figure 2.6). Due to stimulus correlations in natural scenes, it is common for overlapping or neighboring RGCs with similar response properties to receive excitatory inputs in close temporal relation, correlating their membrane potentials. This is the case for the sON α -RGCs and medium sON RGCs as they show similar response properties and extensive stimulus-driven correlations (Figure 2.1I-L, Figure 2.2). In addition, the receptive field overlap between heterotypically coupled pairs is on average even higher than in homotypic pairs, which occurs due to the relative placement of the coupled neurons reflected in the mosaic structure of two independent ganglion cell types (Figure 2.1 insets, Figure 2.2, Figure 2.4) Our results suggest that the medium sON RGCs inherit some of the receptive field features of sON α-RGCs (Figure 2.6). It is therefore tempting to speculate that information is passed from one cell type to another, which may not be available from their presynaptic circuitries. This could be the case for melanopsin signals, for instance, which are generated only at the level of certain ganglion cell types, including sON α-RGCs in mice (Estevez et al., 2012; Schmidt et al., 2014).

2.3.4 Interactions across neuronal pathways

The optic nerve represents a bottleneck in the flow of visual information from the retina to the visual centers of the brain. Therefore, the output of the retina is bound to efficiently use the limited information capacity and is thought to minimize the redundancies of the signals. One consequence of this is the concept of parallel processing in the retina (Wässle, 2004; Nassi & Callaway, 2009). Initially, it is a confusing finding that, after the visual information was segregated with considerable effort into separate pathways, signals are partially mixed again at the output neurons even though there are many instances of potential cross talk within the retinal circuitry. However, the concept of parallel pathways in the retina is not meant in this absolute way, as demonstrated, for instance, by the cross talk in the

inner retina even across ON and OFF pathways (Zaghloul et al., 2003; Hoshi et al., 2009) and the convergence of retinal pathways in the lateral geniculate nucleus (Rompani et al., 2017; Rosón et al., 2019). Therefore, a full assessment of the independence of channels is only possible after the complete circuitries, including the projection targets of the cells and the upstream processing of the signals, are understood. Overall, while we demonstrate here only a single example of heterotypic RGC-to-RGC coupling, our study serves as a counterexample to the common notion of exclusively homotypic coupling, and it shows that the complexity of electrical coupling across neuronal pathways has been underestimated in the previous literature.

2.4 Materials and Methods

2.4.1 Animals and tissue preparation

All experiments were performed in accordance with the institutional guidelines for animal welfare and the laws on animal experimentation issued by the European Union and the German government. Guinea pigs of either sex were killed by an overdose of pentobarbital (Narcoren, Boehringer Ingelheim). Animals at an age of 3–35 months were used for the experiments, and no difference in the prevalence of homotypic or heterotypic RGC coupling was apparent. Animals were housed in a 12 h light/dark cycle, and experiments were performed during daytime hours. Retinas were dissected from the eye-cup under infrared illumination in Ames' solution, pH 7.4 (Sigma-Aldrich) bubbled with carbogen (95% O2 and 5% CO2) at room temperature (RT). MEA recordings were performed at 34°C in the recording chamber. For neurobiotin injections, the tissue was stored under photopic light conditions in Ames' solution at ~30°C.

2.4.2 Multi-electrode array recordings

Retinas were recorded as described previously (Field et al., 2007). Briefly, a 3×3 mm piece of isolated retina from the ventral half of the eye was mounted, ganglion cell side down, on a large-scale CMOS (complementary metal-oxide-semiconductor) array (3Brain). The MEA comprised 4096 electrodes arranged in a 64×64 grid with 42 μ m electrode spacing. Recordings were analyzed offline to isolate the spikes of different cells. Candidate spike events were detected using a threshold on each electrode. The voltage waveforms on the electrode and neighboring electrodes around the time of the spike were extracted. Clusters of similar spike waveforms were identified as candidate neurons if they exhibited a refractory period. Duplicate recordings of the same cell were identified by temporal cross-correlation and removed.

2.4.3 Light stimulation

A random noise stimulus with a natural spatiotemporal frequency falloff was used to characterize the response properties of recorded cells. The stimulus was presented on a CRT monitor at a refresh rate of 120 Hz and a stimulus pixel width of 49 μ m on the retina at photopic light levels at a mean intensity of 2.9 mW/m². Only the green and blue monitor guns were used.

2.4.4 Receptive field and classification analysis

The receptive field was approximated by the spike-triggered average. Since the random noise stimulus was spatiotemporally correlated, the spike-triggered average does not represent an unbiased linear filter but produces a slightly blurred spatial filter.

RGCs were functionally classified into types based on their spatiotemporal receptive field properties and spike autocorrelation function. Receptive field outlines were drawn at the 1 SD contour of two-dimensional Gaussian fits. Receptive field size estimates are reported as the diameter of a circle with the same area as the elliptical Gaussian fit. The receptive field areas of coupled and uncoupled RGCs and of the receptive fields calculated from synchronous and remaining spikes were estimated by the number of stimulus pixels above a threshold (one-third) of the peak amplitude. The distance between these receptive fields were estimated as the distance between the centroids of the selected stimulus pixel. This method had sufficient flexibility to measure asymmetric receptive fields compared with the symmetric Gaussian fit.

2.4.5 Correlated activity measurement

Cross-correlation functions were obtained by binning spikes and computing the correlation coefficient between the resulting spike count vectors, with a temporal offset. Cross-correlation functions were summarized by averaging across neighboring pairs showing reciprocal coupling. Cells with noisy spike-triggered averages, auto-correlation or cross-correlation functions, or electrical images indicative of imperfect spike sorting were excluded from the analysis. Cross-correlation functions were calculated over spike recordings of 50 – 60 min duration in the presence of a random noise stimulus. No apparent timing difference was observed between the left and right peaks in the cross-correlation functions of heterotypic pairs. Therefore, both peaks were included in the reported average offset times for homotypic and heterotypic pairs. For the conditional cross-correlation analysis (see Figure 2.6), we calculated the linear response to the stimulus using the spike-triggered average as the linear filter. As mentioned above, the spike-triggered average of a spatiotemporally correlated stimulus is not an unbiased linear filter but produces a slightly blurred spatiotemporal version. We used this method for its familiarity in the field as no critical influence was expected for the resolution of this analysis. This was confirmed by a logistic regression model that is less sensitive to the stimulus correlations that led to qualitatively similar results (data not shown). Quintiles of the linear responses were used to

subdivide the spikes. We removed the slower correlations elicited by shared network noise, correlations of the light stimulus and artifacts introduced by the spike subdivision by subtracting the average cross-correlation function of uncoupled pairs with a similar average receptive field overlap and spike count.

2.4.6 Electrical Image

The electrical image is the average spatiotemporal spike waveform recorded across the electrode array during the spikes detected from a specific cell (Litke et al., 2004; Field et al., 2007). The electrical image of a given cell was computed from a 10.1 ms window starting 4.48 ms before the peak negative voltage sample for each spike and was averaged over all recorded spikes. The spatiotemporal electrical image was further collapsed across time by taking the minimal voltage deflection at each electrode location, yielding the spatial representation seen in Figure 2.5,A and D. For the analyses of the hot spots of correlated activity in the surrounding area of the soma of the cell, the electrical image was averaged from 2.1 to 0.39 ms before a spike. The analysis was robust over a wide range of time windows. The parameters were adjusted by hand to produce the strongest visually perceived contrast and to avoid any interference of the hot spot signals with those from central somatic spikes or overlapping dendrites. As the signals from the central somatic spikes were much stronger than those of the coupled cells in the hot spots, the time window was chosen with a sufficient distance to this peak. In addition, we chose a time window before the somatic spike, because the electrical activity spreading through the dendritic field overlapped in space and time with the hot spot activity, which hampered visualization of the hot spots in the two-dimensional image.

2.4.7 Electrical Image Model

For the electrical image model, we used the full electrical image from the neighboring RGCs as a template for their electrical signature. If the neighboring RGCs fired a spike within a narrow time frame before or after a spike of the center cell, their electrical image was temporally shifted appropriately and added to the model electrical image. The mean of the model electrical image from 2.1 to 0.39 ms before a spike reproduced the hot spots of activity surrounding the soma of the cell. Next, the bimodal cross-correlation function between each neighbor and the center cell was fitted by the sum of three Gaussians. The bimodal peaks originate from reciprocal electrical coupling via gap junctions, and they are superimposed on slower correlations elicited by shared network noise and correlations of the light stimulus. We randomly shifted the spikes that contribute to the peak in the cross-correlation function, which occurs at approximately -2 ms (see Figure 2.5H, inset) to remove correlated spikes that the neighbor cell fired before the center cell. In this partially decorrelated model, the amplitude of the hot spots was strongly reduced. This is consistent with the idea that the hot spots are mainly based on

precise, gap junction-driven correlated spikes, while the waveforms of less precisely correlated spikes average out.

2.4.8 Neurobiotin injections

We performed intracellular injections of the gap junction-permeable tracer neurobiotin (Vaney, 1991). Pieces of isolated, ventral retinas were mounted on black nitrocellulose filter mem branes with the ganglion cell layer up. For visualization of ganglion cell bodies, the tissue was incubated in acridine orange (0.0001% in Ames' medium; Sigma-Aldrich) for 1 min and then mounted in the bath chamber where the tissue was continuously superfused with Ames' solution. Putative sON α -ganglion cells were identified based on their large polygonal cell bodies in the ganglion cell layer under a 40 × waterimmersion objective (Zeiss). Intracellular injections were performed with sharp borosilicate glass electrodes (175–440M Ω). Electrodes were filled with a solution containing 10% neurobiotin (Vector Laboratories) dissolved in 0.1 M Tris buffer, pH 7.3, and 5mM Invitrogen Alexa Fluor 568 hydrazide (Thermo Fisher Scientific). Electrodes were backfilled with 0.2 M KCl. After the cell body was impaled and visualized by the Alexa Fluor dye fluorescence, neurobiotin was delivered by iontophoresis into the cell with a current of 0.6 nA for 10 min. After cell injections, the tissue was fixed for 20 min in 4% paraformaldehyde (PFA) in 0.01 M PBS, pH 7.4. Following cryoprotection with 30% sucrose in PBS, retinas were stored at -20° C until immunohistochemical labeling was performed.

2.4.9 Immunohistochemistry and light microscopy.

For immunohistochemistry, the tissue was fixed in 4%PFA in PBS for 20 min at RT. The tissue was cryoprotected overnight with 30% sucrose in PBS and stored at -20°C until use. Following dissection, retinal pieces were either used as whole mounts or sectioned vertically at 18-20 μ m using a cryostat (Leica).

Immunohistochemical labeling was performed by an indirect fluorescence method. Vertical sections were incubated overnight at RT with primary antibodies diluted in 5% normal donkey serum (NDS), 0.5% Triton X-100, and 0.02% sodium azide in PBS. Sections were incubated for 1 h with secondary donkey antibodies diluted in the same incubation solution.

Retinal whole mounts were incubated at RT for 2–3 d in the primary antibody solution containing 5% NDS, 1% Triton X-100 and 0.02% sodium azide dissolved in PBS. Primary antibodies used in this study were anti-RBPMS (rabbit, polyclonal, 1:500; catalog #1830-RBPMS, PhosphoSolutions), anti-Neurofilament H, nonphosphorylated (SMI-32, mouse, monoclonal, 1:1000; catalog #801701, BioLegend), anti-choline acetyltransferase (ChAT; goat, polyclonal, 1:200; catalog #AB144P, Merck). Secondary donkey antibodies (1:500, Invitrogen Alexa Fluor 488 and 568, Thermo Fisher Scientific; 1:250, Alexa Fluor 405, Abcam; 1:250, Cy5, Jackson ImmunoResearch; and 1:200, Invitrogen Alexa Fluor 568-conjugated streptavidin, Thermo Fisher Scientific) were incubated at RT for 4 h in the same incubation solution. The tissue was mounted on glass slides and cover slipped with

VECTASHIELD (Vector Laboratories). Spacers between glass slides and coverslips were used to avoid squeezing the tissue.

Image stacks were obtained with confocal laser-scanning microscopes (models TC SP8 and TCS SL, Leica). Overview scans were acquired with 10× or 20× air-objectives. High-resolution image stacks were acquired with 40× oil-immersion objectives (numerical aperture, ≥1.25) and z-axis increments of 0.25–0.5 µm. Image stacks of neurobiotin-injected cells were median filtered in Fiji (Schindelin et al., 2012) to reduce photomultiplier noise (Kerschensteiner et al., 2009). Maximum intensity x/y-or z-projections are shown in all figure panels of microscopic images and were performed in Fiji. The brightness and contrast of the final images were adjusted in Adobe Photoshop.

Cell bodies labeled with RBPMS or neurobiotin were manually outlined, and the corresponding areas were measured in Fiji to calculate the diameters. To analyze the location of tracer-coupled cells relative to the dendritic field of the injected cells, convex hulls were manually placed around the distal tips of individual dendrites in Fiji and the distances of the injected cell bodies to cell bodies of tracer-coupled cells relative to the hulls were measured.

2.4.10 Alignment and matching

After the MEA recordings were completed, images of the retina preparation on the multielectrode array were obtained with a Leica DM LFS epifluorescence microscope equipped with a $10\times$ air-objective and manually aligned in Adobe Photoshop. Subsequently, the tissue was carefully mounted on black nitrocellulose filter membrane with the ganglion cell layer up. Following fixation, cryoprotection, and immunostaining, images of the labeled retina were obtained with a Leica DM6 B epifluorescence microscope equipped with a motorized stage and a $20\times$ air-objective and automatically stitched together in the microscope software (LAS X, Leica). The outline of the tissue while mounted on the multielectrode array was aligned to the image of the successive immunostaining. sON α -RGCs were identified in microscopic image stacks of these retinal whole mounts based on soma size, SMI-32 staining intensity, and stratification levels of the dendrites relative to the ChAT bands. The cells were then marked with the cell counter tool in Fiji in the center of their cell bodies.

To identify the corresponding pairs between recording locations of the large sON RGCs and the marked soma locations, a greedy algorithm was implemented. The recording location was defined as the weighted average of the electrode locations with significant somatic signals. For all recording locations, the distance to the second nearest soma was divided by the distance to the nearest soma. The pair with the largest distance ratio was selected as a corresponding pair. Next, all ratios were updated and the procedure was repeated. To minimize artifacts caused by the border of the preparation and by missing, unidentified cells, potential pairs with distances between the recording and soma location larger than the average nearest neighbor distance were excluded. The robustness of the greedy procedure was tested by the alignment optimization of random permutations of the nonflipped mosaics.

Next, we tested whether the observed alignment of recording and soma locations could have occurred by chance. To calculate the chance expectation, the mosaic of soma locations was flipped and transformed through random rotations and translations. The soma locations were rotated from 0° to 360° in 10 steps and shifted in X and Y direction up to two times the average nearest neighbor distance with steps of $10~\mu m$. The mean distance between corresponding pairs in the observed alignment was smaller than in all random permutations of the flipped mosaic in two independent preparations (see Figure 2.3I, black arrowhead). Therefore, the permutation analysis indicated that the match was inconsistent with chance alignment.

Finally, after testing the match of the two mosaics, the alignment was optimized to account for possible small deviations due to tissue handling and fixation. The scaling, position, and angle were adjusted to minimize the mean distance between recording and soma locations. For the preparation seen in Figure 2.3H, the soma mosaic was scaled to 98%, shifted 1.5 electrode positions in X and 0.4 in Y direction, and was not rotated from the original alignment to reduce the mean distance to 30 μ m (Figure 2.3I, black arrow).

2.4.11 Statistical analyses.

Statistical analyses comprised nonparametric tests. A Wilcoxon rank sum test or a Wilcoxon signed-rank test for paired comparisons was used to test for statistical significance. To test the observed alignment of recording positions and soma locations (Figure 2.3I), a permutation analysis was performed as described above. Outliers were always included in the statistical analysis. Measurements are reported as the mean \pm SD. Shaded regions in figures represent the 95% confidence interval.

3 Asymmetric polyaxonal amacrine cell type delivers directional sensitive inhibition to retinal ganglion cells

Declaration	
I hereby confirm that Elaheh Lotfi contributed to the afor	rementioned study as stated below:
Article:	
Asymmetric polyaxonal amacrine cell type delivers direct ganglion cells	ctional sensitive inhibition to retinal
Elaheh Lotfi, Christian Puller, Christoph T. Block, and M	Martin Greschner
Department of Neuroscience and Research Center Neuro	sensory Science, Carl von Ossietzky
University, 26111 Oldenburg, Germany	
Authors contribution:	
M.G., E.L. designed experiments, C.P., C.B.T., M.G. perfor	med experiments, E.L. analyzed data,
E.L. prepared the figures, E.L. wrote the draft of the manuscri	pt.
	02.04.2014
Prof. Dr. Martin Greschner	Date

Supervisor

3.1 Introduction

The retina is composed of a complex neural network that processes visual information and transmits it to the brain through parallel pathways. A large amount of computation occurs in the inner plexiform layer (IPL), where the input from photoreceptors is modulated by various interneurons before being transmitted by retinal ganglion cells (RGCs) to the higher visual areas.

Among these interneurons, amacrine cells (ACs) are a diverse and intricate class of cells that play a crucial role in visual information processing and transmission in the IPL (Gollisch & Meister, 2010). More than 42 types of ACs have been identified so far (Euler et al., 2014), and they form inhibitory synapses with bipolar cells, RGCs, and other ACs, mediating various visual functions. However, the functional roles and organization of many AC populations remain unclear(Masland, 2012b; Cafaro et al., 2020). ACs can be divided into two major subgroups: small-field ACs, which mainly signal vertically in the IPL, and wide-field ACs, which spread their processes laterally in the IPL (Franke & Baden, 2017). Among wide-field ACs, there are spiking polyaxonal amacrine cells (PACs) that have long axons that can extend to several millimeters over the retina (Dacey, 1988; Vaney et al., 1988; Dacey, 1989; Mariani, 1990; Famiglietti, 1992; Freed et al., 1996; Taylor, 1996; Völgyi et al., 2001; Ölveczky et al., 2003; Wright & Vaney, 2004; Davenport et al., 2007). To enable signal transmission over long distances, they need to generate spikes. Therefore, it is possible to measure the spiking activity of these PACs with multi-electrode arrays. Studies have shown that different types of PACs contribute to the formation of the extra-classical receptive field of ON parasol cells (Greschner et al., 2016) or the size selectivity of the direction-selective RGC circuit (Hoggarth et al., 2015).

This chapter introduces a type of PAC in the guinea pig retina, termed ON asymmetric PAC, and explores its role in shaping the visual coding of medium sON RGC, a type of ON RGC. Large-scale, high-density, multi-electrode array recording, an electrical imaging approach that detects spiking PACs based on their action potential propagation patterns, is utilized to identify and characterize these cells (Litke et al., 2004; Petrusca et al., 2007; Greschner et al., 2014; Greschner et al., 2016). We show that PACs can be distinguished based on their electrical images, and a specific functional type of ON PAC correlates to the previously found medium sON RGCs. The spatial and temporal properties of the correlated activity of these two cell types are investigated. We show that the inhibitory signals of the population of ON asymmetric PACs are direction sensitive. Hence, they may alter the response of medium sON RGCs when exposed to a moving bar stimulus, potentially instilling direction-sensitivity in their response. Subsequently, a conceptual model is developed, illustrating the coherence between the direction-sensitive inhibition by ON asymmetric PACs and the direction-sensitivity observed in medium sON RGCs.

3.2 Results

3.2.1 Functional identification of an ON PAC cell type

The electrical images of cells recorded simultaneously with a large-scale multielectrode array were screened to identify and distinguish PACs from RGCs (Litke et al., 2004; Petrusca et al., 2007; Greschner et al., 2014; Greschner et al., 2016). The electrical image is the spike-triggered electrical activity of a cell across all electrodes, which reveals the spatial organization of the cell when a spike is generated on the soma and propagated through the axon. RGCs of all types showed high-amplitude biphasic somatic spikes surrounded by lower-amplitude opposite-sign dendritic spikes in the nearby electrodes and triphasic spikes traveling in the axons to the optic disk (Figure 3.1C). Conversely, the spatial organization of PACs is described by triphasic axonal spikes that propagate outward from the soma simultaneously in various directions (Figure 3.1A, B) (Petrusca et al., 2007). Further inspection of electrical images of all recorded PACs highlighted a group of ON PACs with a specific axonal pattern. These cells exhibited sparse axonal arbors extended asymmetrically around the soma (Figure 3.1A). Therefore, they are called ON asymmetric PACs in the rest of this study.

3.2.2 Functional organization and light response of ON asymmetric PACs and medium sON RGCs

As described in chapter 2, the medium sON retina ganglion cells were identified as a specific cell type that formed a regular mosaic with their receptive fields ($\emptyset = 313\pm35~\mu m$, n = 89) and exhibited a biphasic temporal filter (Figure 3.2A). Similarly, we investigated whether ON asymmetric PACs form a distinct functional cell type. These cells also displayed homogenous biphasic temporal filters with slight variation within the group (Figure 3.2B right). Moreover, these cells formed a mosaic with their receptive fields ($\emptyset = 266.29 \pm 29.61~\mu m$, n = 51), which is a classic indicator of cell type identity (Wässle et al., 1981). Gaps are typically observed in the mosaics of PACs, which can be attributed to incomplete recording of the population and limitations in spike sorting due to the low spike amplitudes of PACs. This situation was also noted in the mosaic of ON asymmetric PACs.

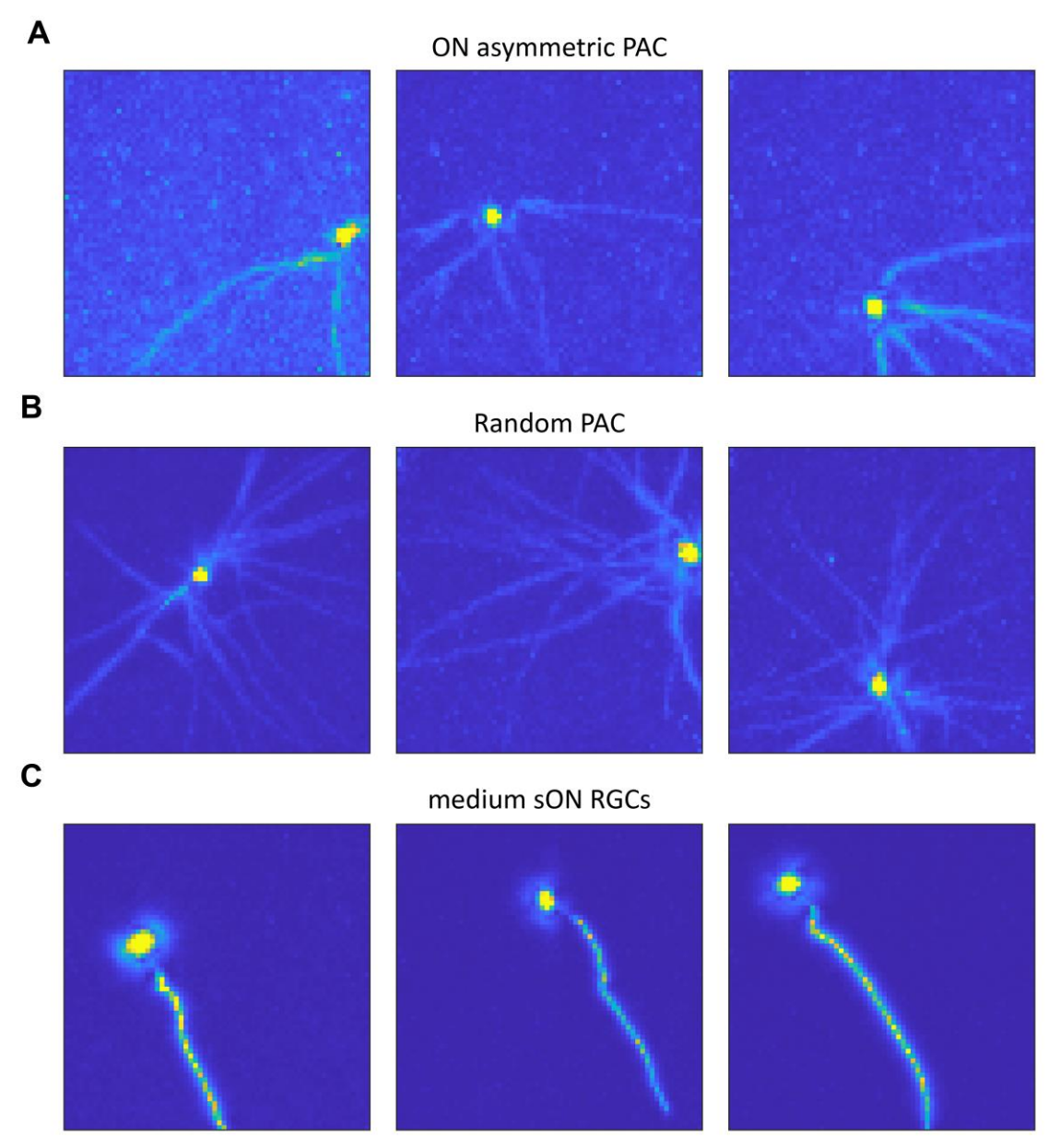


Figure 3.1: Electrical images of ON asymmetric PACs and medium sON RGCs. A, The minimum projection of the spike-triggered electrical activity of three ON asymmetric PACs from 4.48 ms before to 11.2 ms after the somatic spike. Warm colors indicate more negative voltage deflections. B, As in A from random PACs. C, As in A for medium sON RGCs. The multi-electrode array size is $2.6 \times 2.6 \text{ mm}^2$.

3.2.3 Physiological properties of ON asymmetric PACs

3.2.3.1 Axonal pattern

ON asymmetric PACs showed to have a distinct pattern of axonal arbors compared to the other recorded PACs (Figure 3.1A, B). To test whether this pattern is consistent across the population, we used the electrical image of the ON asymmetric PACs to trace their axonal arbors. The ON asymmetric PACs population exhibited an asymmetric spatial arrangement of axonal arbors, with no axon in the upper left of the somas and a high density of axons in the lower left of the somas (Figure 3.3 A, B). The tracing analysis was repeated for a randomly selected subset of the rest of the recorded PACs. Unlike

the previous observations, the axonal arbors of this subset displayed a uniformly distributed pattern of axons encircling the somas (Figure 3.3 C). Thus, the asymmetric spatial arrangement of axonal arbors of the ON asymmetric PACs could be considered as a characteristic feature of this cell type.

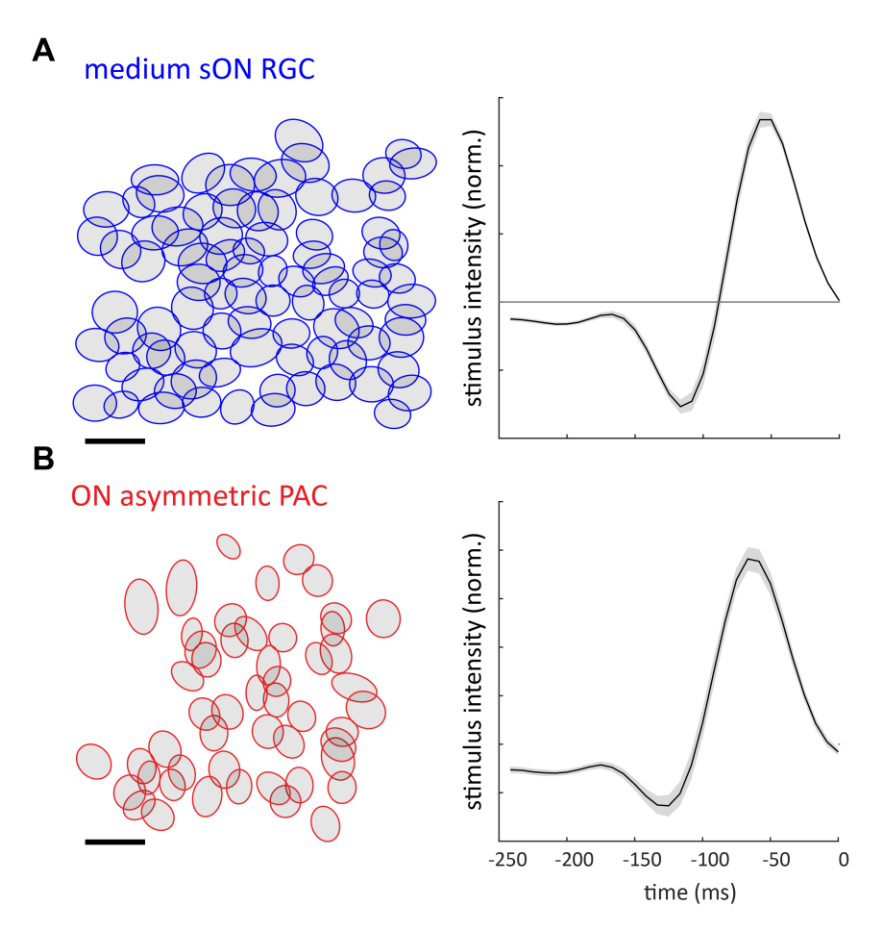


Figure 3.2: Receptive field mosaics of medium sON RGCs and ON asymmetric PACs.A, Receptive field outline of all recorded medium sON RGCs forms a complete mosaic. Receptive field outlines are drawn at the 1 SD contour of two-dimensional Gaussian fits. Right, mean spike-triggered average stimulus time course. Shaded region represents the 95% confidence interval. B, As in A for ON asymmetric PACs. Scale bars: for A, B, 500 μm.

3.2.3.2 Conduction velocity

The conduction velocity of ON asymmetric PACs was ~0.3 m/s and declined as a function of distance from the soma (Figure 3.4 A). The measured conduction velocity was similar to the reported value for the PACs in the macaque retina (Greschner et al., 2014; Greschner et al., 2016). ON asymmetric PACs exhibited a branched axonal structure, where the primary axonal arbors split into two or three branches as they extended from the soma (Figure 3.4 B). It was hypothesized that spike propagation in branched axons would be slower than in primary ones, as seen in some cases (Figure 3.4 A). Hence, a signed rank test was conducted to test this hypothesis. However, the test showed no significant difference in the spike conductance velocity of the primary and branched axonal arbors.

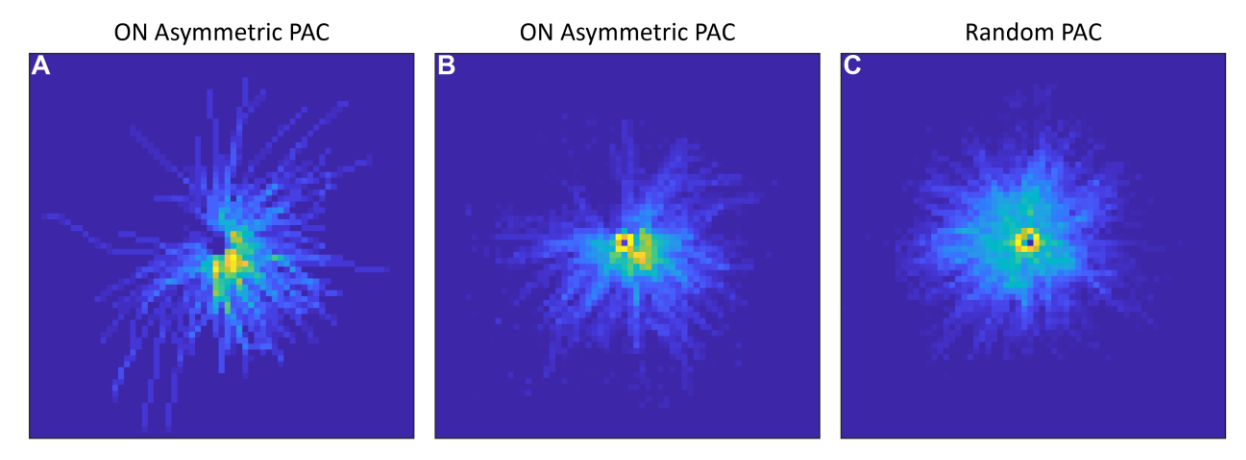


Figure 3.3: Electrical images of ON asymmetric PACs reveal asymmetry in their axonal arbor pattern. A, The average of the minimum projection of the spike-triggered electrical activity of ON asymmetric PACs while they are centered based on their soma location (n = 51). The axonal arbors are marked manually. Warm colors indicate higher axon density. B, As in A while the axonal arbors are marked automatically. C, As in B for a random subset of the rest of the recorded ON PACs (n = 38).

3.2.4 Correlated activity of ON asymmetric PACs and medium sON RGCs

The cross-correlation analysis of the spiking activity between ON asymmetric PACs and all recorded RGCs revealed that medium sON RGC was the only type that exhibited a prominent correlation with ON asymmetric PAC. ON asymmetric PACs and medium sON RGCs with overlapping receptive fields showed a strong positive correlation (Figure 3.5 A, B). This observation was expected because both cell types were ON cells with highly overlapped receptive fields, thus likely to receive shared inputs and show a positive correlation in their response. Additionally, the distinct bimodal peaks with an offset from zero in their cross-correlation function may indicate the presence of heterotypic electrical coupling via gap junctions within a pair, as evidenced by previous studies (Mastronarde, 1983c; Brivanlou et al., 1998; DeVries, 1999; Völgyi et al., 2013). Most of the medium sON RGCs in the close proximity of the axons of ON asymmetric PACs had a delayed trough in their cross-correlation function, while the ones farther away did not (Figure 3.5 A, C). The presence of a delayed negative correlation in the cross-correlation function of the pair, i.e., the reduction of medium sON's firing activity, provides implicit evidence to support the direct inhibitory effect of ON asymmetric PACs on medium sON RGCs. These observations are consistent with previous findings on the GABAergic inhibitory influence of ACs on RGCs (Masland, 2012b). Moreover, the inhibitory effect of ON asymmetric PACs on medium sON RGCs' firing activity resembled that of previously found PAC type on ON Parasol RGCs in the macaque retina (Greschner et al., 2016).

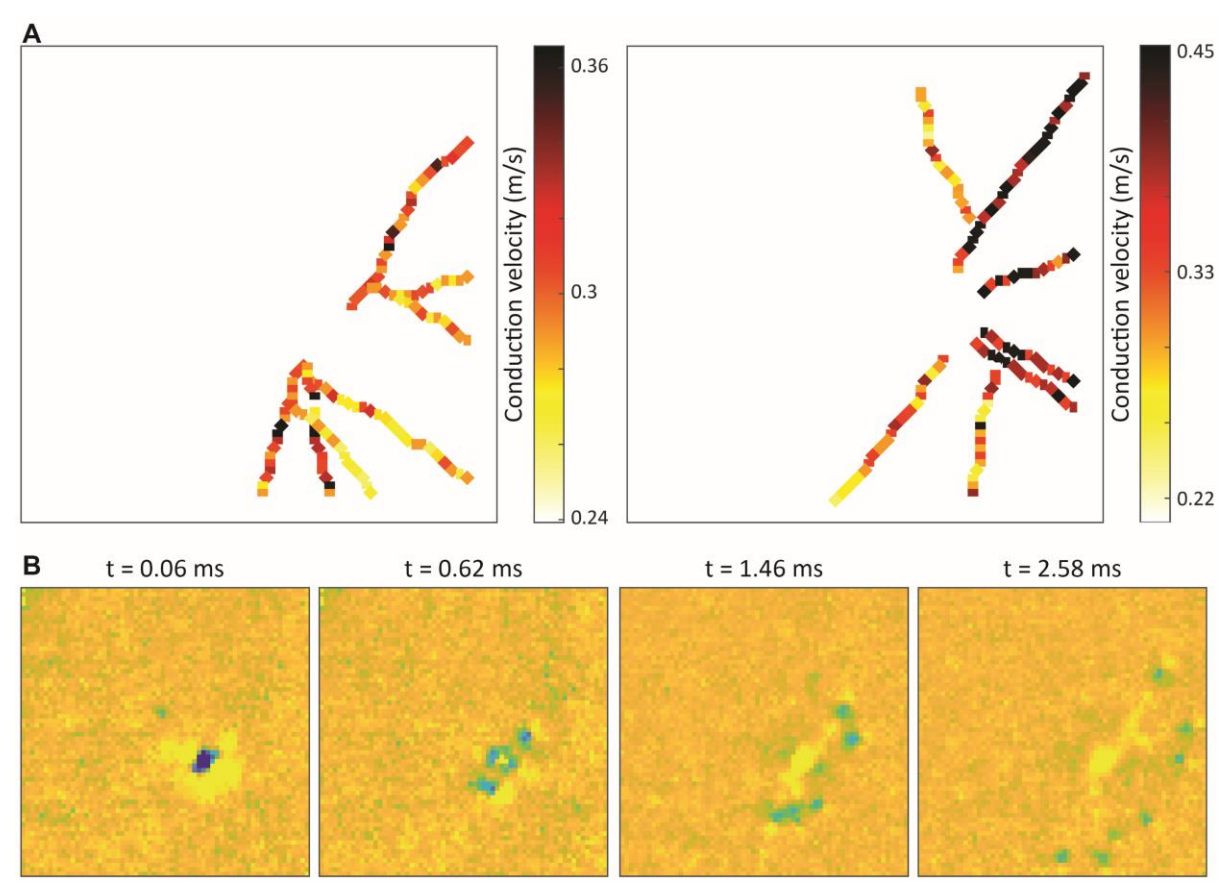


Figure 3.4: Conduction velocity of ON asymmetric PAC's axonal spikes. A, Spatial arrangement of conduction velocity, measured locally, is shown for two ON asymmetric PACs. Local conduction velocity was calculated over overlapping segments of 4 electrodes. **B**, The electrical image of the ON asymmetric PAC in A, left is shown from the initiation of the somatic spike until the signal propagates along the axons throughout the branched structure. Cool colors indicate more negative voltage deflections. The multi-electrode array size is 2.6 × 2.6 mm².

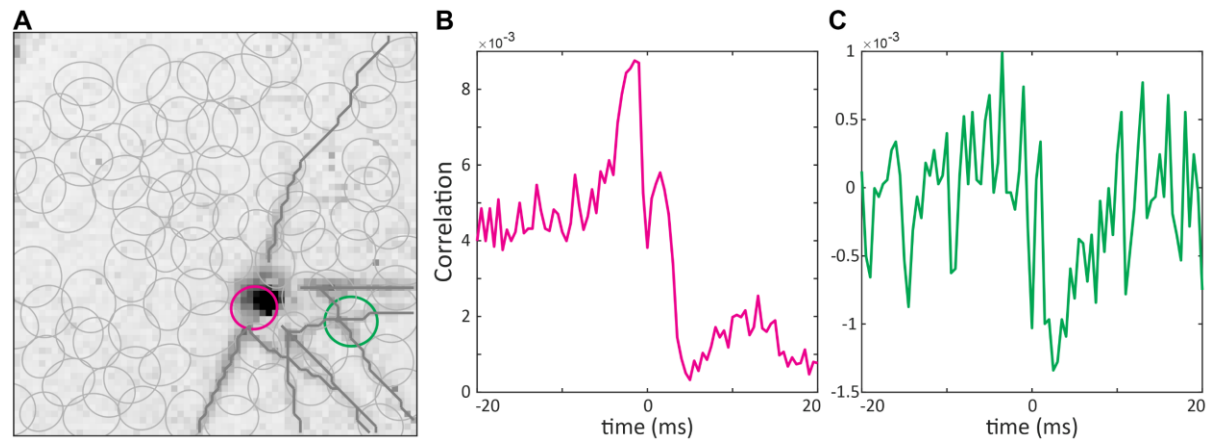


Figure 3.5: Correlated activity of ON asymmetric PACs and medium sON RGCs A, The minimum projection of the electrical image of an ON asymmetric PAC in grayscale, aligned with the medium sON RGCs' receptive field mosaic. Darker intensities indicate more negative voltage deflections. **B**, Cross-correlation function of the ON asymmetric PAC of A and the medium sON RGC marked with magenta in A. C, As in B for the medium sON RGC marked with Green. bin size 0.5 ms. The multi-electrode array size is $2.6 \times 2.6 \text{ mm}^2$.

3.2.4.1 Inhibitory effect of ON asymmetric PACs on medium sON RGCs

Conduction velocity of ON asymmetric PACs decreases with increasing distance from the soma (Greschner et al., 2014; Greschner et al., 2016). Therefore, it is reasonable to assume that the inhibitory effect of ON asymmetric PACs on medium sON RGCs varies with the relative location of their somas. Cross-correlation functions of the spiking activity of an ON asymmetric PAC and some medium sON RGCs in close proximity to the axons of the PAC showed that inhibition occurred at different times depending on the distance of the medium sON RGCs from the PAC's receptive field (Figure 3.6 A, B). The inhibition time was delayed by approximately 5 ms, which increased as the medium sON RGCs were located at the distant locations of the ON asymmetric PAC axons.

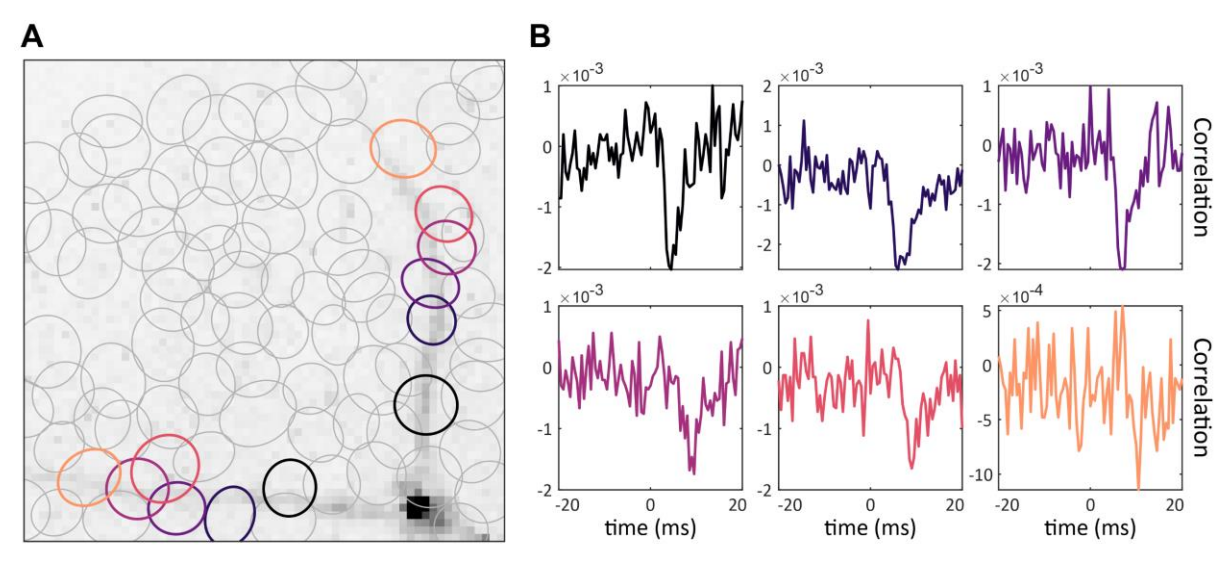


Figure 3.6: Delay in the negative correlation of ON asymmetric PACs and medium sON RGCs is consistent with conduction velocity. A, The minimum projection of the electrical image of an ON asymmetric PAC in grayscale, aligned with the medium sON RGCs' receptive field mosaic. Darker intensities indicate more negative voltage deflections. The receptive field of the medium sON cells that are in close proximity to the PAC's axons are color-coded. **B**, The cross-correlation function between the ON asymmetric PAC and color-coded medium sON RGCs located on the vertical axon of the ON asymmetric PAC of A. bin size 0.5 ms. The multi-electrode array size is $2.6 \times 2.6 \text{ mm}^2$.

To assess the inhibitory impact of ON asymmetric PACs on the population of medium sON RGCs, an inhibition index was defined using the cross-correlation of the spiking activity of each ON asymmetric PAC and all medium sON RGCs. The cross-correlation bin width was set to 6 ms, which was similar to the average duration of the troughs observed in the finely binned cross-correlations (Figure 3.6 B). Prior to cross-correlation calculation, the spike train of medium sON RGCs was shifted according to the conduction time along the ON asymmetric PACs' axons. These adjustments allowed the use of the correlation value at a single bin for all pairs as an inhibition index. The medium sON RGCs that were in close proximity to the receptive field of ON asymmetric PACs were excluded from this analysis, as the stimulus-driven correlation (signal correlation) could interfere with the accurate measurement of the inhibition index.

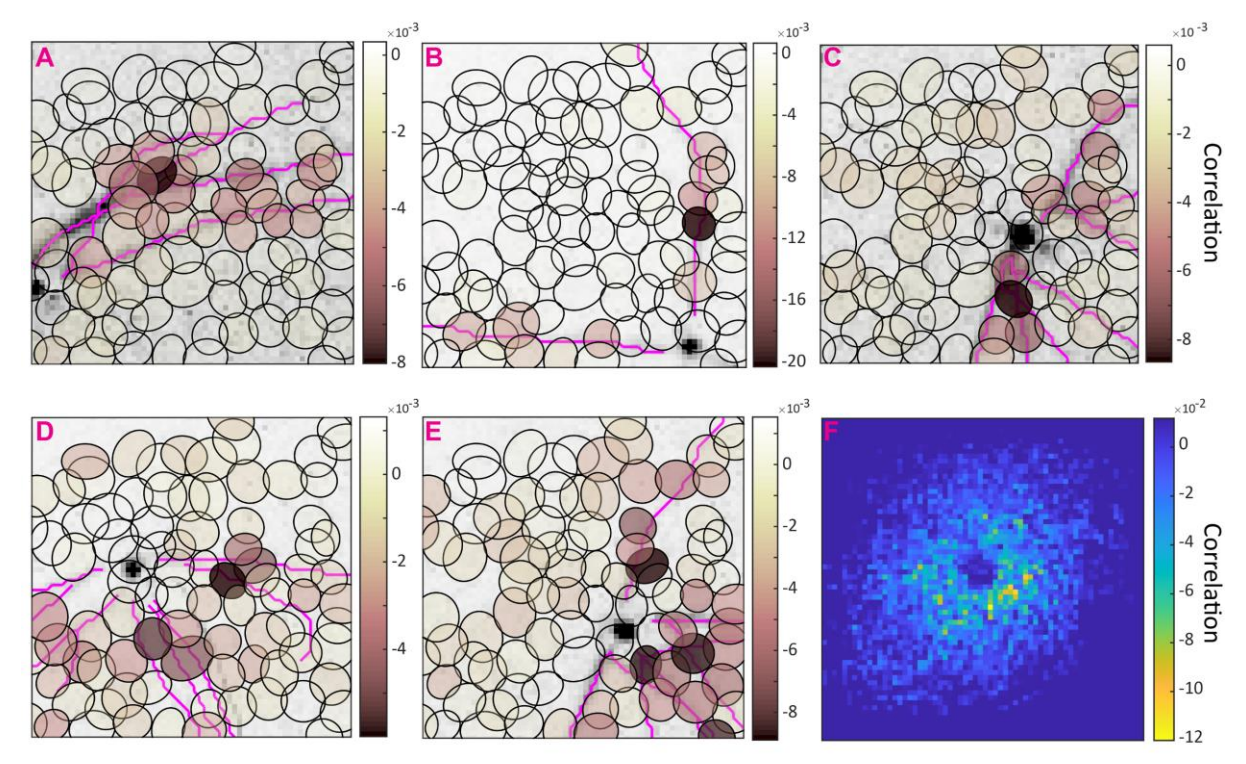


Figure 3.7: Stimulus-driven activity of medium sON RGCs in close proximity to ON asymmetric PAC's axons is inhibited. A-E, The minimum projection of the electrical image of an ON asymmetric PAC is shown in grayscale, aligned with the receptive field mosaic of simultaneously recorded medium sON RGCs. The PAC's axons are marked with magenta for better visibility. Colormap for medium sON RGCs indicates the amplitude of the trough in the cross-correlation function of stimulus-driven activity between the ON asymmetric PAC and medium sON RGCs. Correlations were measured in a 6-ms time interval, shifted according to the conduction time along the ON asymmetric PAC axon. The electrical image is shown for 4.48 ms before to 11.2 ms after the somatic spike. Darker intensities in the electrical image indicate more negative voltage deflections. **F**, Overall inhibition of ON asymmetric PAC population on medium sON RGCs. For each ON asymmetric PAC, the inhibitory effect on the medium sON mosaic was measured as in A-E. Obtained inhibition indices were assigned to the most significant electrodes of their corresponding medium sON cell, resulting in an EI-based spatial inhibition histogram for each ON asymmetric PAC. The average over all the EI-based spatial inhibition histograms centered by the location of the most significant electrodes of their respective ON asymmetric PACs provides an inhibition map that delivers the strength of inhibition of ON asymmetric PACs on medium sON RGCs based on their relative location. The multi-electrode array size is $2.6 \times 2.6 \text{ mm}^2$.

The spatial interaction of several ON asymmetric PACs and the medium sON RGCs population is displayed in Figure 3.7A-E. Most of the medium sON RGCs that were in close proximity to ON asymmetric PAC axons were inhibited by the ON asymmetric PAC. However, those medium sON RGCs that were far from the ON asymmetric PAC axons were unaffected. To further investigate this spatial pattern, we categorized the medium sON RGCs into three groups. This classification was based on the proximity of their receptive fields to the receptive field or axons of the ON asymmetric PACs. The cross-correlation of the spiking activity of each ON asymmetric PAC and three groups of medium sON RGCs was calculated (Figure 3.8). The first group comprised medium sON RGCs that were in close proximity to the ON asymmetric PAC's receptive field but did not overlap with it. A trough with a width of about 6 ms was present in the cross-correlation function of this group and the ON asymmetric PAC (Figure 3.8 A). This trough was superimposed on a slower correlation elicited by shared network noise and correlations of the light stimulus during recordings (Trong & Rieke, 2008; Ala-Laurila et al.,

2011; Greschner et al., 2011). Second group of medium sON RGCs were those with receptive fields in close proximity to ON asymmetric PAC's axons but far away from its receptive field. The third group was located far away from the ON asymmetric PAC's axons and receptive field. The inhibitory effect of ON asymmetric PAC on the second group was clearly exhibited in the cross-correlation function (Figure 3.8 B). However, the slow correlation noted in Figure 3.8A was not present here. This absence was due to the fact that the receptive fields of the second group did not overlap with that of the ON asymmetric PAC, in contrast to the first group. Consequently, they did not share the same presynaptic noise and signal to form a slow, positive correlation. Finally, as expected, the third group of medium sON RGCs did not show any correlated activity with ON asymmetric PAC, consistent with previous reports (Figure 3.8 C) (Greschner et al., 2016).

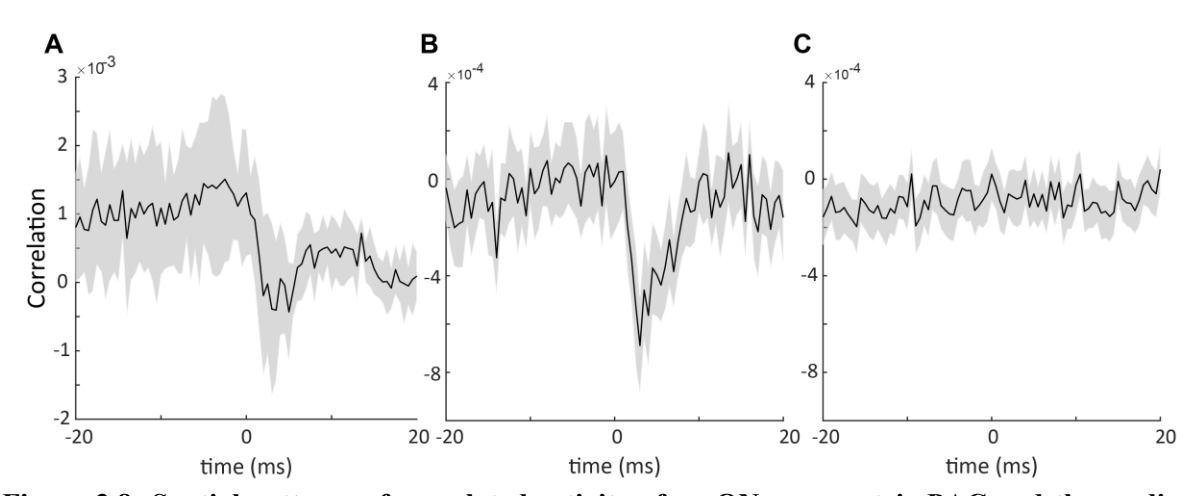


Figure 3.8: Spatial patterns of correlated activity of an ON asymmetric PAC and the medium sON RGCs population. Medium sON RGCs were separated into three groups based on the location of their receptive fields relative to the receptive field and axons of the ON asymmetric PAC. A, Average cross-correlation function between the ON asymmetric PAC of Figure 3.7E and medium sON RGCs in close proximity to the PAC's receptive field (n = 7). B, As in A for medium sON RGCs in close proximity to the PAC's axons and far from its receptive field (n = 22). C, As in A for medium sON RGCs far from the PAC's axons and receptive field (n = 51). Bin size 0.5 ms. Binned spike trains were shifted according to the conduction time along the PAC's axons. The gray shaded region represents the 95% confidence interval.

To evaluate the overall inhibitory impact of ON asymmetric PACs population on medium sON RGCs, the collective inhibition histogram was calculated. The EI-based spatial inhibition histogram of each ON asymmetric PAC was used to obtain the collective inhibition histogram (Figure 3.7 F). The soma of each ON asymmetric PAC was aligned to the center of the 2D histogram, and the medium sON RGC mosaic was adjusted accordingly. Considering that the medium sON RGCs that were in close proximity to the receptive field of ON asymmetric PACs were excluded from the inhibition index calculation due to the impact of positive signal and noise correlation, the collective inhibition histogram did not have any information about the interactions of the two cell types within that distance limit. Therefore, the center of the collective inhibition histogram exhibited a circular region with non defined value. Expectedly, the medium sON RGCs in the lower-right of the ON asymmetric PACs' soma were

most strongly suppressed, while those in the upper-left part were least suppressed. This was consistent with Figure 3.3 A, where the ON asymmetric PACs' axons had the highest density in the lower-right part of their soma and almost no axon in the upper-left part. Thus, the asymmetric axonal pattern of ON asymmetric PACs was the basis for the specific inhibition pattern of the medium sON RGCs' population.

3.2.5 The light response of medium sON RGCs to moving bar stimulus

The guinea pig retina was stimulated with bars of light moving in 8 directions. Although the medium sON RGCs did not respond to the moving bar stimulus in the same way as the classic directionselective ganglion cells, they showed some degree of direction-sensitivity. Figure 3.9 illustrates the response of three medium sON RGCs to the bright and dark moving bar stimuli where the bright stimulus was a gray bar moving on a black background and the dark stimulus was a black bar moving on a white background. Medium sON RGCs exhibited sustained strong firing activity when the leading edge of the bright bar reached their receptive field. When the trailing edge of the light bar left the receptive field, there was a period of silence followed by background activity. However, the background activity of medium sON RGCs was suppressed in a specific direction. In this context, directionsensitivity refers to the suppression of the background activity in a specific direction. This is distinct from direction-selectivity, where ganglion cells fire strongly to motion in their preferred direction and show no activity to motion in the opposite, null, direction. The polar plot, measured in time intervals during the background activity, showed a clear direction-sensitivity in medium sON RGCs' response to moving bar stimulus (Figure 3.9 B). The same pattern of direction-sensitivity was observed during the presentation of the dark moving bar (Figure 3.9 C, D). To verify if direction-sensitivity is prevalent among medium sON RGCs, we examined their response to moving bar stimulus in multiple datasets. Most of the medium sON RGC populations displayed a strong direction-sensitivity, while a few showed a weak effect. Therefore, tt can be inferred that direction-sensitivity is a characteristic of the medium sON RGC population and may serve as a criterion for classifying this cell type.

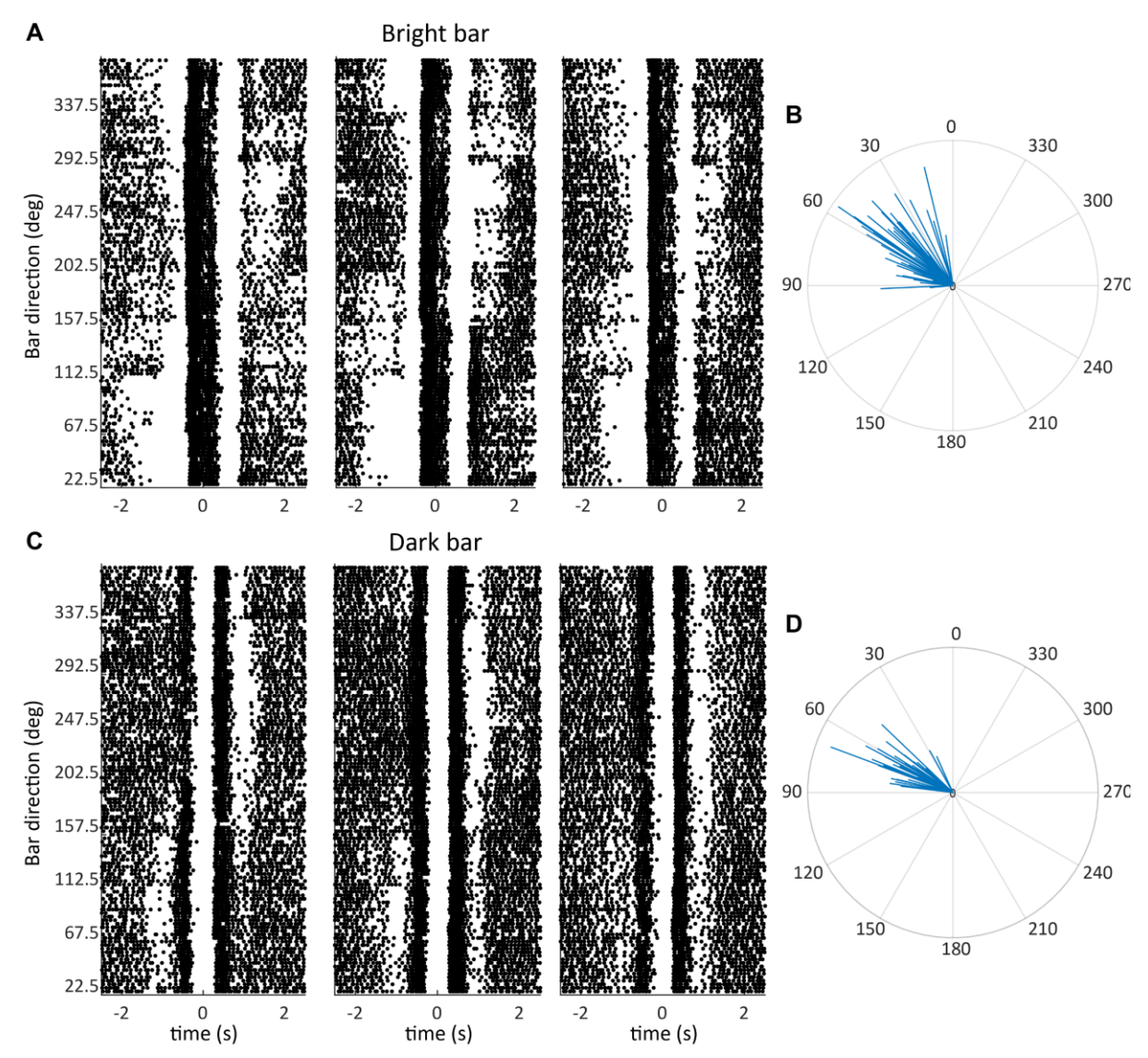


Figure 3.9: Medium sON RGCs response to moving bar stimulus reveals their direction-sensitivity. A, Raster plot of spike responses from three medium sON RGCs in response to a light bar moving in eight different directions. Each row represents a single stimulus trial, with the 15 repetitions of the moving bar's direction displayed as a vertical stack. The time of the spikes in the raster plot for each direction is aligned relative to the time that the middle of the bar reaches the center of the cell's receptive field. **B**, The preferred directions of medium sON RGCs calculated in two specific time intervals from -1.64 s to -0.85 s and from 0.63 s to 1.4 s. Vector sum in blue is flipped for the former time interval (n = 23). **C**, **D** As in A and B, but for the response of the same three medium sON cells to a dark moving bar (n = 20).

3.2.6 ON asymmetric PACs contribute to the direction-sensitivity of medium sON RGCs

ON asymmetric PACs suppressed the light response of medium sON RGCs in close proximity to their axonal arbors (Figure 3.7). Hence, we hypothesized that the direction-sensitivity of medium sON RGCs might be mediated by inhibitory synapses from ON asymmetric PACs. To investigate this hypothesis, we used the cross-correlation function of the spiking activity of each medium sON RGC and all the ON asymmetric PACs to identify the PACs that inhibited the RGC. Figure 3.10A illustrates a medium sON RGC (in black) and the ON asymmetric PACs (in colors) that inhibited it. ON asymmetric PACs fired transiently when the leading edge of the bright bar reached their receptive field.

The timing of ON asymmetric PACs' activation in response to the moving bar, their pattern of firing activity, and the strength of the inhibitory signals they imposed on medium sON RGCs—based on the relative locations of the axonal arbors of ON asymmetric PACs and the receptive field of medium sON RGCs—indicated that ON asymmetric PACs produced a directional sensitive inhibitory signal. The timing of the directional sensitive inhibitory signal from the ON asymmetric PACs was observed to align with the direction-sensitive response of the medium sON RGCs. ON asymmetric PACs exhibited strong inhibition in the time intervals that the medium sON RGC showed no activity in response to the moving bar (Figure 3.10B). Given that the medium sON RGCs that exhibited a negative correlation with the ON asymmetric PACs were in close proximity to the axons of these PACs, we inferred that the negative correlation was indicative of direct inhibition. This close proximity led us to deduce that no other cell types were involved, thereby suggesting that the ON asymmetric PACs contribute to the direction sensitivity of the medium sON RGCs. Since the recorded mosaic of ON asymmetric PACs was incomplete to inspect the impact of the full mosaic on direction-sensitivity of medium sON RGCs, a conceptual model of ON asymmetric PAC population was developed. In this model, we used measured values from recordings without adjusting any parameters to assess the observed phenomenon. To develop the parameter-free model, we created synthetic mosaics of ON asymmetric PACs and determined the inhibition index for the PAC and RGC pair from the inhibition map shown in Figure 3.7F. The average effect of the synthetic mosaics of ON asymmetric PACs on the direction-sensitivity of medium sON RGCs was similar to that observed in the recorded mosaic (Figure 3.10C). Therefore, both the model and the empirical data indicate that ON asymmetric PACs, which exert inhibitory signals on medium sON RGCs, contribute to the direction-sensitivity of this type of RGC.

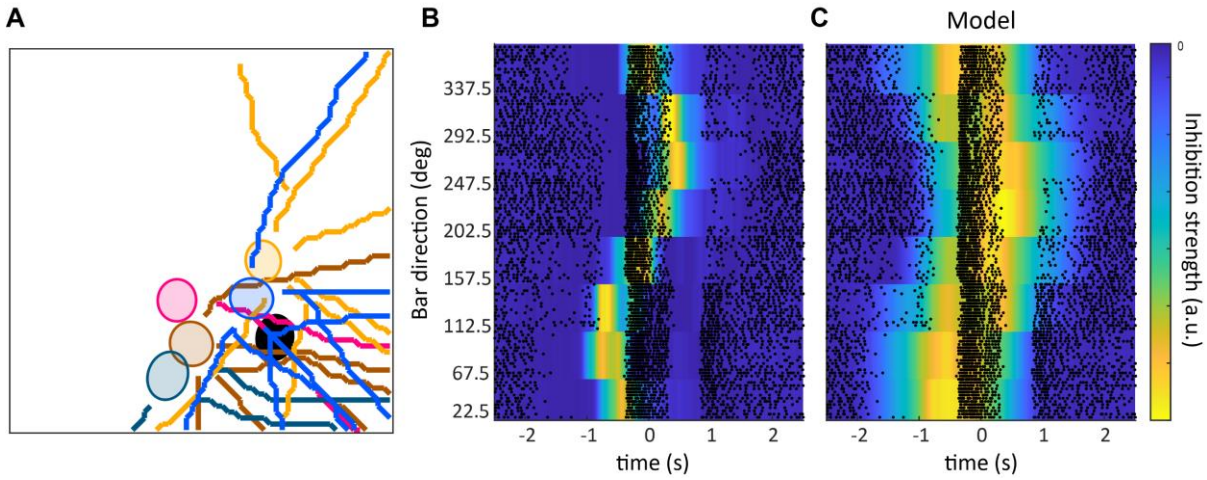


Figure 3.10: Direction-sensitive inhibition of medium sON RGCs through ON asymmetric PACs. A, spatial arrangement of a medium sON cell (black) and the ON asymmetric ACs (colored) that have an inhibitory effect on its response. Axons of each ON asymmetric PAC are marked with a color similar to that of its receptive field. **B**, Raster plot of spike responses from the medium sON cell of A in response to light bar moving in eight different directions, aligned with the inhibitory signal from five ON asymmetric PACs of A. The timing and strength of inhibition is in line with the pattern of inhibition observed in the raster plot. **C**, As in B, but the inhibitory signals were obtained from an average response of modeled populations of ON asymmetric PACs to light moving bar stimulus.

3.3 Discussion

This study investigated the role of ON asymmetric PACs in the direction-sensitivity of medium sON RGCs in the guinea pig retina. Utilizing electrical images from large-scale multi-electrode array recordings, we were able to differentiate PACs from RGCs based on their unique axonal patterns. Our findings reveal that ON asymmetric PACs are a distinct functional cell type characterized by sparse and asymmetric axonal arbors, specialized light response properties, and regular mosaic formation. Additionally, we observed that ON asymmetric PACs display strong positive correlated activity with medium sON RGCs that share a receptive field, as well as a negative correlation with medium sON RGCs located in close proximity to their axons. Finally, our results indicate that the directional sensitive inhibitory signal from ON asymmetric PACs contributes to the direction-sensitive response of medium sON RGCs.

3.3.1 Modulatory effect of ON asymmetric PACs: positive and negative correlation

A time lag was noted in the negatively correlated activity between the ON asymmetric PACs and medium sON RGCs. Additionally, the medium sON RGCs located in close proximity to the distal parts of the PACs' axons showed a greater delay and weaker negative correlation than those in close proximity to the initial segments of the axons. These findings align with previous research on PAC types in the primate retina (Greschner et al., 2014; Greschner et al., 2016). PACs possess thinner axons than ganglion cells, leading to a smaller signal that tends to diminish slightly as it travels along the axon, and their conduction velocity decreases as well. Thus, the observed variations in the strength and timing of the negative correlation among different medium sON RGCs along the axons can be attributed to the differences in conduction velocity and signal strength in the PACs' axons.

Medium sON RGCs and ON asymmetric PACs that had receptive field overlap exhibited a strong positive asymmetric correlation. Since both cell types are ON cells, it is possible for them to receive shared noise, mainly originating from cones, and shared signals from spatially correlated stimulus, forming a positively correlated activity (Trong & Rieke, 2008; Ala-Laurila et al., 2011; Greschner et al., 2011). The asymmetry in the correlated activity could arise from their different presynaptic circuitries and their intrinsic properties. Additionally, the observation of sharp peaks at approximately ±2 ms offset from zero could indicate heterotypic electrical coupling between the medium sON RGCs and the ON asymmetric PACs with overlapping receptive fields, which is a common case for PACs to form heterotypic electrical coupling with RGCs (Völgyi et al., 2001; Ackert et al., 2006; Greschner et al., 2016; Roy et al., 2017). However, to confirm the existence of heterotypic electrical coupling between the medium sON RGCs and ON asymmetric PACs, further investigations, such as the use of tracer injections, are needed.

3.3.2 Direction sensitivity of medium sON RGCs by ON asymmetric PACs

Direction-selective RGCs respond strongly to the motion along their preferred direction and exhibit no activity in the opposite, null, direction. Previous studies have identified two functional types of ON and ON-OFF direction-selective RGCs in mammals. The ON and ON-OFF direction-selective RGCs have three and four subtypes respectively, which are tuned to cardinal directions (Barlow & Hill, 1963; Barlow et al., 1964; Barlow & Levick, 1965). However, direction selectivity is not a unique feature of this classic direction-selective RGCs and it has been observed in other RGC types such as J-RGCs, F mini-On and F mini-OFF in mouse retina. These RGC types have different circuitries for direction selectivity that do not involve starburst amacrine cells (Kim et al., 2008; Joesch & Meister, 2016; Nath & Schwartz, 2017; Wei, 2018). Similarly, medium sON RGCs in guinea pig retina showed robust direction sensitivity that can be used as a feature for the classification of this cell type. A conceptual model was used to illustrate the contribution of direction-sensitive inhibitory signals from the ON asymmetric PAC population in mediating the direction sensitivity of medium sON RGCs. The preferred direction of medium sON RGCs was toward the ventral direction across multiple preparations, which aligns with the overall direction of ON asymmetric ACs' axons. This suggests that the asymmetry of the axonal pattern of the ON asymmetric PACs may play a role in determining the preferred direction of the medium sON RGCs. Indeed, asymmetric morphology has been reported to be a mechanism for direction selectivity in other cell types, such as J-RGCs and classic direction-selective RGCs (Bloomfield, 1994; Murphy-Baum & Taylor, 2015; Nath & Schwartz, 2017; Wei, 2018).

3.3.3 ON asymmetric PACs: sparse and asymmetric axonal arbors

This study introduces a polyaxonal amacrine cell with sparse asymmetric radiating axonal processes that span more than 1 mm over the retina surface. Among the more than 42 amacrine cell types that have been identified, a subset of which are PACs (Badea & Nathans, 2004; Lin & Masland, 2006), most of them have dense symmetric axonal processes. But there are also examples of PACs with sparse axonal arbors such as W4A-1 in mouse retina that has its soma located in the GCL and its sparse axonal arbors ramify in the S4/S5 sublamina of IPL, where the sustained ON RGCs also stratify their dendrites (Badea & Nathans, 2004; Wässle, 2004; Lin & Masland, 2006; Jia et al., 2020). However, the anatomical identification of the ON asymmetric PAC is beyond the scope of this study, as different techniques such as immunohistochemistry and neurobiotin injection are required to determine the chemical phenotype and measure the size, shape, and stratification depth of this recorded PAC and compare it with known types of PACs.

3.3.4 Prospects for future studies

In conclusion, this study revealed how ON asymmetric PACs influence the direction-sensitivity of medium sON RGCs in the guinea pig retina. However, some limitations need to be addressed in future studies. First, in this study, a conceptual model was used to suggest that ON asymmetric PACs contribute to direction-sensitivity of medium sON RGCs. However, direct experimental evidence and a circuitry for direction-sensitivity of medium sON RGCs should be provided to verify the role of ON asymmetric PACs in mediating direction-sensitivity of medium sON RGCs. This could involve using pharmacological methods. Second, our preliminary studies, which included recordings from various retinal regions such as the peripheral ventral area and the area near the central retina, revealed that medium sON RGCs exhibit direction-sensitive responses. To comprehend the functional significance of this direction sensitivity, it is crucial to investigate the topographic variations in direction sensitivity within this cell type. Finally, the ON asymmetric PACs recorded by large-scale multi-electrode array should be characterized by their chemical identity and their detailed morphology to compare and confirm their distinctiveness with the known types of PACs. This could be achieved by using methods such as immunohistochemistry and neurobiotin injection.

3.4 Materials and Methods

3.4.1 Animals and tissue preparation

All experiments were performed in accordance with the institutional guidelines for animal welfare and the laws on animal experimentation issued by the European Union and the German government. The preparation was performed as described in section 2.4.1.

3.4.2 Multi-electrode array recordings

Recording of RGCs activity under two stimulus presentations was performed as described in section 2.4.2.

3.4.3 Light stimulation

A random noise stimulus with a natural spatiotemporal frequency falloff was used to characterize the response properties of recorded cells. The stimulus was presented on a CRT monitor at a refresh rate of 120 Hz and a stimulus pixel width of 49 μ m on the retina at photopic light levels at a mean intensity of 2.9 mW/m². Only the green and blue monitor guns were used.

Another stimulus used in this study was a light bar of $620 \, \mu m$ width that moved in 8 directions with an interval of 22.5° at a speed of $985 \, \mu m/s$. The contrast of the moving bar was varied by changing the background and the bar color. The bar was either gray on a black background (bright bar) or black

on a white background (dark bar). Moving bars of different contrasts were presented in separate sessions and for 10 minutes. In a pseudo-random fashion, the bar moved along each direction across the retina for 15 times with a presentation time of 5 seconds.

3.4.4 Receptive field and classification analysis

RGCs were functionally classified into types as described in section 2.4.4. The PACs were distinguished by screening the electrical images as they exhibit very different axonal pattern from RGCs, having multiple axons radiating from the soma outward. The ON asymmetric PACs were characterized from the rest of PACs based on their distinct sparse and asymmetric axonal processes.

3.4.5 Correlated activity measurement

The Cross-correlation functions were calculated by binning the spikes into 0.5 ms time bins and computing the correlation coefficient between the spike count vectors as a function of temporal offset. Binned spike trains were shifted according to the conduction time along the PAC's axon. Medium sON RGCs were separated into three groups based on their receptive field location relative to the receptive field and axons of the ON asymmetric PAC. The groups were: (1) medium sON cells whose receptive field was in close proximity to the receptive field of the ON asymmetric PAC but did not overlap with it (Figure 3.8A); (2) medium sON cells whose receptive field was located less than one standard deviation away from the ON asymmetric AC axons and far from its receptive field (Figure 3.8B); and (3) medium sON cells whose receptive field was located more than two standard deviations away from the ON asymmetric PAC axons and far from its receptive field (Figure 3.8 C).

The inhibition index for each pair of ON asymmetric PAC and medium sON RGC was quantified by calculating the cross-correlation function of their shifted spiking activity with coarse binning (6 ms). The bin size was chosen based on the average width of the inhibitory trough in the finely calculated cross-correlation functions. The spike times were shifted as described earlier, so that the maximum effect (inhibition or excitation) of the PAC on the medium sON RGC activity would occur in a fixed bin, regardless of their spatial relationship. The correlation coefficient value of this bin was used as the inhibition index. To better visualize the inhibitory impact of PACs on the medium sON RGC population, the medium sON RGCs that exhibited strong positive correlation (Figure 3.5 B) or had their suppression by the PAC masked by the positive noise and signal correlation (Figure 3.8A) were excluded and their inhibition index was set to not defined value. The EI-based spatial inhibition histogram of the reference cell was computed using the inhibition indices of each ON asymmetric PAC and medium sON RGCs population. For each medium sON RGC, electrode locations with significant somatic signals were defined as significant electrodes. Inhibition indices were assigned to corresponding significant electrodes, generating a 2D inhibition histogram for each ON asymmetric PAC. These histograms were centered based on the location of their reference cell's significant electrode and then averaged to produce the collective inhibition histogram of ON asymmetric PACs.

3.4.6 Measurement of conduction velocity of PAC

The electrodes along which the axons were positioned were identified manually using the electrical image of the PAC. The occurrence time of the spike was obtained for each electrode on the axon. For each electrode, the conduction velocity along the axon was calculated as an average velocity across a set of four electrodes. This was achieved by using the time interval between the spike's occurrence on the reference electrode and the third subsequent electrode as the time delay. The distance was determined by the displacement of the signal between the reference electrode and the third one following it. The velocity was then measured as the ratio of this distance to the time interval.

3.4.7 Polar and raster plots

The firing activity of medium sON RGCs during moving bar presentation is illustrated with a raster plot. Dots in vertical lines represent the action potentials elicited during the 5-second stimulations. To evaluate the cell's response to different bar directions regardless of its location in the mosaic, the reference time 0 was set as the time when the center of the bar reached the receptive field centroid and the raster plot was calculated accordingly. The receptive field was considered as an ellipse with known parameters and the moving bar's initial location, width, velocity and direction were used to calculate the reference time. The preferred direction of the cell (θ_{pref}) was determined by defining the response to each stimulus direction as a vector $V_{\theta} = R_{\theta}e^{i\theta}$; R_{θ} is the average spike count of each direction normalized by the total number of spikes evoked during stimulation with all directions. The summation of vectors over all directions results in a vector sum where its norm and angle describe the tuning strength and preferred direction of the cell.

3.4.8 Model

A simple model based on the interactions of medium sON RGCs and ON asymmetric PACs was developed to explain the direction-sensitivity of medium sON RGCs in response to a moving bar stimulus. The response of ON asymmetric PACs to moving bar stimulus and the amplitude of negative correlations between the ON asymmetric PACs and the desired medium sON RGC were used to calculate the overall inhibitory signal. Due to spike sorting limitations, only a few ON asymmetric PACs had their moving bar response available. Therefore, a Poisson spike train similar to that of existing ON asymmetric PACs was generated for each ON asymmetric PAC. The reference time 0 was set as the time when the middle of the bar reached the center of the desired medium sON receptive field. Then the timing of the response to the moving bar stimulus for each recorded ON asymmetric PAC that inhibits the medium sON cell was determined according to the relative location of the pair and the moving bar velocity. The signal propagation time was negligible compared to the moving bar travel time; therefore, it was not considered in the model. A weighted average of the response of all inhibitory ON asymmetric PACs in response to the moving bar for eight different directions, using the amplitude

of negative correlations between each pair as a strength of inhibition, provided the inhibitory signal of the ON asymmetric PAC mosaic to the desired medium sON cell. To observe the effect of the complete mosaic of ON asymmetric PACs on the direction-sensitivity of medium sON cells, a synthetic mosaic of that was generated based on spatial properties of the receptive field of recorded ON asymmetric PACs. The same procedure was conducted to obtain the overall inhibitory signal from the synthetic ON asymmetric PAC mosaic. The inhibition map introduced in Figure 3.7F was used to determine the weight of inhibition for each pair of ON asymmetric PAC and the desired medium sON cell. Several synthetic mosaics were generated and the average inhibitory effect of them on the desired medium sON RGC is displayed in Figure 3.10C.

4 Multineuronal firing patterns in retinal ganglion cells of guinea pig

Declaration		
I hereby confirm that Elaheh Lotfi contributed to the aforen	nentioned study as stated below:	
Article:		
Multineuronal firing patterns in retinal ganglion cells of gui	nea pig	
Elaheh Lotfi, Christian Puller, Christoph T. Block, and Martin Greschner		
Department of Neuroscience and Research Center Neuroser	nsory Science, Carl von Ossietzky	
University, 26111 Oldenburg, Germany		
Authors contribution:		
M.G., E.L. designed experiments, C.P., C.B.T., M.G. performe	d experiments, E.L. analyzed data,	
E.L. prepared the figures, E.L. wrote the draft of the manuscript.	1 , , , , ,	
	02.04.2014	
Prof. Dr. Martin Greschner	Date	
Supervisor		

4.1 Introduction

Correlated activity is a fundamental characteristic of signaling within neural circuits. This indicates that neurons have a tendency to fire simultaneously more frequently than would be expected by chance. As a result, they cannot be fully examined as individual encoders but rather as a collective, which complicates the study of neural networks. To acquire a definitive understanding of correlated activity in a network and its effects on signal processing, it is essential to understand its underlying mechanisms. In line with many neural circuits, correlated activity has been observed in retinal ganglion cells across various species. The retina represents an accessible neural circuit with a distinct biological function. Hence, comprehending the significance of correlated activity in the retina may shed light on similar phenomena within neural circuits in other areas of the brain.

Correlated activity in the retina was first documented by a series of seminal studies in cat (Mastronarde, 1983a, 1983b, 1983c). Correlated activity between RGCs is shown to be mediated by common input or reciprocal interactions. Common input consists of the shared presynaptic inputs that mainly originate from cone photoreceptors' noise. The reciprocal interactions mediate correlation directly between or indirectly via the presence of a third cell, which is mainly an amacrine cell (Mastronarde, 1983a, 1983b, 1983c; Brivanlou et al., 1998; DeVries, 1999; Hu & Bloomfield, 2003; Trong & Rieke, 2008; Ala-Laurila et al., 2011). Additionally, a stimulus with a correlated spatial structure can also induce correlation to the response of RGCs. Based on the correlation's origin and mechanism, it can occur on various time scales. Reciprocal interactions involving gap junctions mediate fast correlations at a time scale of 2 ms while correlations mediated by common input are slower.

In this study, using large-scale, high-density, multi-electrode array recording, we survey the structure of correlated activity within and across six RGC types in the guinea pig. We show that the correlation exhibits several general patterns across cell types and has a specific spatial structure. Moreover, we study the receptive field features of synchronous spikes of RGC pairs within cell types. Pairwise synchronous spikes exhibited a stronger localized sensitivity to the stimulus compared to the pairwise asynchronous spikes.

4.2 Results

Large-scale multi-electrode array recordings from adult guinea pig retinas (four retinas) were performed. The cell types were classified based on their spatiotemporal receptive field features, obtained from reverse correlation with random noise stimuli (Chichilnisky, 2001), their autocorrelation function, and their direction-selectivity. Six RGC types that showed consistent responses throughout the recordings and formed a regular mosaic in all four retinas were selected for further analysis. Three of them were the well-known alpha cell types found in rodents: transient ON alpha (tON alpha), transient OFF alpha (tOFF alpha), and sustained OFF alpha (sOFF alpha) (Krieger et al., 2017). The

other three were the medium sON (see chapters 2 and 3), a medium-sized transient OFF cell type (medium tOFF) and a small ON cell type (small tON) (Figure 4.1).

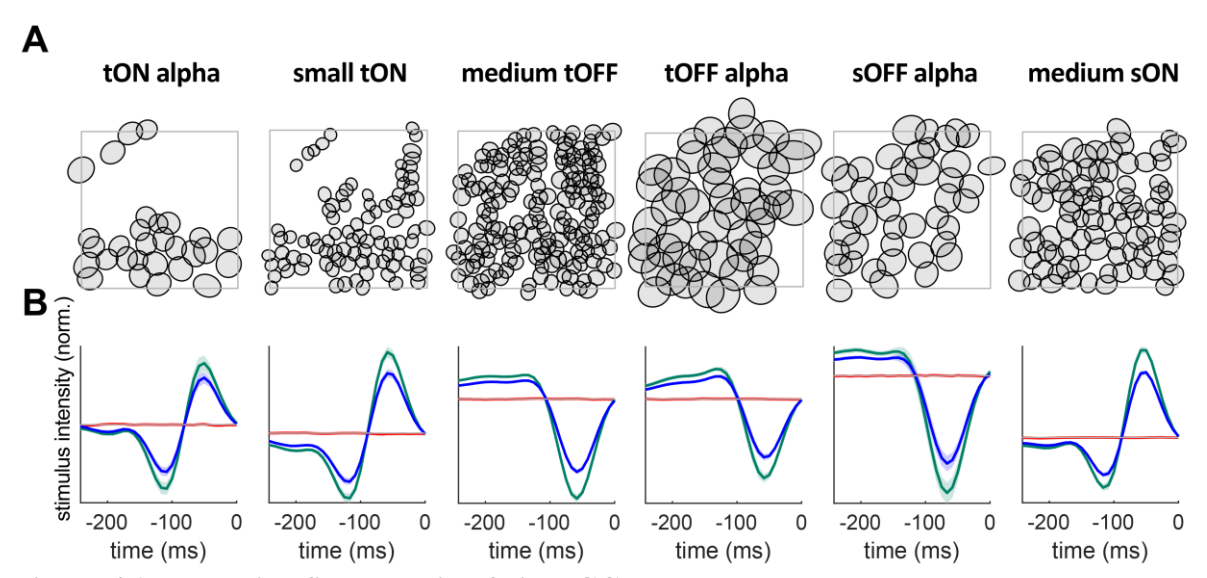


Figure 4.1: Receptive field mosaic of six RGC types. A, Receptive field outlines of each cell type superimposed on the outline of the 4096-electrode array $(2.6 \times 2.6 \text{ mm})$. The receptive fields of each cell type formed a regular mosaic tiling the region of retina recorded. Receptive field outlines are drawn at the 1 SD contour of two-dimensional Gaussian fits. **B**, Mean spike-triggered average stimulus time course of each cell type for each of the three display primaries (red, green, and blue). Shaded region represents the 95% confidence interval.

4.2.1 Spatial organization of correlated activity

Studying the correlated activity of RGCs within and across cell types exhibited several patterns. All RGC pairs exhibited a positive correlation within a type (Figure 4.2A, diagonal). However, the cross-type correlation could be positive or negative based on the polarity of the two cell types (Figure 4.2A, off-diagonal). Cell types with the same polarity showed a positive correlation, while cell types with opposite polarity showed a negative correlation. The strength of correlation showed to be mainly stronger for pairs that belonged to the same type and their cross-correlation function was symmetric, although the strength of correlation across cell types varied. While pairs from different cell types exhibited asymmetric cross-correlation functions, which could be due to the difference in their response kinetics. Pairs of some different cell types, such as tON alpha and small tON exhibited strong symmetric cross-correlation functions. Both of these cell types are ON, same polarity, so they might receive input from a shared circuitry which could give rise to their strong correlation and their similar light response kinetics (Figure 4.1 B) may underlie the symmetric cross-correlation function.

RGCs exhibited to have a specific spatial characteristic in their correlated activity. The spatial extent of the correlated activity of RGC types was evaluated by calculating the correlation coefficient of every pair at zero time lag as a function of distance (Figure 4.2B). The correlation strength of pairs decreased gradually within 1-2 receptive field diameters and became negligible beyond that distance. The 1-2 receptive field diameter is the distance that the first direct neighbors of a cell in the mosaic are located (marked with red dots in Figure 4.2B, diagonal). Therefore, the majority of the cells showed to

have correlations only with their immediate neighbors. However, some cell types such as medium sON and tOFF alpha exhibited that RGCs could have a weak correlation beyond their immediate neighbors. This could be due to the involvement of an amacrine cell (see Chapter 3) or chain coupling. To study the pattern of correlation within each cell type more in detail, cross-correlation functions of immediate neighboring pairs in mosaics of each cell type were calculated with fine binning (Figure 4.2Figure 4.2C). medium sON and tOFF alpha RGCs exhibited bimodal peaks with $\sim \pm 2$ ms offset from zero which suggested the existence of homotypic electrical coupling via gap junctions (Mastronarde, 1983c; DeVries, 1999; Hu & Bloomfield, 2003).

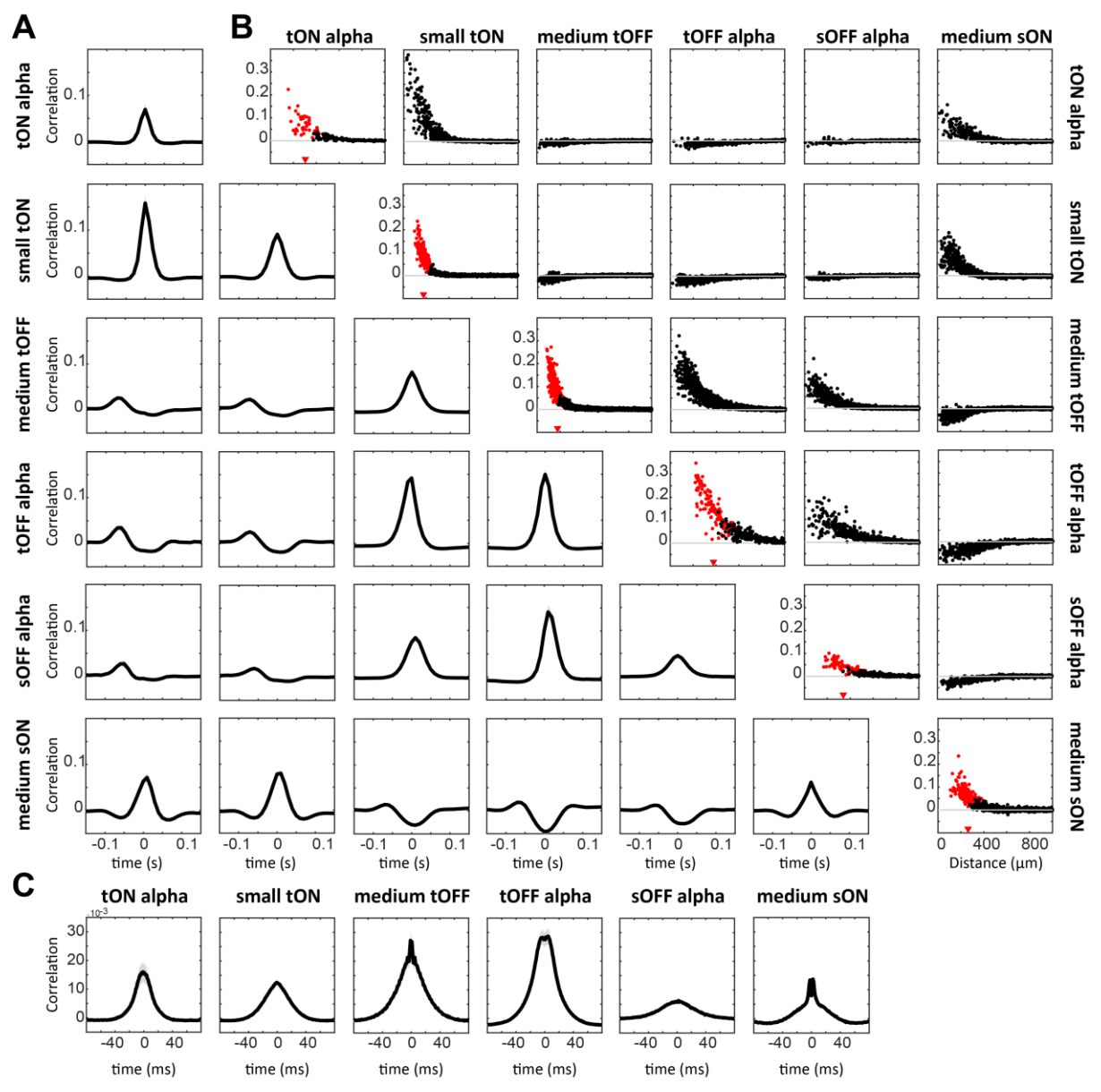


Figure 4.2: Spatial organization of correlated spiking activity within and across RGC types. A, Average cross-correlation function of first direct neighboring RGC pairs within each cell type, and for cross-type RGC pairs with distance of less than 200 μm. Bin size, 10 ms. B, Correlation coefficient at time zero as a function of distance between cells. First direct neighboring pairs of cells in the mosaic are indicated with red points, other cell pairs are represented with black points. The average distance of first direct neighboring racked with an arrowhead on the abscissa. Bin size, 10 ms. C, As in A for within-type first direct neighboring RGCs with finer

bin size to inspect homotypic gap junction coupling. Bin size, 1 ms. Shaded region represents the 95% confidence interval.

4.2.2 Receptive field properties of pairwise synchronous and asynchronous spikes

To understand what synchronous spikes convey to the brain beyond the spikes of their component cells, we introduced two types of spike trains for each pair containing synchronous spikes and asynchronous spikes. Per our definition, the spikes of a pair that occurred within the time limit of \pm 5 ms from each other were synchronous spikes and those spikes of a pair that occurred beyond this time limit were asynchronous spikes (see Materials and Methods). In this study, we only focused on pairs that belong to the same cell type. The spike-triggered average (STA) is a linear estimate of how the brain perceives the visual world, and an approximation of the spatial and temporal receptive field of a cell can be obtained from it. Therefore, we used it to study the difference in the receptive fields of synchronous and asynchronous spikes of pairs. Figure 4.3A illustrates the spatial receptive field of a pair of immediate neighbors in the mosaic of each cell type. Pairwise synchronous spikes in all cell types exhibited a smaller spatial receptive field compared to the pairwise asynchronous spikes. Moreover, the spatial receptive field of pairwise synchronous spikes was smaller than the union of the spatial receptive field of its component cells (Figure 4.3 B, C). The amplitude of the STA in all cell types was ~ 2 times larger for the pairwise synchronous spikes than the pairwise asynchronous spike (Figure 4.3 B, C). This was also observable from the temporal STA of all cell types where the peak of the temporal STA for pairwise synchronous spikes was larger than the pairwise asynchronous spikes (Figure 4.4 A). The z-scores exhibited that the main difference in the amplitude of the spatial STA of synchronous and asynchronous spikes was in the overlap area of the spatial receptive field of their component cells (Figure 4.3 D). The z-score was calculated using the spatial STA of the synchronous spikes relative to the spatial STA of 50 bootstraps of asynchronous spikes. To get an impression if the difference in the spatial receptive field of pairwise synchronous and asynchronous spikes was only conducted by the amplitude of the STA, we normalized the STAs of pairwise synchronous and asynchronous spikes based on the maximum and minimum values of the STAs individually and calculated the z-score as before. The z-score of the normalized spatial STA of pairwise synchronous and asynchronous spikes showed a consistent pattern across the majority of cell types. However, some cell types displayed not specific pattern (Figure 4.3 E). Two clusters of pixels with negative values (blue color) were located along the major axis of the receptive field outlines. These clusters were situated on either side of a smaller, centrally located cluster of pixels with positive values (yellow color). Both zscore analyses indicated that the significant difference of the spatial receptive field of pairwise synchronous and asynchronous spikes was mainly in the overlap area of the component cells' receptive fields. Therefore, in analyzing the temporal receptive field, we concentrated on the time course of the pairwise synchronous and asynchronous spikes within the overlapping receptive field areas of the component cells. Pairwise synchronous and asynchronous spikes exhibited time courses with similar

kinetics across all cell types. However, there was a time shift between the two time courses, where in some cell types the time course of the pairwise synchronous spikes displayed a shorter latency than that of the pairwise asynchronous spikes (Figure 4.4 B).

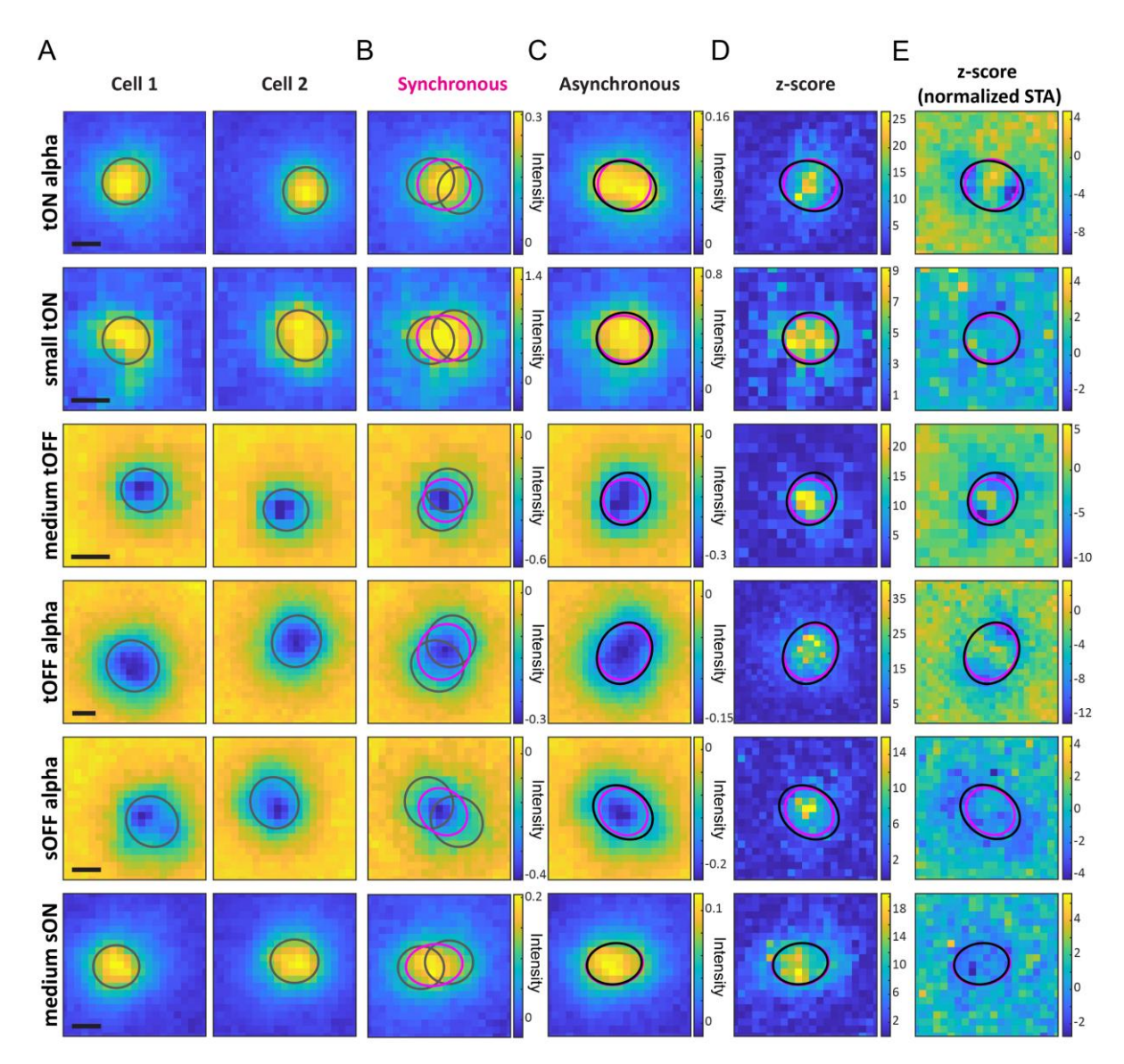


Figure 4.3: The spatial receptive field of the synchronous and asynchronous spike trains. A, The spatial receptive field of two neighboring ganglion cells of the same cell type. The average of the three strongest frames of the STA is used to obtain the spatial receptive field. Receptive field outlines are drawn at the 1 SD contour of two-dimensional Gaussian fits. B, The spatial receptive field of the synchronous spikes of pairs in A. Synchronous spikes of a pair are spikes that have a time lag of less than 5 ms from each other. The receptive field outlines of the pair and the synchronous spikes are shown in gray and magenta respectively. C, The average spatial receptive field of 50 bootstraps of asynchronous spike trains of the pair in A. Asynchronous spikes of a pair are spikes that have a time lag of more the 5 ms from each other. The number of spikes used to calculate the STAs in B and C are equal. The receptive outlines of the synchronous (magenta) and asynchronous (black) spikes are superimposed on the average spatial STA of 50 bootstraps of asynchronous spike trains. D, The z-score of the spatial STA of the synchronous spikes of B relative to the spatial STA of 50 bootstraps of asynchronous spikes of C. The ellipses show the receptive field outlines as in C. E, As in D, for normalized spatial STAs. Scale bars: 200μm

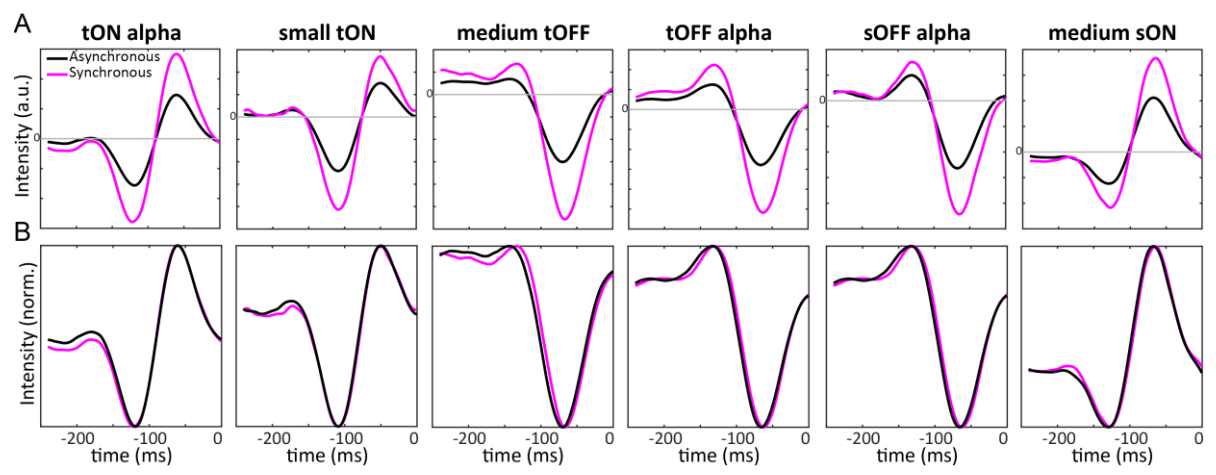


Figure 4.4: The temporal receptive field of synchronous and asynchronous spike trains. A, The temporal receptive field of the synchronous spike train of pairs of Figure 4.3 and the mean temporal receptive field of the 50 bootstraps of asynchronous spike trains of the same pairs calculated in the overlap area of the spatial receptive fields of the two component cells. B, The normalized temporal receptive fields of synchronous and asynchronous spike trains of A.

4.2.3 Quantification of the receptive field properties of pairwise synchronous and asynchronous spikes across cell types

To investigate the general patterns in the receptive fields of pairwise synchronous and asynchronous spikes across cell types, we randomly selected several immediate neighbouring pairs, similar to those depicted in Figure 4.3, for each cell type in four retinas. The receptive field features such as size, intensity, and latency for pairwise synchronous and asynchronous spikes in these samples were depicted in violin plots (Figure 4.5). The size of the receptive field was evaluated based on two measurements: the radius of the receptive field outline, in which the receptive outline was the 1 SD contour of the two-dimensional Gaussian fit to the spatial STA, and the area of the spatial STA above a certain threshold (two-thirds). Figure 4.5 A and B depict the ratio for the radius and area of the receptive field of pairwise synchronous spikes to the mean radius and mean area of the receptive fields of 50 bootstraps of pairwise asynchronous spikes, where each dot represents a single pair. All cell types, consistently in each of the four retinas, exhibited a smaller radius and area for the receptive field of pairwise synchronous spikes compared to the receptive field of pairwise asynchronous spikes. The comparison between the radius of the receptive field of the pairwise synchronous spikes and the mean radius of the receptive field of the component cells showed no significant difference across cell types (ratio, medium tOFF: 0.99 ± 0.05 , tON alpha: 0.99 ± 0.06 , medium sON: 1.02 ± 0.05 , tOFF alpha: 1.06 \pm 0.12, sOFF alpha: 1.04 \pm 0.06) except for small tON that showed a smaller receptive field for pairwise synchronous spikes compared to the component cells (ratio = 0.85 ± 0.11). The STA of pairwise synchronous spikes showed a higher amplitude than the pairwise asynchronous spikes across cell types (Figure 4.3 D and Figure 4.4 A). Investigation of this observation in a sample population showed a consistent pattern across all cell types in the four retinas. The amplitude ratio of the STA for pairwise synchronous spikes, when compared to the average amplitude of the STA from 50 bootstrapped pairwise asynchronous spikes, revealed a distribution with an average value ranging from 1.5 to 2 (Figure 4.5 C). Pairwise synchronous spikes showed smaller latency than the pairwise asynchronous spikes in some cell types (Figure 4.4 B). To quantify this pattern, the latency difference of the time course of 50 bootstrapped pairwise asynchronous spikes compared to the mean time course of the same 50 bootstrapped pairwise asynchronous spikes was calculated. This measure for sample pairs across all cell types showed to have a Gaussian distribution with zero mean (Figure 4.5 D, white violin plots). Similarly, the latency difference in the time course of the pairwise synchronous spikes and the mean time course of the 50 bootstrapped asynchronous spikes of each pair was calculated. For each cell type and retina, we plotted this measure for sample pairs against the violin plot representing the same measure for pairwise asynchronous spikes (Figure 4.5 D, blue dots vs white violin plots). All cell types except for tON alpha and small tON exhibited shorter latency in the time course of pairwise synchronous spikes compared to the time course of pairwise asynchronous spikes. The Wilcoxon rank sum test showed the significance of this observation (data not shown). However, this test for tON alpha and small tON showed that the latency of the time course of pairwise synchronous spikes was not significantly different from the latency of the time course of pairwise asynchronous spikes.

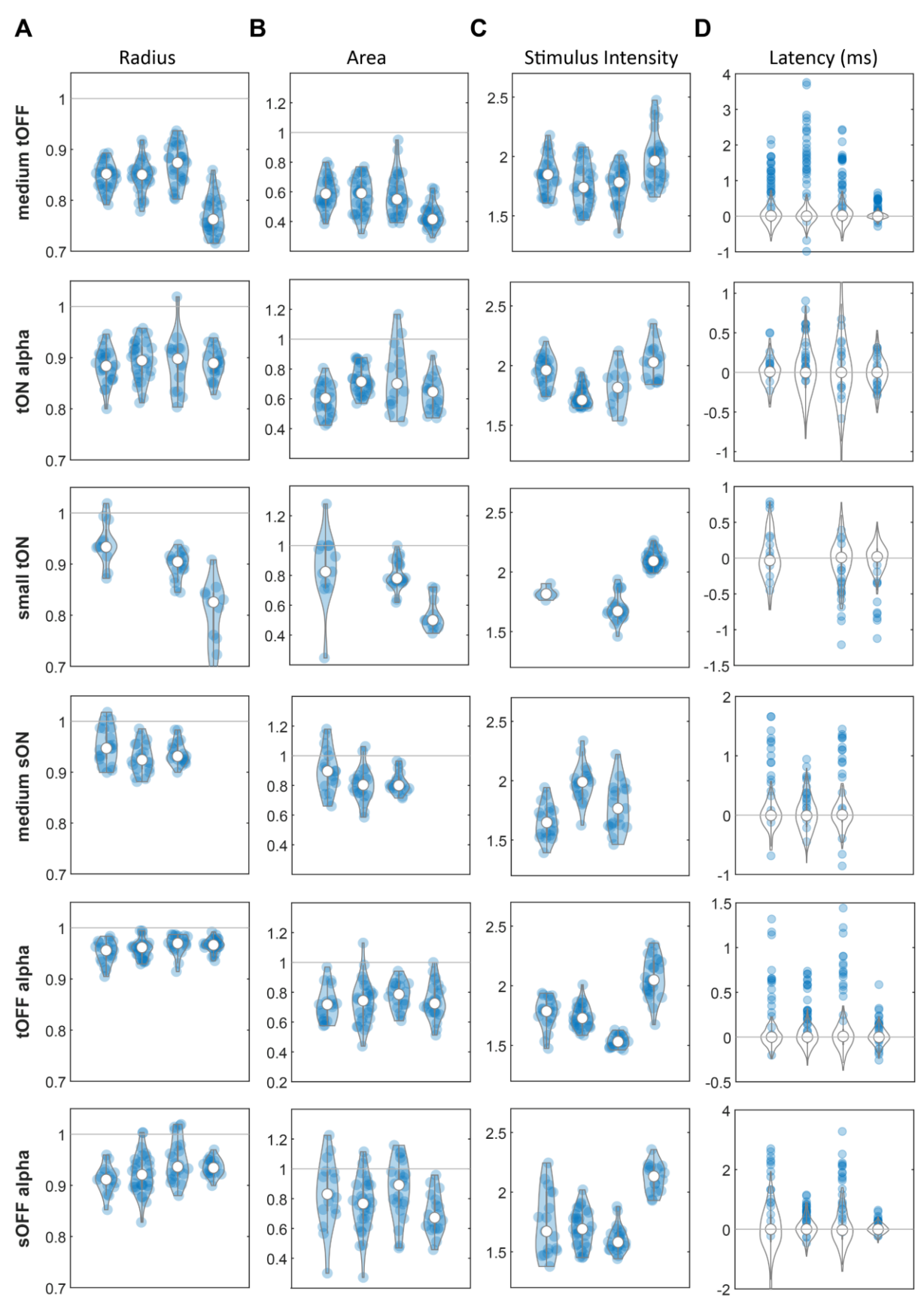


Figure 4.5: Quantification of the receptive field of pairwise synchronous and asynchronous spikes across cell types. A, The ratio of the receptive field radius for pairwise synchronous spikes compared to the average radius of the receptive fields of 50 bootstrapped pairwise asynchronous spikes. Radii are determined from the radial radius of the elliptical Gaussian fits. Each row represents the data for a specific ganglion cell type in

four different datasets. **B**, The ratio of the area covered by the spatial receptive field for pairwise synchronous spikes at a certain threshold to the average area covered by the spatial receptive fields for 50 bootstrapped pairwise asynchronous spikes at the same threshold. **C**, The peak amplitude ratio calculated by comparing the peak of the temporal receptive field for pairwise synchronous spikes to the average peak of temporal receptive fields for 50 bootstrapped pairwise asynchronous spikes. **D**, The distribution of the latencies for the time courses of 50 bootstrapped pairwise asynchronous spikes, compared to their mean latencies. Each Blue circle represents the time course latency of pairwise synchronous spikes relative to mean latency of the time courses of 50 bootstrapped pairwise asynchronous spikes. Positive values indicate shorter latency.

4.3 Discussion

In this study, we quantitatively characterized the correlated activities within and across six RGC types in the guinea pig. Our findings align with prior research conducted on different species. Moreover, we explored the variance in linear responses between pairwise synchronous and pairwise asynchronous spikes across various cell types. Our analysis revealed that the features of the receptive field—namely size, intensity, and latency—of pairwise synchronous spikes differ from those of pairwise asynchronous spikes within the same pair.

4.3.1 Structure of correlated activity

Correlated activity in the retina is mediated by reciprocal interactions and common input that can be noise originating mainly from photoreceptors (noise correlation) or signal from a shared stimulus with spatial correlated structure (signal correlation) (Mastronarde, 1983a, 1983b, 1983c; Brivanlou et al., 1998; DeVries, 1999; Hu & Bloomfield, 2003; Trong & Rieke, 2008; Ala-Laurila et al., 2011). Our results on the correlated activity of six RGC types in the guinea pig retina showed consistent patterns, as was seen in various species previously (Mastronarde, 1983c; DeVries, 1999; Greschner et al., 2011). Correlated activity was observed to be positive among pairs of the same cell type or those with the same light response polarity. Conversely, pairs with opposite light response polarities (ON and OFF) exhibited negative correlated activity. This pattern is expected because ON cells are activated by increases in light intensity, while OFF cells respond to decreases. When one type is active, the other mainly remains inactive, resulting in the negative correlation observed. Similarly, cells of the same polarity, such as ON cells, may have little shared presynaptic circuits, but they share common cone inputs, leading to the positive correlation seen in their responses. Pairs of the same cell types exhibited symmetric cross-correlation functions, while pairs of different types mainly exhibited asymmetric cross-correlation functions. This asymmetry could be attributed to the fact that, although cone photoreceptors are the primary source of noise correlation, the presynaptic circuitry and intrinsic properties of the cells, such as nonlinearities, can modify the correlated presynaptic input between the pair, resulting in asymmetric correlation. However, there were examples of cross-type pairs, tON alpha and small tON, that exhibited nearly symmetric positive correlated activity. This could be explained by the similar kinetics of their temporal receptive field (Figure 4.1B).

Observations of the cross-correlation function on a finer time scale revealed sharp bimodal peaks with ± 2 ms offset from zero in medium sON and tOFF alpha RGCs. This pattern is indicative of

reciprocal interactions mainly mediated via gap junction (Mastronarde, 1983c; DeVries, 1999). The cross-correlation function revealed this rapid correlation superimposed upon a slower noise correlation stemming from shared inputs. Furthermore, the broad and shallow patterns seen in the cross-correlation functions indicate signal correlation, driven by a stimulus with a correlated structure. In general, Correlations mediated from different mechanisms (noise and signal correlation) are thought to be additive and can be isolated using the shuffling method. Separate observations of signal and noise correlations have shown that rapid noise correlations overlay the slow signal correlation. Utilizing a random noise stimulus with a correlated structure in our experiments, the cross-correlation functions displayed a mix of slow and fast correlations, with the majority being attributed to noise correlation. (figure 4.2A, diagonal).

Our findings suggest that the reduction in correlation with distance is a fundamental principle observed among various cell types (Mastronarde, 1983a; DeVries, 1999; Shlens et al., 2006; Greschner et al., 2011). The correlated activity of all RGC types as a function of distance showed correlation mainly existed between first direct neighboring pairs and as the distance of the pairs increased, the correlation became negligible. This spatial structure of the correlated activity refers to the mosaic organization of the RGCs' receptive field. As the RGC pairs grow apart, the number of shared cones that provide presynaptic input to the pair decreases in comparison to the RGC pairs with overlapped receptive fields, hence the correlated activity of the distant pairs becomes smaller. The medium sON and tOFF alpha RCG types exhibited a relatively weak positive correlation for pairs (within-type) located beyond their first direct neighbors. This correlation could be mediated by an intermediate cell, such as an amacrine cell, or by chain homotypic electrical coupling via gap junctions. Notably, the medium sON RGCs were negatively correlated with a polyaxonal amacrine cell (PAC) type when their receptive fields were in close proximity to the axons of the PAC (see Chapter 3). This negative correlation was suggestive of the inhibitory effect of the PAC on the neighbouring medium sON RGCs along the PAC's axon. Consequently, this inhibition, which is received with a slight delay, may lead to a weak positive correlation among medium sON RGC pairs that are not directly adjacent.

4.3.2 Synchronous spikes vs asynchronous spikes

Synchronous spikes of an RGC pair are thought to convey a different message about the stimulus to the brain compared to their component cells. Studies in salamander retina reported that the synchronous spikes provide finer spatial details than the spatial details that the receptive field of the component cells conveys to the brain (Meister et al., 1995; Schnitzer & Meister, 2003). We evaluated this observation in six RGC types of guinea pigs. We used spike-triggered average as a linear model of ganglion cell's receptive field. STA provides information on the spatial and temporal domains of the receptive field (Chichilnisky, 2001). Pairwise synchronous spikes across all cell types exhibited smaller receptive field size, higher stimulus intensity and shorter response latency compared to the pairwise asynchronous spikes (Figure 4.5). Cells of the same type respond synchronously when they receive

common input. If we calculate the STA for the synchronous spikes of a distant pair, the spatial STA exhibits two distinct regions that are the location of the receptive field of each cell in the mosaic. This indicates that for a distant pair to fire synchronously, they should be stimulated by similar inputs at their receptive field. However, if the pair are neighbouring cells with receptive field overlap, stimulating the pair at the overlap of their receptive fields leads them to fire synchronously while stimulating them in an area that lies in the center of the receptive field of one and the surround of the receptive field of the other one leads to negative correlation meaning the first cell fires strongly and the other one is suppressed. Pairwise synchronous spikes across all cell types showed the same pattern of smaller-sized receptive fields localized in the overlap of the receptive field of their component cells compared to the receptive fields of the pairwise asynchronous spikes. Moreover, the amplitude of the STA in the overlap area of the component cells' receptive field, which indicates the intensity of the cell's response to the stimulus in its receptive field, for pairwise synchronous spikes was higher than for the pairwise asynchronous spikes across all cell types. These two observations may indicate that the pairwise synchronous spikes were produced by strong stimulation in the overlap area of the pair's receptive field while pairwise asynchronous spikes were produced by an average stimulus that may elicit a spike in one cell but not in the other cell. Except for two cell types, all cell types exhibited shorter latency in the time course of the pairwise synchronous spikes relative to the time course of the pairwise asynchronous spikes. This may also arise because cells mainly tend to fire faster in response to a strong stimulus as opposed to an average one.

4.3.3 Prospects for future studies

In this study, a random noise with a natural spatiotemporal frequency falloff was used to characterize the response properties of recorded cells. This stimulus is spatially correlated, hence can induce correlation in the response of RGCs. Therefore, the most standard test is to use a white noise stimulus to assess the consistency of the observations under both stimulations. In a preliminary test, we used a white noise stimulus for one of the retinas and observed similar results regarding the higher amplitude of the STA for the pairwise synchronous spikes in the overlap area of the component cells' receptive field. However, due to the brief duration of the stimulus, the resulting STAs were too noisy, preventing us from assessing the receptive field size and latency.

The use of STA as a linear estimator of the receptive field could potentially impact our observations. STA provides an unbiased linear estimate of the receptive field only when applied to white noise stimulus; however, our study's use of spatially correlated random noise introduces a bias. Moreover, to capture the effect of the nonlinearities of the receptive field, we could improve the study further by employing nonlinear models, such as linear-nonlinear (LN) models. Our findings indicate that certain RGC types exhibit positive, nearly symmetric cross-type correlations. Therefore, it would be insightful to study the characteristics of the linear and non-linear filters of synchronous spikes of pairs that do not belong to the same type but show a strong correlated activity.

4.4 Materials and Methods

4.4.1 Animals and tissue preparation

All experiments were performed in accordance with the institutional guidelines for animal welfare and the laws on animal experimentation issued by the European Union and the German government. The preparation was performed as described in section 2.4.1.

4.4.2 Multi-electrode array recordings

Recording of RGCs activity under two stimulus presentations was performed as described in section 2.4.2.

4.4.3 Light stimulation

A random noise stimulus with a natural spatiotemporal frequency falloff was used to characterize the response properties of recorded cells. The stimulus was presented on a CRT monitor at a refresh rate of 120 Hz and a stimulus pixel width of 49 μ m on the retina at photopic light levels at a mean intensity of 2.9 mW/m². Only the green and blue monitor guns were used. Another stimulus used in this study was a white noise stimulus presented on a CRT monitor at a refresh rate of 120 Hz and a stimulus pixel width of 24 μ m on the retina.

4.4.4 Receptive field and classification analysis

RGCs were functionally classified into types as described in section 2.4.4.

4.4.5 Correlated activity measurement

Cells with noisy spike-triggered averages, auto-correlation or cross-correlation functions, or electrical images that indicated poor spike sorting quality were excluded from the analysis. The cross-correlation function analysis was performed on spike recordings of 50–60 min duration under a random noise stimulus. Cross-correlation functions were obtained by binning spikes and computing the correlation coefficient between the resulting spike count vectors, with a temporal offset. The cross-correlation function value at zero lag was used to quantify the correlation strength within and between different cell types and to examine how it depends on the spatial distance of the cell pairs. The distance of each pair was the distance of the center of the elliptical Gaussian fits. The first direct neighbors of each retinal ganglion cell were identified based on their receptive field location in the mosaic, and the average distance of these neighboring pairs for each cell type was calculated. The cross-correlation functions were averaged across the first direct neighboring pairs for within-type correlations, and across the pairs with a distance of less than 200 µm for cross-type correlations.

4.4.6 Synchronous spike trains

The pairwise synchronous spikes of retinal ganglion cells within each cell type were investigated. Since across all cell types, the first direct neighbors exhibited the strongest positive correlated activity and the strength of correlation decreased tremendously beyond that we used only the first direct neighbors for further analysis. The cross-correlation functions of these pairs exhibited a prominent peak centered at zero lag and the main correlated activity was restricted to the time window of ±5 ms (Shlens et al., 2006; Trong & Rieke, 2008; Greschner et al., 2011). Based on this observation, a time window of ±5 ms was used to obtain the synchronous spikes of the RGC pairs. For every RGC pair, A and B, using A as a reference cell, the spikes of B that occurred within a ±5 ms window around each spike of A were identified as synchronous spike pairs. A third spike train C was generated to represent the synchronous spikes of A and B (Schnitzer & Meister, 2003). For each synchronous spike pair, a spike was added to C that had a firing time at the midpoint of the firing times of its parent spikes. For a comparison, a new type of spike train called asynchronous was introduced. Any synchronous spikes of cell A and B that had a corresponding spike in cell C were removed, resulting in spike trains A' and B'. Then, a distribution of 50 asynchronous spike trains with the same number of spikes as cell C were generated, using the spikes of cells A' and B' with equal contributions.

4.4.7 STA calculation and receptive field parameters

The spike-triggered average (STA) was computed from the binned spike trains elicited by random noise stimuli. N preceding frames were summed for each bin with a spike and then averaged over all spike-containing bins. STAs were calculated with both fine and coarse time resolutions. For the coarse STA, the bin size matched the stimulus refresh cycle (8.33 ms) and N was 30. For the fine STA, the stimulus was interpolated by a factor of 20, resulting in a bin size of 0.41 ms and N of 600. The fine STA was only used to compare the latency of the time course of synchronous and asynchronous spikes. To make the STAs of synchronous and asynchronous spikes comparable, the same number of spike-containing bins was ensured for both to keep the noise levels similar.

The STA was calculated using only the blue and green channels of the stimulus, since red is not detected by guinea pig photoreceptors. Similar kinetics were shown by the temporal STA for both channels across different cell types, except that a slightly higher amplitude was elicited by the green channel than the blue channel. For example, the peak amplitude of the green channel temporal STA for medium sON cells was 1.34 ± 0.04 larger than that of the blue channel temporal STA. A high correlation coefficient of 0.998 ± 0.001 was obtained by the normalized green and blue temporal STA curves, indicating that a comparable preference for both colors was exhibited by this cell type. Therefore, a weighted average of the green and blue channel STAs was computed, using the peak amplitude of each channel's temporal STA as a weight. The weight value depended on the cell type.

Receptive field outlines were drawn at the 1 SD contour of two-dimensional Gaussian fits. Receptive field size estimates are reported as the diameter of a circle with the same area as the elliptical Gaussian fit.

4.4.8 Quantification

Radius and area. The radius of the receptive fields was calculated as the radius of a circle with the same area as the elliptical Gaussian fit. Calculation of the area is independent of the Gaussian fit and is the area of the receptive field in which the amplitude of the STA is above a certain threshold (two-thirds). The distribution of the ratio of the radius and area of the receptive field of the pairwise synchronous spikes and the mean radius and area of the receptive field of 50 bootstrapped pairwise asynchronous spikes for pairs within a cell type are calculated.

Intensity. The amplitude of the STA was extracted from the amplitude of the peak (ON cells) or trough (OFF cells) of the temporal receptive fields. For each pair, the ratio of the amplitude of the STA for pairwise synchronous spikes and the mean amplitude of the STAs of 50 bootstrapped pairwise asynchronous spikes were calculated. The distribution of the amplitude ratios of the pairs within each cell type is calculated. Observations from the white noise stimulus also showed similar results as random noise stimulus with spatially correlated structure (white noise, ratio: medium tOFF: 2.58 ± 0.49 , small tON: 2.41 ± 0.33 , tOFF alpha: 2.16 ± 0.29 , sOFF alpha: 2.28 ± 0.33).

Latency. To measure the latency of the time course of pairwise synchronous and asynchronous spikes, the cross-correlation function of the time course of the STA of pairwise synchronous and asynchronous spikes with the mean time course of the STAs of 50 bootstrapped pairwise asynchronous spikes for each pair was computed. The fine STA calculation was used in this analysis to increase the resolution. The time of the maximum of the cross-correlation function was used as the latency measure. The latencies of time course of the STA of 50 bootstrapped pairwise asynchronous spikes are exhibited as a distribution and the latency of the time course of the STA of pairwise synchronous spikes is exhibited as sample points.

4.4.9 Violin plot

A Violin Plot is used to visualize the distribution of the data and its probability density function. The white dot in the middle is the median value and the thick gray bar in the center represents the interquartile range. The thin gray line extending from it represents the range of the data.

5 General Discussion

RGCs in the retina are not independent encoders but rather display correlated activity with different time scales. Correlation affects the response of RGCs and hence the signal conveyed to the brain by these output channels of the retina. By studying the circuits that mediate correlation, we can gain insight into how RGCs encode visual signals that they transmit as parallel pathways to the brain. The correlation can be mediated by reciprocal interactions via gap junctions and by shared presynaptic noise, originating mainly from cone photoreceptors. A different mechanism that induces correlation in the RGCs response is the stimulus-driven correlation origination from a highly spatiotemporally correlated stimulus. Each type of correlation can have a distinct impact on information coding in the retina and ignoring them while decoding the visual information sent via RGCs to the brain may compromise the amount of decoded information.

In this thesis, we used large-scale multielectrode array recording that allows us to capture the simultaneous firing activity of thousands of RGCs and spiking ACs. With this recording method, we could study the correlation of RGCs within and across different types. In Project 1, we investigated the presence of heterotypic gap junction coupling between two RGC types. This was the first observation of heterotypic coupling among RGCs. All previous studies had reported only homotypic gap junction coupling or heterotypic gap junction coupling between RGCs and ACs consistent with the notion of parallel coding of visual information in the retina. In Project 2, we explored the interactions of a specific RGC type with a polyaxonal AC type. This PAC type exhibited a strong positive correlation with RGCs whose receptive fields overlapped with the PAC's receptive field, and at the same time, a negative correlation with RGCs of the same type that were in close proximity of the PAC's axons. Using a conceptual model, we showed that these interactions were sufficient to explain the direction-sensitivity of this RGC type. In Project 3, we provided a quantitative description of correlated activity within and across six RGC types and showed that the correlated activity exhibits a systematic pattern across all cell types. Moreover, the strength of correlation systematically depends on the distance of the pair. We showed in six RGC types that the synchronous firing activity of RGC pairs within the type possesses a different spatiotemporal linear filter than asynchronous firing activities.

5.1 Electrical coupling between parallel pathways of different RGC types

Retinal ganglion cells are the output channels of the retina that convey visual information to higher visual areas. About 30 functionally and morphologically distinct RGC types have been identified in mice, each of which covers the retina uniformly and forms an independent parallel pathway (Baden et al., 2016; Bae et al., 2018). Different RGC types encode different features of the stimulus (Kerschensteiner, 2022). Some RGC types form electrical coupling via gap junctions within the same type (homotypic coupling) (Vaney, 1991; DeVries, 1999; Hu & Bloomfield, 2003; Hidaka et al., 2004;

Trong & Rieke, 2008; Greschner et al., 2011; Trenholm et al., 2013; Völgyi et al., 2013; Trenholm et al., 2014). Additionally, RGCs form electrical coupling with different amacrine cell types (heterotypic coupling) (Ackert et al., 2006; Völgyi et al., 2013; Greschner et al., 2016). Homotypic coupling of RGCs is thought to increase the signal-to-noise ratio and the accuracy of neuronal signalling (Bloomfield & Völgyi, 2009; Trenholm et al., 2013; Yao et al., 2018). The heterotypic coupling of RGCs with amacrine cells serves various functions and shapes the response of RGCs (Greschner et al., 2016; Roy et al., 2017). However, our published study (chapter 2) in guinea pigs, followed by a similar study in mice a year later, revealed the existence of heterotypic coupling between RGCs for the first time (Puller et al., 2020; Cooler & Schwartz, 2021). In chapter 2, we used large-scale multi-electrode array recording and tracer-coupling injections to discover heterotypic coupling between two RGC types: the well-studied sustained ON alpha RGC and the medium sustained ON (medium sON) RGC, which has a medium-sized receptive field. Both cell types formed a regular mosaic with their receptive fields and showed distinct tri-phasic and bi-phasic temporal filters for sustained ON alpha and medium sON, respectively. We observed bimodal cross-correlation functions with sharp peaks at ±~2 ms centered around zero for sustained ON alpha and medium sON pairs, suggesting heterotypic coupling (Mastronarde, 1983c; Brivanlou et al., 1998; DeVries, 1999; Völgyi et al., 2013). Furthermore, neurobiotin injections to sustained ON alpha RGCs, which can be easily identified by their large cell bodies, showed connections of the target sustained ON alpha with the cells of the same type and a smaller-sized RGC. The electrical image of the medium sON RGCs also had the footprint of sustained ON alpha RGCs (only soma) superimposed on it. These are all evidence that supports the existence of heterotypic coupling between sustained ON alpha and medium sON RGCs. This observation could challenge the general rule of parallel information processing in the retina. However, similar cross-talks also exist in different levels of the retina, such as the inner plexiform layer (Zaghloul et al., 2003; Hoshi et al., 2009), or the lateral geniculate nucleus (Rompani et al., 2017; Rosón et al., 2019). Therefore, this study could be an example of how much more needs to be discovered about the circuitries, projection sites, and information processing in the higher visual areas to understand the parallel processing of information in the retina.

5.2 Direction-sensitive response of medium sON RGCs

The visual system computes the direction of motion in several stages, starting from the retina. Retinal ganglion cells are one of the cell classes that exhibit direction-selectivity, which means they respond differently to stimuli moving in different directions. This property was first discovered in the rabbit retina by Barlow and his colleagues in the 1960s (Barlow & Hill, 1963; Barlow et al., 1964; Barlow & Levick, 1965). Direction-selective RGCs (DSGCs) can be divided into two major categories: ON DSGCs and ON-OFF DSGCs. ON DSGCs are activated by light increments, while ON-OFF DSGCs are activated by both light increments and decrements. Each category has several subtypes,

with three subtypes of ON DSGCs and four subtypes of ON-OFF DSGCs identified so far (Mauss et al., 2017; Wei, 2018; Reinhard et al., 2020). However, a recent study reported a fourth subtype of ON DSGCs in the mouse retina (Sabbah et al., 2017). The direction-selectivity of both ON and ON-OFF DSGCs is mediated by a common circuit involving starburst amacrine cells (SACs), which are interneurons that release both inhibitory and excitatory neurotransmitters (Famiglietti Jr, 1983; Famiglietti, 1991). The SACs inhibit the DSGCs in a direction-dependent manner, resulting in a preferential response to one direction of motion (Fried et al., 2002; Briggman et al., 2011; Wei et al., 2011; Yonehara et al., 2011).

Besides the classic ON and ON-OFF DSGCs, there are other RGC types that show directionselectivity in addition to their original functions. These include J-RGCs, F-mini On, and F-mini OFF cells in the mouse retina. These cells do not costratify with the SACs, suggesting that they use different circuits to generate direction-selectivity (Kim et al., 2008; Joesch & Meister, 2016; Rousso et al., 2016; Nath & Schwartz, 2017; Cooler & Schwartz, 2021). In Project 2, we revealed that medium sON RGCs display direction sensitivity. Specifically, these cells exhibited a preference in their background activity for bars moving in the ventral direction when positioned distally relative to their receptive fields. Additionally, we observed a negative correlation between the firing activity of medium sON RGCs and ON asymmetric PACs when in close proximity to the PACs' axons. Conversely, medium sON RGCs with receptive fields located further from the PACs' axons did not exhibit correlated activity. This spatially dependent negative correlation suggests a direct interaction, likely indicative of GABAergic inhibition of medium sON RGCs by ON asymmetric PACs. Our research also showed that the inhibitory signals from ON asymmetric PACs to medium sON RGCs are direction-sensitive, aligning with the direction sensitivity observed in medium sON RGCs. The development of a parameter-free conceptual model, based on the interactions between medium sON RGCs and ON asymmetric PACs, indicated that the directional inhibitory signals from PACs sufficiently explain the direction sensitivity of medium sON RGCs. However, our study does not describe a detailed circuit diagram for the direction sensitivity of medium sON RGCs. Further research, employing pharmacological methods and recording both presynaptic inhibitory and excitatory inputs to these cells, is necessary to fully elucidate the underlying circuitry. We investigated the presence of direction sensitivity in medium sON RGCs across several retinal preparations, both peripherally and near the central retina. In all examined regions, medium sON RGCs consistently exhibited direction sensitivity (data not shown). A comprehensive understanding of the topographic variation in direction sensitivity among medium sON RGCs throughout the retina is crucial for discovering the functional significance of this feature. Furthermore, identifying the downstream brain targets of this cell type will enhance our comprehension of its role in visual processing.

5.3 A Polyaxonal amacrine cell population in the guinea pig retina

Amacrine cells are a diverse and less understood class of retinal cells that modulate the signals of bipolar cells and retinal ganglion cells. Based on their morphology, neurotransmitter, and synaptic connections, at least 42 distinct types of ACs have been identified (Masland, 2012b; Euler et al., 2014). ACs can be broadly divided into two categories: small-field and wide-field, which differ in their size, shape, chemical properties, and functional roles (Wässle, 2004; Masland, 2012a; Franke & Baden, 2017). A subset of wide-field ACs are PACs, which were first discovered by Vaney et al. (1988) in the rabbit retina (Vaney et al., 1988). PACs have separate dendritic and axonal arbors that span several millimeters across the retina (Dacey, 1988; Vaney et al., 1988; Dacey, 1989; Mariani, 1990; Famiglietti, 1992; Freed et al., 1996; Taylor, 1996; Völgyi et al., 2001; Ölveczky et al., 2003; Wright & Vaney, 2004; Davenport et al., 2007). PACs generate action potentials similar to RGCs, which allow them to transmit signals over long distances. ACs are thought to be involved in various computations in the inner plexiform layer (IPL), but their exact circuitry and population-level function remain unclear (Gollisch & Meister, 2010). As for PACs, only a few studies have systematically investigated their role in specific visual tasks, such as object motion detection and orientation selectivity (Baccus et al., 2008; Greschner et al., 2014; Murphy-Baum & Taylor, 2015).

Recent advances in multi-electrode array recordings have enabled the simultaneous recording of RGCs and spiking ACs, such as PACs. This provides an opportunity to study the collective response of PACs and their influence on the output of RGCs. In Project 2, we analyzed the electrical images of all recorded cells and differentiated PACs and RGCs based on their distinctive axonal patterns (Litke et al., 2004; Petrusca et al., 2007). Using this approach, we characterized a population of PACs that had a sparse and asymmetric axonal distribution, mainly oriented toward the ventral direction. These PACs, which we called ON asymmetric PACs, formed a regular mosaic with their spatial receptive fields and had homogenous temporal filters. These common features suggested that they constituted a single functional cell type (Devries & Baylor, 1997; Field & Chichilnisky, 2007). Furthermore, we examined the cross-correlation function of these PACs with RGCs and found that they formed excitatory and inhibitory interactions with a specific RGC type, the medium sON. Their collective inhibitory effect on the response of medium sON RGCs was consistent with the medium sON RGC's direction sensitivity. For subsequent research, employing immunohistochemical markers to visualize the cell morphology and ascertain the level of dendritic and axonal stratification will help in identifying this particular type of polyaxonal amacrine cell. All this accumulated systematic knowledge of ACs would enable us to better evaluate their role in the retina, and whether they participate in specialized circuits and serve specific functions, or whether they are involved in multiple mechanisms and serve general functions (Franke & Baden, 2017).

5.4 Systematic patterns of correlated activity across six RGC types

Correlated activity is a common phenomenon in neural circuits, where neurons tend to fire more frequently than expected by chance (Averbeck et al., 2006; Shlens et al., 2008). The first report of the correlated activity of ganglion cells in the mammalian retina came from David Mastronarde, based on a series of semantic studies on the cat retina (Mastronarde, 1983a, 1983b, 1983c). Subsequent studies revealed that the correlation in retinal ganglion cells is mediated by two main mechanisms: common input from cone photoreceptors and reciprocal coupling via gap junctions (Mastronarde, 1983a, 1983b; Brivanlou et al., 1998; DeVries, 1999; Trong & Rieke, 2008; Ala-Laurila et al., 2011). Besides intrinsic correlations, the statistical properties of the stimulus can induce correlation in the response of RGCs (Simoncelli & Olshausen, 2001; Averbeck et al., 2006). We investigated the structure of correlated activity in six functional RGC types in the guinea pig. We observed several systematic patterns: strong positive within-type correlation, negative correlation between pairs of opposite polarity, rapid correlated activity in some cell types, varying strengths of correlation across cell types, and systematic dependence of correlation to distance. These observations mirror the mechanisms underlying correlated activity. Notably, correlation strength decreased significantly beyond the first direct neighbors, suggesting that the mosaic organization of RGCs influences the extent of correlation. However, for certain cell types such as medium sON and tOFF alpha RGCs, we found that the within-type positive correlated activity extended to the second direct neighbors, consistent with previous findings in ON parasol RGCs in primates (Greschner et al., 2011). This could be due to chain coupling or the involvement of an amacrine cell. For instance, a PAC positively correlates with nearby RGCs but inhibits several others along its axons. If another AC inhibits this PAC, the resulting disinhibition could extend correlated activity to more distant neighbors. The asymmetry observed in the cross-correlation function of cross-type RGC pairs suggests the modificatory role of presynaptic circuitries and the intrinsic features of the cell types.

5.5 Linear response of synchronous and asynchronous firing activities

The significance of correlation in the ganglion cell layer has been a matter of debate (Averbeck et al., 2006; Shlens et al., 2008). Meister and colleagues suggested that the synchronous firing activity of a population of RGCs produces a multiplex code, which means that the synchronous spikes form a distinct channel to encode the information of presynaptic cells, such as amacrine cells, and transmit them to higher visual areas without requiring extra fibres (Meister et al., 1995; Meister, 1996; Schnitzer & Meister, 2003). In support of this idea, several studies showed that synchronous and asynchronous firing patterns of RGCs encode different stimulus features (Ishikane et al., 2005; Schwartz et al., 2007; Deny et al., 2017). In Project 3, we used large-scale multi-electrode array recordings to compare the linear responses of synchronous and asynchronous firing activities across various cell types. We used spike-triggered average (STA) as a linear estimate of receptive fields. The receptive field contains the

stimulus-response properties of a cell. Thus, by analyzing the STA of a pair's synchronous firing activities, we gain insights into how synchrony influences the stimulus-response properties of the cell. The spatiotemporal features of the STA such as size, stimulus intensity and latency varied between synchronous and asynchronous firing activities. All RGC types exhibited systematic patterns such as smaller spatial STA, higher stimulus intensity, and shorter latency in the time course of STA for synchronous firing activities, implying a difference in the stimulus strength that elicits synchronous and asynchronous firing activities. To further investigate the receptive field of synchronous firing activities we could use nonlinear models such as LNP models that can capture the intrinsic nonlinearity of the receptive field. Additionally, extending our analysis to include cross-type correlations could broaden our understanding of the general notion of parallel visual coding in retina.

5.6 Final remarks

Over five decades ago, observations of correlated activity in the retina began a new era of research into visual information processing. Groundbreaking studies by David Mastronarde unveiled the mechanisms behind this activity, leading to numerous subsequent studies aimed at understanding its role, benefits, and drawbacks in coding, as well as how it integrates with established principles like parallel visual processing and efficient coding in the retina.

Advancements in experimental techniques, such as multi-electrode array recordings, have granted access to a vast number of spiking cells, including a large population of RGCs and hundreds of polyaxonal amacrine cells. Leveraging the detailed knowledge from earlier foundational work, we were able to characterize various RGC types and systematically study the structure of correlated activity across many RGC types, yielding consistent results that align with the understood mechanisms of correlation. Furthermore, simultaneous recordings of populations of PACs alongside RGCs facilitated the examination of the collective impact of interactions between specific PAC types and RGC types on the latter's responses. Finally, by combining anatomical and physiological techniques, we revisited the longstanding concept of parallel visual processing in the retina, uncovering counterexamples to this general rule.

Thus, previous foundational research has paved the way for current studies, and the advent of new experimental techniques is enhancing our understanding of retinal circuits. Each new discovery prompts further questions about the function and prevalence of these findings, driving the field forward.

Abbreviations

°C degree Celsius

aRGC alpha retinal ganglion cell

AC amacrine cell BC bipolar cell

c cone

Ca²⁺ calcium ion

ChAT choline acetyltransferase

CMOS complementary metal-oxide-semiconductor

CNS central nervous system
CRT Cathode Ray Tube

Cx connexin d day

dLGN dorsal-lateral geniculate nucleus e.g. for example (lat. exempli gratia)

et al. and others (lat. et alii)
GCL ganglion cell layer

GABA gamma-aminobutyric acid

h hour

HC horizontal cell

Hz hertz

i.e. that is (lat. Id est)INL inner nuclear layerIPL inner plexiform layerKCL potassium chloride

M Molar

MEA multielectrode array

 $\begin{array}{ccc} \text{Min} & \text{minute} \\ \text{Mm} & \text{millimeter} \\ \text{mM} & \text{millimoles} \\ \text{ms} & \text{millisecond} \\ \text{M}\Omega & \text{megaohm} \\ \text{n} & \text{total number} \end{array}$

NA numerical aperture

NB neurobiotin

NDS normal donkey serum
NMDA N-methyl-D-aspartic acid

ONL outer nuclear layer
OPL outer plexiform layer
PFA paraformaldehyde

pH potential of hydrogen (lat. pondus hydrogenii)

r rod

RGC retinal ganglion cell

RBPMS RNA-binding protein with multiple splicing

RT room temperature SD standard deviation

Sec. second

sON sustained ON micrometer

Curriculum Vitae

Elaheh Lotfi

PERSONAL INFORMATION

Date of Birth: 24.03.1989 Cell-Phone: +98 (921) 4722370

E-mail: elahehlotfi@yahoo.com

EDUCATION

PhD Student, Department of Neuroscience, Carl von Ossietzky University, Oldenburg, *April 2019 – now*

- Thesis Title: 'Correlated activity in the mammalian retina'
- Supervision: Prof. Dr. Martin Greschner

MSc in Electrical Engineering – Control, School of Electrical and Computer Engineering, University of Tehran, Tehran, Iran, *September 2011- August 2014*

- GPA: 17.90/20
- Thesis Title: 'Model-based Decoding of V1 Multi-Electrode Activity'
- Advisors: Prof. Babak Nadjar Araabi (From University of Tehran)
 Prof. Majid Nili Ahmadabadi (From University of Tehran)
 Dr. Lars Schwabe (From University of Rostock)

BSc in Electrical Engineering – Control, School of Electrical and Computer Engineering, University of Tehran, *September 2007 - August 2011*

- GPA: 17.20/20
- Thesis Title: 'Speed Control Methods for MFL PIG'
- Advisor: Prof. Majid Nili Ahmadabadi

FURTHER ENGAGEMENTS

- Staff scientist with Prof. Dr. Martin Greschner, Department of Neuroscience, Carl von Ossietzky University, Oldenburg, *February 2016 April 2019*
- Research visit, laboratory of Dr. Lars Schwabe, University of Rostock (DAAD scholarship), *June 2012- December 2012*

PUBLICATIONS

 Puller C*, Duda S*, Lotfi E*, Arzhangnia Y, Block CT, Ahlers MT, Greschner M. (2020) Electrical Coupling of Heterotypic Ganglion Cells in the Mammalian Retina. The Journal of Neuroscience 40(6):1302– 1310

CONFERENCES

- Elaheh Lotfi*, Christian Puller*, Yousef Arzhangnia, Martin Greschner, "Electrical Coupling among Heterotypic Ganglion Cells" 11th FENS Forum of Neuroscience, Berlin 2018.
- E. Lotfi, B. N. Araabi, M. N. Ahmadabadi and L. Schwabe, "Biological Constrained Learning of Parameters in a Recurrent Neural Network-based Model of the Primary Visual Cortex", 21th Iranian Conference on Biomedical Engineering (ICBME 2014), Tehran, 2014.

TEACHING EXPERIENCE

Teaching Assistant:

- Modern Control, University of Tehran, Fall 2013.
- Engineering Mathematics, University of Tehran, Spring 2010.

List of publications

Puller C*, Duda S*, **Lotfi E***, Arzhangnia Y, Block CT, Ahlers MT, Greschner M. (2020) Electrical Coupling of Heterotypic Ganglion Cells in the Mammalian Retina. The Journal of Neuroscience 40(6):1302–1310

Participation in conferences

2018 FENS Forum of Neuroscience, Berlin – Germany Poster presentation: "Electrical Coupling among Heterotypic Ganglion Cells."

References

- Ackert, J. M., Wu, S. H., Lee, J. C., Abrams, J., Hu, E. H., Perlman, I., & Bloomfield, S. A. (2006). Light-induced changes in spike synchronization between coupled ON direction selective ganglion cells in the mammalian retina. *Journal of Neuroscience*, 26(16), 4206-4215.
- Ala-Laurila, P., Greschner, M., Chichilnisky, E., & Rieke, F. (2011). Cone photoreceptor contributions to noise and correlations in the retinal output. *Nature neuroscience*, *14*(10), 1309-1316.
- Arnett, D. (1978). Statistical dependence between neighboring retinal ganglion cells in goldfish. *Experimental Brain Research*, 32, 49-53.
- Atick, J. J., & Redlich, A. N. (1990). Towards a theory of early visual processing. *Neural computation*, 2(3), 308-320.
- Attneave, F. (1954). Some informational aspects of visual perception. *Psychological review*, 61(3), 183.
- Averbeck, B. B., Latham, P. E., & Pouget, A. (2006). Neural correlations, population coding and computation. *Nature Reviews Neuroscience*, 7(5), 358-366.
- Averbeck, B. B., & Lee, D. (2004). Coding and transmission of information by neural ensembles. *Trends in neurosciences*, 27(4), 225-230.
- Awatramani, G. B., & Slaughter, M. M. (2000). Origin of transient and sustained responses in ganglion cells of the retina. *Journal of Neuroscience*, 20(18), 7087-7095.
- Baccus, S. A., Ölveczky, B. P., Manu, M., & Meister, M. (2008). A retinal circuit that computes object motion. *Journal of Neuroscience*, 28(27), 6807-6817.
- Badea, T. C., & Nathans, J. (2004). Quantitative analysis of neuronal morphologies in the mouse retina visualized by using a genetically directed reporter. *Journal of Comparative Neurology*, 480(4), 331-351.
- Baden, T., Berens, P., Franke, K., Román Rosón, M., Bethge, M., & Euler, T. (2016). The functional diversity of retinal ganglion cells in the mouse. *Nature*, *529*(7586), 345-350.
- Bae, J. A., Mu, S., Kim, J. S., Turner, N. L., Tartavull, I., Kemnitz, N., Jordan, C. S., Norton, A. D., Silversmith, W. M., & Prentki, R. (2018). Digital museum of retinal ganglion cells with dense anatomy and physiology. *Cell*, *173*(5), 1293-1306. e1219.
- Barlow, H. (2001). Redundancy reduction revisited. *Network: computation in neural systems*, 12(3), 241.
- Barlow, H., Hill, R., & Levick, W. (1964). Retinal ganglion cells responding selectively to direction and speed of image motion in the rabbit. *The Journal of physiology*, 173(3), 377.
- Barlow, H., & Levick, W. R. (1965). The mechanism of directionally selective units in rabbit's retina. *The Journal of physiology*, 178(3), 477.
- Barlow, H. B., & Hill, R. M. (1963). Selective sensitivity to direction of movement in ganglion cells of the rabbit retina. *Science*, *139*(3553), 412-414.

- Beaudoin, D. L., Kupershtok, M., & Demb, J. B. (2019). Selective synaptic connections in the retinal pathway for night vision. *Journal of Comparative Neurology*, 527(1), 117-132.
- Bleckert, A., Schwartz, G. W., Turner, M. H., Rieke, F., & Wong, R. O. (2014). Visual space is represented by nonmatching topographies of distinct mouse retinal ganglion cell types. *Current Biology*, 24(3), 310-315.
- Bloomfield, S. A. (1994). Orientation-sensitive amacrine and ganglion cells in the rabbit retina. *Journal of Neurophysiology*, 71(5), 1672-1691.
- Bloomfield, S. A., & Völgyi, B. (2009). The diverse functional roles and regulation of neuronal gap junctions in the retina. *Nature Reviews Neuroscience*, 10(7), 495-506.
- Brackbill, N., Rhoades, C., Kling, A., Shah, N. P., Sher, A., Litke, A. M., & Chichilnisky, E. (2020). Reconstruction of natural images from responses of primate retinal ganglion cells. *Elife*, 9, e58516.
- Brandstätter, J. H., Koulen, P., & Wässle, H. (1998). Diversity of glutamate receptors in the mammalian retina. *Vision research*, *38*(10), 1385-1397.
- Briggman, K. L., Helmstaedter, M., & Denk, W. (2011). Wiring specificity in the direction-selectivity circuit of the retina. *Nature*, 471(7337), 183-188.
- Brivanlou, I. H., Warland, D. K., & Meister, M. (1998). Mechanisms of concerted firing among retinal ganglion cells. *Neuron*, 20(3), 527-539.
- Cafaro, J., Zylberberg, J., & Field, G. D. (2020). Global motion processing by populations of direction-selective retinal ganglion cells. *Journal of Neuroscience*, 40(30), 5807-5819.
- Cajal, S. R. y (1893) La rétine des vertébrés. La cellule, 9, 119-257.
- Chapot, C. A., Euler, T., & Schubert, T. (2017). How do horizontal cells 'talk' to cone photoreceptors? Different levels of complexity at the cone—horizontal cell synapse. *The Journal of physiology*, 595(16), 5495-5506.
- Chichilnisky, E. (2001). A simple white noise analysis of neuronal light responses. *Network:* computation in neural systems, 12(2), 199.
- Contini, M., & Raviola, E. (2003). GABAergic synapses made by a retinal dopaminergic neuron. *Proceedings of the National Academy of Sciences*, 100(3), 1358-1363.
- Cooler, S., & Schwartz, G. W. (2021). An offset ON-OFF receptive field is created by gap junctions between distinct types of retinal ganglion cells. *Nature neuroscience*, 24(1), 105-115.
- Coombs, J., Van Der List, D., Wang, G.-Y., & Chalupa, L. (2006). Morphological properties of mouse retinal ganglion cells. *Neuroscience*, *140*(1), 123-136.
- Dacey, D. M. (1988). Dopamine-accumulating retinal neurons revealed by in vitro fluorescence display a unique morphology. *Science*, 240(4856), 1196-1198.
- Dacey, D. M. (1989). Axon-bearing amacrine cells of the macaque monkey retina. *Journal of Comparative Neurology*, 284(2), 275-293.
- Dacey, D. M., & Brace, S. (1992). A coupled network for parasol but not midget ganglion cells in the primate retina. *Visual neuroscience*, *9*(3-4), 279-290.

- Davenport, C. M., Detwiler, P. B., & Dacey, D. M. (2007). Functional polarity of dendrites and axons of primate A1 amacrine cells. *Visual neuroscience*, 24(4), 449-457.
- Demb, J. B., Haarsma, L., Freed, M. A., & Sterling, P. (1999). Functional circuitry of the retinal ganglion cell's nonlinear receptive field. *Journal of Neuroscience*, 19(22), 9756-9767.
- Deny, S., Ferrari, U., Mace, E., Yger, P., Caplette, R., Picaud, S., Tkačik, G., & Marre, O. (2017). Multiplexed computations in retinal ganglion cells of a single type. *Nature communications*, 8(1), 1964.
- DeVries, S. H. (1999). Correlated firing in rabbit retinal ganglion cells. *Journal of Neurophysiology*, 81(2), 908-920.
- DeVries, S. H. (2000). Bipolar cells use kainate and AMPA receptors to filter visual information into separate channels. *Neuron*, 28(3), 847-856.
- Devries, S. H., & Baylor, D. A. (1997). Mosaic arrangement of ganglion cell receptive fields in rabbit retina. *Journal of Neurophysiology*, 78(4), 2048-2060.
- Diamond, J. S. (2017). Inhibitory interneurons in the retina: types, circuitry, and function. *Annual review of vision science*, *3*, 1-24.
- Dumitrescu, O. N., Protti, D. A., Majumdar, S., Zeilhofer, H. U., & Wässle, H. (2006). Ionotropic glutamate receptors of amacrine cells of the mouse retina. *Visual neuroscience*, 23(1), 79-90.
- Estevez, M. E., Fogerson, P. M., Ilardi, M. C., Borghuis, B. G., Chan, E., Weng, S., Auferkorte, O. N., Demb, J. B., & Berson, D. M. (2012). Form and function of the M4 cell, an intrinsically photosensitive retinal ganglion cell type contributing to geniculocortical vision. *Journal of Neuroscience*, 32(39), 13608-13620.
- Euler, T., Haverkamp, S., Schubert, T., & Baden, T. (2014). Retinal bipolar cells: elementary building blocks of vision. *Nature Reviews Neuroscience*, *15*(8), 507-519.
- Famiglietti, E. V. (1991). Synaptic organization of starburst amacrine cells in rabbit retina: analysis of serial thin sections by electron microscopy and graphic reconstruction. *Journal of Comparative Neurology*, 309(1), 40-70.
- Famiglietti, E. V. (1992). Polyaxonal amacrine cells of rabbit retina: morphology and stratification of PA1 cells. *Journal of Comparative Neurology*, *316*(4), 391-405.
- Famiglietti Jr, E. V. (1983). 'Starburst'amacrine cells and cholinergic neurons: mirror-symmetric ON and OFF amacrine cells of rabbit retina. *Brain research*, 261(1), 138-144.
- Field, G. D., & Chichilnisky, E. (2007). Information processing in the primate retina: circuitry and coding. *Annu. Rev. Neurosci.*, *30*, 1-30.
- Field, G. D., Sher, A., Gauthier, J. L., Greschner, M., Shlens, J., Litke, A. M., & Chichilnisky, E. (2007). Spatial properties and functional organization of small bistratified ganglion cells in primate retina. *Journal of Neuroscience*, 27(48), 13261-13272.
- Franke, F., Fiscella, M., Sevelev, M., Roska, B., Hierlemann, A., & da Silveira, R. A. (2016). Structures of neural correlation and how they favor coding. *Neuron*, 89(2), 409-422.
- Franke, K., & Baden, T. (2017). General features of inhibition in the inner retina. *The Journal of physiology*, 595(16), 5507-5515.

- Freed, M. A., Pflug, R., Kolb, H., & Nelson, R. (1996). ON-OFF amacrine cells in cat retina. *Journal of Comparative Neurology*, 364(3), 556-566.
- Fried, S. I., Münch, T. A., & Werblin, F. S. (2002). Mechanisms and circuitry underlying directional selectivity in the retina. *Nature*, 420(6914), 411-414.
- Gauthier, J. L., Field, G. D., Sher, A., Greschner, M., Shlens, J., Litke, A. M., & Chichilnisky, E. (2009). Receptive fields in primate retina are coordinated to sample visual space more uniformly. *PLoS biology*, 7(4), e1000063.
- Gollisch, T., & Meister, M. (2010). Eye smarter than scientists believed: neural computations in circuits of the retina. *Neuron*, 65(2), 150-164.
- Greschner, M., Field, G. D., Li, P. H., Schiff, M. L., Gauthier, J. L., Ahn, D., Sher, A., Litke, A. M., & Chichilnisky, E. (2014). A polyaxonal amacrine cell population in the primate retina. *Journal of Neuroscience*, 34(10), 3597-3606.
- Greschner, M., Heitman, A. K., Field, G. D., Li, P. H., Ahn, D., Sher, A., Litke, A. M., & Chichilnisky, E. (2016). Identification of a retinal circuit for recurrent suppression using indirect electrical imaging. *Current Biology*, 26(15), 1935-1942.
- Greschner, M., Shlens, J., Bakolitsa, C., Field, G. D., Gauthier, J. L., Jepson, L. H., Sher, A., Litke, A. M., & Chichilnisky, E. (2011). Correlated firing among major ganglion cell types in primate retina. *The Journal of physiology*, 589(1), 75-86.
- Grimes, W. N., Songco-Aguas, A., & Rieke, F. (2018). Parallel processing of rod and cone signals: retinal function and human perception. *Annual review of vision science*, 4, 123-141.
- Hall, J. E., & Hall, M. E. (2020). Guyton and Hall textbook of medical physiology e-Book. Elsevier Health Sciences.
- Hartveit, E., & Veruki, M. L. (2012). Electrical synapses between AII amacrine cells in the retina: function and modulation. *Brain research*, 1487, 160-172.
- Helmstaedter, M., Briggman, K. L., Turaga, S. C., Jain, V., Seung, H. S., & Denk, W. (2013). Connectomic reconstruction of the inner plexiform layer in the mouse retina. *Nature*, 500(7461), 168-174.
- Hidaka, S., Akahori, Y., & Kurosawa, Y. (2004). Dendrodendritic electrical synapses between mammalian retinal ganglion cells. *Journal of Neuroscience*, 24(46), 10553-10567.
- Hoggarth, A., McLaughlin, A. J., Ronellenfitch, K., Trenholm, S., Vasandani, R., Sethuramanujam, S., Schwab, D., Briggman, K. L., & Awatramani, G. B. (2015). Specific wiring of distinct amacrine cells in the directionally selective retinal circuit permits independent coding of direction and size. *Neuron*, 86(1), 276-291.
- Hoshi, H., Liu, W.-L., Massey, S. C., & Mills, S. L. (2009). ON inputs to the OFF layer: bipolar cells that break the stratification rules of the retina. *Journal of Neuroscience*, 29(28), 8875-8883.
- Hu, E. H., & Bloomfield, S. A. (2003). Gap junctional coupling underlies the short-latency spike synchrony of retinal α ganglion cells. *Journal of Neuroscience*, 23(17), 6768-6777.
- Ishikane, H., Gangi, M., Honda, S., & Tachibana, M. (2005). Synchronized retinal oscillations encode essential information for escape behavior in frogs. *Nature neuroscience*, 8(8), 1087-1095.

- Jackman, S. L., Babai, N., Chambers, J. J., Thoreson, W. B., & Kramer, R. H. (2011). A positive feedback synapse from retinal horizontal cells to cone photoreceptors. *PLoS Biol*, 9(5), e1001057.
- Jia, Y., Lee, S., Zhuo, Y., & Zhou, Z. J. (2020). A retinal circuit for the suppressed-by-contrast receptive field of a polyaxonal amacrine cell. *Proceedings of the National Academy of Sciences*, 117(17), 9577-9583.
- Joesch, M., & Meister, M. (2016). A neuronal circuit for colour vision based on rod–cone opponency. *Nature*, *532*(7598), 236-239.
- Kerschensteiner, D. (2022). Feature detection by retinal ganglion cells. *Annual review of vision science*, 8, 135-169.
- Kerschensteiner, D., Morgan, J. L., Parker, E. D., Lewis, R. M., & Wong, R. O. (2009). Neurotransmission selectively regulates synapse formation in parallel circuits in vivo. *Nature*, 460(7258), 1016-1020.
- Kim, I.-J., Zhang, Y., Yamagata, M., Meister, M., & Sanes, J. R. (2008). Molecular identification of a retinal cell type that responds to upward motion. *Nature*, 452(7186), 478-482.
- Kong, J. H., Fish, D. R., Rockhill, R. L., & Masland, R. H. (2005). Diversity of ganglion cells in the mouse retina: unsupervised morphological classification and its limits. *Journal of Comparative Neurology*, 489(3), 293-310.
- Kovács-Öller, T., Debertin, G., Balogh, M., Ganczer, A., Orbán, J., Nyitrai, M., Balogh, L., Kántor, O., & Völgyi, B. (2017). Connexin36 expression in the mammalian retina: a multiple-species comparison. *Frontiers in Cellular Neuroscience*, 11, 65.
- Krieger, B., Qiao, M., Rousso, D. L., Sanes, J. R., & Meister, M. (2017). Four alpha ganglion cell types in mouse retina: Function, structure, and molecular signatures. *PloS one*, *12*(7), e0180091.
- Lee, S., Chen, L., Chen, M., Ye, M., Seal, R. P., & Zhou, Z. J. (2014). An unconventional glutamatergic circuit in the retina formed by vGluT3 amacrine cells. *Neuron*, 84(4), 708-715.
- Li, P. H., Gauthier, J. L., Schiff, M., Sher, A., Ahn, D., Field, G. D., Greschner, M., Callaway, E. M., Litke, A. M., & Chichilnisky, E. (2015). Anatomical identification of extracellularly recorded cells in large-scale multielectrode recordings. *Journal of Neuroscience*, *35*(11), 4663-4675.
- Lin, B., & Masland, R. H. (2006). Populations of wide-field amacrine cells in the mouse retina. *Journal of Comparative Neurology*, 499(5), 797-809.
- Litke, A., Bezayiff, N., Chichilnisky, E., Cunningham, W., Dabrowski, W., Grillo, A., Grivich, M., Grybos, P., Hottowy, P., & Kachiguine, S. (2004). What does the eye tell the brain?: Development of a system for the large-scale recording of retinal output activity. *IEEE Transactions on Nuclear Science*, 51(4), 1434-1440.
- MacNeil, M. A., & Masland, R. H. (1998). Extreme diversity among amacrine cells: implications for function. *Neuron*, 20(5), 971-982.
- Manookin, M. B., Beaudoin, D. L., Ernst, Z. R., Flagel, L. J., & Demb, J. B. (2008). Disinhibition combines with excitation to extend the operating range of the OFF visual pathway in daylight. *Journal of Neuroscience*, 28(16), 4136-4150.

- Marc, R. E., Sigulinsky, C. L., Pfeiffer, R. L., Emrich, D., Anderson, J. R., & Jones, B. W. (2018). Heterocellular coupling between amacrine cells and ganglion cells. *Frontiers in Neural Circuits*, 12, 90.
- Mariani, A. P. (1990). Amacrine cells of the rhesus monkey retina. *Journal of Comparative Neurology*, 301(3), 382-400.
- Masland, R. H. (2012a). The neuronal organization of the retina. *Neuron*, 76(2), 266-280.
- Masland, R. H. (2012b). The tasks of amacrine cells. Visual neuroscience, 29(1), 3.
- Massey, S. C., & Miller, R. F. (1988). Glutamate receptors of ganglion cells in the rabbit retina: evidence for glutamate as a bipolar cell transmitter. *The Journal of physiology*, 405(1), 635-655.
- Mastronarde, D. N. (1983a). Correlated firing of cat retinal ganglion cells. I. Spontaneously active inputs to X-and Y-cells. *Journal of Neurophysiology*, 49(2), 303-324.
- Mastronarde, D. N. (1983b). Correlated firing of cat retinal ganglion cells. II. Responses of X- and Y-cells to single quantal events. *Journal of Neurophysiology*, 49(2), 325-349.
- Mastronarde, D. N. (1983c). Interactions between ganglion cells in cat retina. *Journal of Neurophysiology*, 49(2), 350-365.
- Mauss, A. S., Vlasits, A., Borst, A., & Feller, M. (2017). Visual circuits for direction selectivity. *Annual review of neuroscience*, 40, 211-230.
- Meister, M. (1996). Multineuronal codes in retinal signaling. *Proceedings of the National Academy of Sciences*, 93(2), 609-614.
- Meister, M., Lagnado, L., & Baylor, D. A. (1995). Concerted signaling by retinal ganglion cells. *Science*, 270(5239), 1207-1210.
- Menger, N., Pow, D. V., & Wässle, H. (1998). Glycinergic amacrine cells of the rat retina. *Journal of Comparative Neurology*, 401(1), 34-46.
- Mueller, L. P. D. S., Dedek, K., Janssen-Bienhold, U., Meyer, A., Kreuzberg, M. M., Lorenz, S., Willecke, K., & Weiler, R. (2010). Expression and modulation of connexin30. 2, a novel gap junction protein in the mouse retina. *Visual neuroscience*, 27(3-4), 91-101.
- Murphy-Baum, B. L., & Taylor, W. R. (2015). The synaptic and morphological basis of orientation selectivity in a polyaxonal amacrine cell of the rabbit retina. *Journal of Neuroscience*, *35*(39), 13336-13350.
- Mustafi, D., Engel, A. H., & Palczewski, K. (2009). Structure of cone photoreceptors. *Progress in retinal and eye research*, 28(4), 289-302.
- Nassi, J. J., & Callaway, E. M. (2009). Parallel processing strategies of the primate visual system. *Nature Reviews Neuroscience*, 10(5), 360-372.
- Nath, A., & Schwartz, G. W. (2017). Electrical synapses convey orientation selectivity in the mouse retina. *Nature communications*, 8(1), 2025.
- Nirenberg, S., Carcieri, S. M., Jacobs, A. L., & Latham, P. E. (2001). Retinal ganglion cells act largely as independent encoders. *Nature*, *411*(6838), 698-701.

- O'Brien, J., & Bloomfield, S. A. (2018). Plasticity of retinal gap junctions: roles in synaptic physiology and disease. *Annual review of vision science*, 4, 79-100.
- Ölveczky, B. P., Baccus, S. A., & Meister, M. (2003). Segregation of object and background motion in the retina. *Nature*, 423(6938), 401-408.
- Pan, F., Paul, D. L., Bloomfield, S. A., & Völgyi, B. (2010). Connexin36 is required for gap junctional coupling of most ganglion cell subtypes in the mouse retina. *Journal of Comparative Neurology*, 518(6), 911-927.
- Penn, A., Wong, R., & Shatz, C. (1994). Neuronal coupling in the developing mammalian retina. *Journal of Neuroscience*, 14(6), 3805-3815.
- Perkel, D. H., Gerstein, G. L., & Moore, G. P. (1967). Neuronal spike trains and stochastic point processes: II. Simultaneous spike trains. *Biophysical journal*, 7(4), 419-440.
- Petrusca, D., Grivich, M. I., Sher, A., Field, G. D., Gauthier, J. L., Greschner, M., Shlens, J., Chichilnisky, E., & Litke, A. M. (2007). Identification and characterization of a Y-like primate retinal ganglion cell type. *Journal of Neuroscience*, 27(41), 11019-11027.
- Pillow, J. W., Shlens, J., Paninski, L., Sher, A., Litke, A. M., Chichilnisky, E., & Simoncelli, E. P. (2008). Spatio-temporal correlations and visual signalling in a complete neuronal population. *Nature*, 454(7207), 995-999.
- Pourcho, R. G., & Goebel, D. J. (1983). Neuronal subpopulations in cat retina which accumulate the GABA agonist,(3H) muscimol: a combined Golgi and autoradiographic study. *Journal of Comparative Neurology*, 219(1), 25-35.
- Puchalla, J. L., Schneidman, E., Harris, R. A., & Berry, M. J. (2005). Redundancy in the population code of the retina. *Neuron*, 46(3), 493-504.
- Puller, C., Duda, S., Lotfi, E., Arzhangnia, Y., Block, C. T., Ahlers, M. T., & Greschner, M. (2020). Electrical coupling of heterotypic ganglion cells in the mammalian retina. *Journal of Neuroscience*, 40(6), 1302-1310.
- Puller, C., Ivanova, E., Euler, T., Haverkamp, S., & Schubert, T. (2013). OFF bipolar cells express distinct types of dendritic glutamate receptors in the mouse retina. *Neuroscience*, 243, 136-148.
- Reinhard, K., Kühn, N., & Farrow, K. (2020). Direction selectivity in the retina and beyond.
- Rodieck, R. (1967). Maintained activity of cat retinal ganglion cells. *Journal of Neurophysiology*, *30*(5), 1043-1071.
- Rodriguez, A. R., de Sevilla Müller, L. P., & Brecha, N. C. (2014). The RNA binding protein RBPMS is a selective marker of ganglion cells in the mammalian retina. *Journal of Comparative Neurology*, 522(6), 1411-1443.
- Rompani, S. B., Muellner, F. E., Wanner, A., Zhang, C., Roth, C. N., Yonehara, K., & Roska, B. (2017). Different modes of visual integration in the lateral geniculate nucleus revealed by single-cell-initiated transsynaptic tracing. *Neuron*, *93*(4), 767-776. e766.
- Rosón, M. R., Bauer, Y., Kotkat, A. H., Berens, P., Euler, T., & Busse, L. (2019). Mouse dLGN receives functional input from a diverse population of retinal ganglion cells with limited convergence. *Neuron*, 102(2), 462-476. e468.

- Rousso, D. L., Qiao, M., Kagan, R. D., Yamagata, M., Palmiter, R. D., & Sanes, J. R. (2016). Two pairs of ON and OFF retinal ganglion cells are defined by intersectional patterns of transcription factor expression. *Cell reports*, 15(9), 1930-1944.
- Roy, K., Kumar, S., & Bloomfield, S. A. (2017). Gap junctional coupling between retinal amacrine and ganglion cells underlies coherent activity integral to global object perception. *Proceedings of the National Academy of Sciences*, 114(48), E10484-E10493.
- Ruda, K., Zylberberg, J., & Field, G. D. (2020). Ignoring correlated activity causes a failure of retinal population codes. *Nature communications*, 11(1), 4605.
- Sabbah, S., Gemmer, J. A., Bhatia-Lin, A., Manoff, G., Castro, G., Siegel, J. K., Jeffery, N., & Berson, D. M. (2017). A retinal code for motion along the gravitational and body axes. *Nature*, 546(7659), 492-497.
- Schindelin, J., Arganda-Carreras, I., Frise, E., Kaynig, V., Longair, M., Pietzsch, T., Preibisch, S., Rueden, C., Saalfeld, S., & Schmid, B. (2012). Fiji: an open-source platform for biological-image analysis. *Nature methods*, *9*(7), 676-682.
- Schmidt, T. M., Alam, N. M., Chen, S., Kofuji, P., Li, W., Prusky, G. T., & Hattar, S. (2014). A role for melanopsin in alpha retinal ganglion cells and contrast detection. *Neuron*, 82(4), 781-788.
- Schnitzer, M. J., & Meister, M. (2003). Multineuronal firing patterns in the signal from eye to brain. *Neuron*, *37*(3), 499-511.
- Schubert, T., Degen, J., Willecke, K., Hormuzdi, S. G., Monyer, H., & Weiler, R. (2005). Connexin36 mediates gap junctional coupling of alpha-ganglion cells in mouse retina. *Journal of Comparative Neurology*, 485(3), 191-201.
- Schubert, T., Maxeiner, S., Krüger, O., Willecke, K., & Weiler, R. (2005). Connexin45 mediates gap junctional coupling of bistratified ganglion cells in the mouse retina. *Journal of Comparative Neurology*, 490(1), 29-39.
- Schwartz, G., Taylor, S., Fisher, C., Harris, R., & Berry, M. J. (2007). Synchronized firing among retinal ganglion cells signals motion reversal. *Neuron*, *55*(6), 958-969.
- Shekhar, K., Lapan, S. W., Whitney, I. E., Tran, N. M., Macosko, E. Z., Kowalczyk, M., Adiconis, X., Levin, J. Z., Nemesh, J., & Goldman, M. (2016). Comprehensive classification of retinal bipolar neurons by single-cell transcriptomics. *Cell*, 166(5), 1308-1323. e1330.
- Shlens, J., Field, G. D., Gauthier, J. L., Grivich, M. I., Petrusca, D., Sher, A., Litke, A. M., & Chichilnisky, E. (2006). The structure of multi-neuron firing patterns in primate retina. *Journal of Neuroscience*, 26(32), 8254-8266.
- Shlens, J., Rieke, F., & Chichilnisky, E. (2008). Synchronized firing in the retina. *Current opinion in neurobiology*, 18(4), 396-402.
- Simoncelli, E. P., & Olshausen, B. A. (2001). Natural image statistics and neural representation. *Annual review of neuroscience*, 24(1), 1193-1216.
- Stafford, D. K., & Dacey, D. M. (1997). Physiology of the A1 amacrine: a spiking, axon-bearing interneuron of the macaque monkey retina. *Visual neuroscience*, 14(3), 507-522.
- sterling, P., & Demb, J. B. (2004). Retina. In G. M. Shepherd (Ed.), *The Synaptic Organization of the Brain*. Oxford university press.

- Sümbül, U., Song, S., McCulloch, K., Becker, M., Lin, B., Sanes, J. R., Masland, R. H., & Seung, H. S. (2014). A genetic and computational approach to structurally classify neuronal types. *Nature communications*, *5*(1), 1-12.
- Taylor, W. R. (1996). Response properties of long-range axon-bearing amacrine cells in the dark-adapted rabbit retina. *Visual neuroscience*, 13(4), 599-604.
- Traub, R. D., Whittington, M. A., Gutiérrez, R., & Draguhn, A. (2018). Electrical coupling between hippocampal neurons: contrasting roles of principal cell gap junctions and interneuron gap junctions. *Cell and tissue research*, 373, 671-691.
- Trenholm, S., McLaughlin, A. J., Schwab, D. J., Turner, M. H., Smith, R. G., Rieke, F., & Awatramani, G. B. (2014). Nonlinear dendritic integration of electrical and chemical synaptic inputs drives fine-scale correlations. *Nature neuroscience*, 17(12), 1759-1766.
- Trenholm, S., Schwab, D. J., Balasubramanian, V., & Awatramani, G. B. (2013). Lag normalization in an electrically coupled neural network. *Nature neuroscience*, 16(2), 154-156.
- Trong, P. K., & Rieke, F. (2008). Origin of correlated activity between parasol retinal ganglion cells. *Nature neuroscience*, 11(11), 1343-1351.
- Usrey, W. M., & Reid, R. C. (1999). Synchronous activity in the visual system. *Annual review of physiology*, 61(1), 435-456.
- Vaney, D. I. (1991). Many diverse types of retinal neurons show tracer coupling when injected with biocytin or Neurobiotin. *Neuroscience letters*, 125(2), 187-190.
- Vaney, D. I., Peichl, L., & Boycott, B. B. (1988). Neurofibrillar long-range amacrine cells in mammalian retinae. *Proceedings of the Royal society of London. Series B. Biological sciences*, 235(1280), 203-219.
- Vardi, N., Duvoisin, R., Wu, G., & Sterling, P. (2000). Localization of mGluR6 to dendrites of ON bipolar cells in primate retina. *Journal of Comparative Neurology*, 423(3), 402-412.
- Veruki, M. L., & Hartveit, E. (2002). AII (Rod) amacrine cells form a network of electrically coupled interneurons in the mammalian retina. *Neuron*, 33(6), 935-946.
- Völgyi, B., Abrams, J., Paul, D. L., & Bloomfield, S. A. (2005). Morphology and tracer coupling pattern of alpha ganglion cells in the mouse retina. *Journal of Comparative Neurology*, 492(1), 66-77.
- Völgyi, B., Chheda, S., & Bloomfield, S. A. (2009). Tracer coupling patterns of the ganglion cell subtypes in the mouse retina. *Journal of Comparative Neurology*, 512(5), 664-687.
- Völgyi, B., Pan, F., Paul, D. L., Wang, J. T., Huberman, A. D., & Bloomfield, S. A. (2013). Gap junctions are essential for generating the correlated spike activity of neighboring retinal ganglion cells. *PloS one*, 8(7), e69426.
- Völgyi, B., Xin, D., Amarillo, Y., & Bloomfield, S. A. (2001). Morphology and physiology of the polyaxonal amacrine cells in the rabbit retina. *Journal of Comparative Neurology*, 440(1), 109-125.
- Vroman, R., Klaassen, L. J., Howlett, M. H., Cenedese, V., Klooster, J., Sjoerdsma, T., & Kamermans, M. (2014). Extracellular ATP hydrolysis inhibits synaptic transmission by increasing ph buffering in the synaptic cleft. *PLoS Biol*, *12*(5), e1001864.

- Warland, D. K., Reinagel, P., & Meister, M. (1997). Decoding visual information from a population of retinal ganglion cells. *Journal of Neurophysiology*, 78(5), 2336-2350.
- Wässle, H. (2004). Parallel processing in the mammalian retina. *Nature Reviews Neuroscience*, 5(10), 747-757.
- Wässle, H., Peichl, L., & Boycott, B. (1981). Dendritic territories of cat retinal ganglion cells. *Nature*, 292(5821), 344-345.
- Wässle, H., Puller, C., Müller, F., & Haverkamp, S. (2009). Cone contacts, mosaics, and territories of bipolar cells in the mouse retina. *Journal of Neuroscience*, 29(1), 106-117.
- Wei, W. (2018). Neural mechanisms of motion processing in the mammalian retina. *Annual review of vision science*, 4, 165-192.
- Wei, W., Hamby, A. M., Zhou, K., & Feller, M. B. (2011). Development of asymmetric inhibition underlying direction selectivity in the retina. *Nature*, 469(7330), 402-406.
- Wright, L. L., & Vaney, D. I. (2004). The type 1 polyaxonal amacrine cells of the rabbit retina: a tracer-coupling study. *Visual neuroscience*, 21(2), 145-155.
- Wu, S. M., Gao, F., & Maple, B. R. (2000). Functional architecture of synapses in the inner retina: segregation of visual signals by stratification of bipolar cell axon terminals. *Journal of Neuroscience*, 20(12), 4462-4470.
- Xin, D., & Bloomfield, S. A. (1997). Tracer coupling pattern of amacrine and ganglion cells in the rabbit retina. *Journal of Comparative Neurology*, 383(4), 512-528.
- Yang, X.-L. (2004). Characterization of receptors for glutamate and GABA in retinal neurons. *Progress in neurobiology*, 73(2), 127-150.
- Yao, X., Cafaro, J., McLaughlin, A. J., Postma, F. R., Paul, D. L., Awatramani, G., & Field, G. D. (2018). Gap junctions contribute to differential light adaptation across direction-selective retinal ganglion cells. *Neuron*, 100(1), 216-228. e216.
- Yonehara, K., Balint, K., Noda, M., Nagel, G., Bamberg, E., & Roska, B. (2011). Spatially asymmetric reorganization of inhibition establishes a motion-sensitive circuit. *Nature*, 469(7330), 407-410.
- Zaghloul, K. A., Boahen, K., & Demb, J. B. (2003). Different circuits for ON and OFF retinal ganglion cells cause different contrast sensitivities. *Journal of Neuroscience*, 23(7), 2645-2654.
- Zhang, J., Li, W., Hoshi, H., Mills, S. L., & Massey, S. C. (2005). Stratification of alpha ganglion cells and ON/OFF directionally selective ganglion cells in the rabbit retina. *Visual neuroscience*, 22(4), 535-549.
- Zylberberg, J., Cafaro, J., Turner, M. H., Shea-Brown, E., & Rieke, F. (2016). Direction-selective circuits shape noise to ensure a precise population code. *Neuron*, 89(2), 369-383.

Acknowledgments

At this moment, I want to express my sincere thanks to everyone who supported me during my doctorate.

Foremost, I express my profound appreciation to Prof. Dr. Martin Greschner for granting me the opportunity to pursue my studies in the fascinating field of neuroscience. Coming from a very different background, I am particularly thankful for his patience, invaluable assistance, and the guidance that facilitated my swift integration and progress. I am grateful to Martin for his exceptional mentorship and the confidence he placed in my capabilities.

I also want to thank the members of the retina lab at the University of Oldenburg. My gratitude starts with Dr. Christian Puller, who always shared his smart and helpful ideas. A big thank you to Bettina and Patrick for their constant support and friendly help, which greatly eased my transition to life in Germany. Thanks to Malte, Dipti, Sabrina, and Matteo for creating a welcoming and friendly lab environment.

A huge thanks to Yousef and Christoph for always being there to help me with their programming skills.

Finally, I must thank my family, especially my sister, for always believing in me and providing the greatest support during this time.

Erklärung

Hiermit versichere ich, dass diese Dissertation von mir selbst und ohne unerlaubte Hilfe angefertigt worden ist. Es wurden keine anderen als die von mir angegebenen Hilfsmittel und Quellen benutzt. Ferner erkläre ich, dass die vorliegende Arbeit an keiner anderen Hochschule als Dissertation eingereicht wurde.

Elaheh Lotfi Karkan

Tehran, Iran, 02.04.2024